Spring 2008

Density relaxation of granular matter through Monte Carlo and granular dynamics simulations

Oleksandr M. Dybenko
New Jersey Institute of Technology

ABSTRACT

DENSITY RELAXATION OF GRANULAR MATTER THROUGH MONTE CARLO AND GRANULAR DYNAMICS SIMULATIONS

by
Oleksandr M. Dybenko

Granular materials are the principal ingredients of the industrial complex involved with the handling and processing of bulk solids including pharmaceuticals, chemicals, agricultural and mining materials. Despite the enormous importance of these materials in society, their behavior is not well-understood; in fact, there is no known model available that is capable of predicting the wide range of phenomenon that have been observed. One of the most important of these is known as density relaxation. Here, a granular material undergoes an increase in solids fraction as a result of the application of discrete taps or continuous vibrations.

In this dissertation, the density relaxation phenomenon is promoted by the application of discrete taps to a periodic system of monodisperse spheres. Both stochastic (Monte Carlo) and deterministic (granular dynamics) simulations are employed in this work. The granular microstructure of the system particles was analyzed via radial distribution function, coordination number, and the distribution of sphere centers in the vertical direction.

In the MC simulations, the effect of a tap applied to the system is modeled using two different approaches: (1) vertical position-dependent expansion of the particles, and (2) uniformly lifting the entire ensemble on a small displacement above the supporting floor. Both methods resulted in an increase in the system density after numerous

thousands of taps. However, method (1) exhibited a strong dependence of the final system density on the fill height, which has not been experimentally reported in the literature. On the other hand, this dependency was not seen when the expansion of type (2) was used. The MC evolution of the bulk solids fraction was found to be in qualitative agreement with an inverse log form that has been reported in the experimental literature. The simulated results illustrated that the bulk density is related to amount of the lift in method (2), with a critical value producing the most favorable results. Most striking is the finding that as the taps evolve, the particles self-organize into quasi-crystalline layers, initiated by the planar floor.

The granular dynamics approach makes use of uniform, inelastic, and frictional spheres that interact via laws from well-founded collision-mechanics principles. The equations of motion are numerically integrated to obtain the positions and velocities of the particles. The tapping disturbance consisted of a harmonic intermittent oscillation of the floor. The same type of self-organization into quasi-crystalline layers first identified in the MC simulations was also found here, strongly supporting the conjecture that this is a universal mechanism of the density relaxation process.

DENSITY RELAXATION OF GRANULAR MATTER THROUGH MONTE CARLO AND GRANULAR DYNAMICS SIMULATIONS

by
Oleksandr M. Dybenko

A Dissertation
Submitted to the Faculty of
New Jersey Institute of Technology
In Partial Fulfillment of the Requirements for the Degree of
Doctor of Philosophy in Mechanical Engineering

Department of Mechanical Engineering

May 2008

APPROVAL PAGE

DENSITY RELAXATION OF GRANULAR MATTER THROUGH MONTE CARLO AND GRANULAR DYNAMICS SIMULATIONS

Oleksandr M. Dybenko

5/12/2008

Dr. Anthony Rosato, Dissertation Advisor — Date
Professor of Mechanical Engineering, NJIT

5-13-2008

Dr. David Horntrop, Dissertation Co-Advisor, Committee Member — Date
Associate Professor of Mathematical Sciences, NJIT

5/8/08

Dr. Pushpendra Singh, Committee Member — Date
Professor of Mechanical Engineering, NJIT

04/15/08

Dr. Ernest Geskin, Committee Member — Date
Professor of Mechanical Engineering, NJIT

4/18/08

Dr. I. Joga Rao, Committee Member — Date
Associate Professor of Mechanical Engineering, NJIT

BIOGRAPHICAL SKETCH

Author: Oleksandr M. Dybenko

Degree: Doctor of Philosophy

Date: May 2008

Undergraduate and Graduate Education:

- Doctor of Philosophy in Mechanical Engineering
  New Jersey Institute of Technology, Newark, NJ, USA, 2008

- Master of Science in Applied Physics and Mathematics
  Moscow Institute of Physics and Technology, Moscow, Russia, 2001

- Bachelor of Science in Applied Physics and Mathematics
  Moscow Institute of Physics and Technology, Moscow, Russia, 1999

Major: Mechanical Engineering

Presentations and Publications:

Oleksandr Dybenko, Anthony D. Rosato
"Monte Carlo Simulation of Bulk Density Relaxation", Gordon Research Conference on Granular and Granular-fluid Flow, Oxford UK, July 2006.

Oleksandr Dybenko, Anthony D. Rosato and David Horntrop
"Monte Carlo Modeling of Density Relaxation Induced by Energetic Taps", Frontiers in Applied and Computational Mathematics Conference, New Jersey Insitute of Technology, Newark, NJ, USA, May 2007.

Oleksandr Dybenko, Anthony D. Rosato and David Horntrop
"Three-dimensional Monte Carlo Simulations of Density Relaxation", KONA, vol. 25, p. 133-144, Japan, 2007.

L.Kondic, O.M.Dybenko, R.P.Behringer
"Signal Propagation through Dense Granular Systems", Phys. Review Letters (submitted April 2008)

This dissertation is dedicated to the family Dybenko

whose love and support were crucial to complete this work

ACKNOWLEDGMENT

I would like to express my sincere gratitude to my dissertation advisor Dr. Anthony Rosato, for guidance and support throughout this research. Special thanks are given to dissertation co-advisor Dr. David Horntrop, and Dr. Pushpendra Singh, Dr. I. Joga Rao, and Dr. Ernest Geskin for their active participation in my dissertation committee. The author is also thankful to Dr. Lou Kondic, Dr. Oleg Petrenko and Dr. Ivan Zorych for helpful discussions, along with their supportive remarks. Author would like to acknowledge the support from NSF Grants DMS-0605857 and DMR-0555431 without which this research would be incomplete. Computing resources were provided by the Pittsburgh Supercomputer Center (Grant CTS050015P) and an NSF-MRI grant (DMS-0420590). The author is grateful to D. L. Blackmore and O. R. Walton for their interest and discussions of this work. I am glad to recognize the efforts and persistence of Shawn Chester, Vishagan Ratnaswamy, Meng Cui and Tai Duong - the students who have diligently worked with me in the Granular Science Laboratory and helped to review and discuss the various aspects of present dissertation.

TABLE OF CONTENTS

TABLE OF CONTENTS
(Continued)

TABLE OF CONTENTS
(Continued)

Chapter **Page**

LIST OF TABLES

LIST OF FIGURES

LIST OF FIGURES
(Continued)

Figure **Page**

LIST OF FIGURES
(Continued)

Figure **Page**

LIST OF FIGURES
(Continued)

Figure **Page**

LIST OF FIGURES
(Continued)

Figure **Page**

LIST OF SYMBOLS

d	Particle diameter
D	Diameter of the cylindrical vessel
R	Particle radius
ν	Solids fraction
N_T	Number of taps
μ_p	Limiting particle-particle friction coefficient
ρ	Particle mass density
γ	Vertical lift intensity in MC
g	Gravitational constant $\left(9.81 {}^{m}/_{\sec^2}\right)$
π	Mathematical constant (3.1415926)
f	Frequency of sine-wave tapping in DEM
b	Displacement amplitude of sine-wave tapping in DEM
Γ	Dimensionless acceleration in DEM
Δt	Time step
K_2	Normal unloading stiffness
α	Relative overlap between contacting bodies
$\underset{\sim}{x}_i$	Position vector of particle i

CHAPTER 1

INTRODUCTION AND LITERATURE SURVEY

1.1 Overview

The compaction and densification of granular matter is an issue of importance in the industrial sector in that an increase in packing efficiency in the processing of bulk solids is often desirable in reducing costs and in meeting consumer demands. However, in some situations, the compaction resulting from tapping or vibrations in handling operations and long term transport may be detrimental to the quality of the end product. Beyond these practical matters, the ability of a bulk solid to undergo a change in its bulk density due to external disturbances is a fundamental attribute of granular materials that is not well-understood. Indeed, the factors that have a bearing on the phenomenon (e.g., particle properties, containment geometry, environmental conditions, and the nature of the imposed disturbances) are rather broad and consequently the relationship between them requires further study.

The increase in bulk density experienced by contained granular materials subjected to taps and/or continuous vibrations (often referred to as 'density relaxation') has been well-documented in the early literature. From a broader perspective, research on this phenomenon has its foundations in the many fundamental studies on the packing of particles (for example, see [2-15]). In recognition of the importance of developing a better understanding of the nature of the granular state, and motivated in part by recent experiments, density relaxation has received renewed interest as evidenced by the recent

upsurge in both modeling and computational studies, such as in Monte Carlo and Discrete Element Modeling Simulations.

In this dissertation, the effect of discrete taps applied to a vessel of granular material is modeled using a Monte Carlo approach in three-dimensions. This methodology does not consider the detailed dynamical interactions between particles, as would be the case with dissipative molecular dynamics simulations. Rather, the effect of the intensity of the taps on the equilibrium bulk solids fraction is examined. In this regard, the intensities that were selected roughly correspond to relatively large accelerations of the vessel. A broad set of tap intensities was used, thereby allowing us to obtain a correspondingly wide range of solids fractions, from a loose configuration, rather like a 'poured' assembly, to a relatively dense structure with local crystalline order. The vessel itself was chosen to have a smooth (i.e., not bumpy) floor so as not to preclude the well-known 'ordering' effect of a flat plane on packing of uniform spheres [16, 17].

Also we have studied the crystal order propagation using Discrete Element Method. This method is based on the approximation of the collisional interactions between particles using idealized force models that dissipate energy, integration of system equations of motion and following determination of the individual particle positions and velocities [18]. Finally, we compute relevant transport quantities, bulk properties and analyze evolving microstructure of interest. The external tapping of the bottom in this case was provided via consecutive intermittent harmonic oscillations of the floor. The results obtained by DEM validated the formation of hexagonal close packing crystal microstructure observed in Monte Carlo method.

1.2 Evolution of Solids Fraction in Published Literature

The compaction process of the granular matter has an extensive history and the time evolution of bulk solids fraction is widely represented in the literature. The formation of regular and irregular configurations of particles during granular compaction is naturally accompanied by study of the microstructure geometry. This section is constructed to provide an overview of the experimental, theoretical and simulation approaches that have been applied to the problem of density relaxation. To begin, a brief chronological survey will be given based on the most relevant publications on density relaxation. More specifically, experiments involving discrete taps and continuous vibrations of particulate systems will be reviewed, following by related numerical simulations involving Monte Carlo and discrete element methods. Finally, a discussion on various theories that have been developed will be given.

1.2.1 Experimental Work

This subsection provides a concise review of the experimental results reported in the literature in which continuous vibrations and discrete taps have been used.

1.2.1.1 Study of Continuous Vibration. In an early paper [19], Stewart has found that the maximum improvement of the solids fraction was observed in the experiments in which the bed of granular particles had undergone a high-frequency vertical vibration with a low amplitude. Similar results were obtained by Evans [20]. Henceforth, the characterization of the floor response to the vibration was described by dimensionless

floor acceleration Γ, which is provided by the following combination of amplitude (a) and frequency (f) of oscillations:

$$\Gamma = \frac{4\pi^2 f^2}{g} a \tag{1.1}$$

Further experimental work in continuous vibration was performed by Ayer and Soppet [21] who observed that maximum density of single-component packing of steel shots might be achieved when the cylindrical shaker acceleration Γ is set in the range from 6 to 12. They also analyzed the dependence of the solids fraction for different container-to-sphere diameter ratios $\left(D/d\right)$ and proposed following relationship for the limiting solids fraction $\nu_{\max}$:

$$\nu_{\max} = 0.635 - 0.216 \cdot e^{-0.313 D/d} \tag{1.2}$$

In the successive experiments by D'Appolonia et al. [22] using dry sand, the highest solids fraction was obtained when acceleration of vertical oscillations was about 2. These results were produced by harmonic shaking of the sand in a cylindrical container (with a maximum displacement corresponding to 0.25 mm and the highest frequency equal to 60 Hz). An increase of vibratory acceleration $\Gamma > 2$ led to the elimination of stable configuration and an ensuing decrease of solids fraction. Later Dobry and Whitman [23] noticed that the most rapid densification of the granular matter in a cylinder took place at accelerations Γ in the range from 0.9 to 1.1, while the highest bulk density was obtained when $1.1 \le \Gamma \le 1.3$. More recently, Zhang and Rosato [24] have expanded the selection of experimental quantities (amplitudes $0.04 \le a/d \le 0.24$ and frequencies $25Hz \le \omega \le 100Hz$) which correspond to the range of dimensionless

accelerations Γ from 0.94 to 11.54. For each frequency-amplitude combination, they vibrated a cylindrical vessel of uniform acrylic spheres for ten minutes, after which the improvement of solids fraction (from the poured system) was measured. The highest growth (> 5%) was found to correspond to accelerations (Γ) between 5 and 7, and displacement amplitudes (*a*) from 0.06 to 0.1 diameters, while an augmentation of amplitude to 0.24 diameters revealed almost indistinguishable bulk density improvement over what was seen at the lower displacement amplitudes.

1.2.1.2 Tapping of Granular Matter. The tapping of the container filled with granular particles involves the harmonic oscillation of the vessel floor followed by a "relaxation period" during which time the agitated particulates settle to a stable configuration with zero kinetic energy. As early as in 1957, Macrae [25] studied the effect of taps applied to a cylindrical vessel filled with powders of coal and zirconium. He observed that a sufficiently large increase of impact velocity (or in other words, the energy absorbed by the bed) lead to the destruction of existing particle assemblies. He hypothesized that this was caused by a reduction the surface friction, and thereby weakening the force network maintaining the system in a 'metastable' equilibrium configuration. That is, the system's internal force network responsible for maintaining its structural integrity was disrupted. Evolution of the system to states having greater bulk densities could be achieved by applying taps of impact velocity smaller than the critical value.

In later experimental work, Takahashi and Suzuki [26] proposed an empirical expression for the tapping density evolution in terms of first-order rate kinetics as a function of the reciprocal of the tap number,

$$\frac{dV^*}{dn} = -kV^* \tag{1.3}$$

where $n = 1/N$ is the reciprocal tap number and $V^* = \frac{V_0 - V}{V_0 - V_\infty}$ is the fractional volume compaction. Here, V_0 and V_∞ is the initial (poured) and final fractional volume, respectively. The compaction parameter V^* was considered as the integration of the continuous distribution of different types of microscopic holes with a different filling rate constants *k*:

$$V^* = \int_0^\infty f(k)\exp\left(-\frac{k}{N}\right)dk \tag{1.4}$$

Later they found that the compaction function could be well fit by the applying Weibull's distribution function:

$$f(k) = b \cdot m \cdot k^{m-1}\exp(-bk^m) \tag{1.5}$$

and finally for $k = 1$ obtain the Kawakita's compaction equation for ceramic powders [27]:

$$V^* = \int_0^\infty b\exp(-bk)\exp\left(-k/N\right)dk \tag{1.6}$$

In addition to their theoretical results, the authors tapped four different powders (titanium, Kibushi clay, glass beads, and fly ash) in a cylindrical container. The tapping amplitude was set at 1 cm and frequency of 1 Hz that provides acceleration Γ=0.4. Measuring the volume fraction of the granular vessel after every 10 to 50 cycles, they analyzed the dependence of the fractional volume compaction V^* on reciprocal tap numbers and reported the agreement between experimental and theoretical results defined by Equation 1.6.

A series of experiments was carried out by Knight et al. [28] using glass spheres in a tall cylindrical container. Their experimental technique involved randomly pouring glass particles into a narrow tube and exposing the tube to a sequence of vertical taps. The solids fraction was measured using a capacitance probe technique at several positions from the top surface of the container. The tapping was performed by applying a full cycle of a 30 Hz sine wave to the cylinder using an electromagnetic vibration exciter. The magnitude or intensity of a tap was characterized by its peak acceleration amplitude Γ. After each tap, the system was subsequently allowed to relax to a stable state; and after the application of many thousands of taps, the solids fraction ν was gradually reduced to an equilibrium value ν_∞. Continuation of the taps after this simply resulted in fluctuations of the solids fraction about the equilibrium value. The value of $\nu_\infty$was found to be strongly dependent on the vibration intensity Γ.

Knight et al. [28] have reported two functional formulas for the fitting of granular relaxation with four parameters. The first fit introduced was a stretched exponential Kohlraush-William-Watts (KWW) law:

$$\nu(t) = \nu_\infty - \Delta\nu_\infty \exp\left[-\left(\frac{t}{\tau}\right)^\beta\right] \qquad \textbf{(1.7)}$$

Although the KWW law worked well for the initial phase of experiment (10^1-10^2 taps), its use remains an open question due to significant deviations of the fitting data from experimental solids fraction in the final period (10^3-10^4 taps). To cope with logarithmically long times to reach the steady state, the second functional expression was found to be inverse logarithmic law:

$$\nu(t) = \nu_{\infty} - \frac{\Delta\nu_{\infty}}{1 + B\ln\left(1 + \frac{t}{\tau}\right)} \tag{1.8}$$

In successive works [29-32] the group observed and reported reversible-irreversible behavior of solids fraction ν depending on increasing-decreasing vibration intensity Γ.

Very promising experimental work was reported by Nicolas et al. [33]. They studied the behavior of cyclically sheared spherical glass beads in a parallelepiped. The shear deformation was performed by the action of the sidewalls, which rotated in parallel clockwise and counterclockwise through an angle θ, where θ = 0 corresponded to the walls being vertical. They observed the characteristic stroboscopic increase of solids fraction from an initial value 0.61 up to a value of 0.66 for a fixed $\theta=2.7^0$. An increase of the angle amplitude lead to greater compaction (for instance, 0.68 for angle amplitude $\theta=5.4^0$ and 0.693 for $\theta=10.7^0$). The spheres were arranged in a crystalline hexagonal close packing (HCP). The other important observation reported was the effect of reversible-irreversible volume fraction evolution depending on variable shear angle, somewhat analogous to the results of Nowak's tapping [32].

A quasi two-dimensional experimental study of tapping of spherical particles that were positioned between two vertical planes was performed by Lumay, Ludewig, and Vandewalle [34]. For several different tap intensities the solids fraction obtained was in good agreement with a stretched exponential law of the form,

$$\nu(n) = \sqrt{1 - \exp\left(-\sqrt{\frac{n}{\tau}}\right)} \tag{1.9}$$

Case studies for a range of tap intensities as measured by dimensionless acceleration $2 \leq \Gamma \leq 10$, where $\Gamma = a\omega^2/g$, was carried out. However, the equilibrium state was not

obtained because of the small number of taps applied to the packing (N_T=100) in these experiments.

1.2.2 Simulation Studies

In what follows, a succinct review of Monte Carlo and Discrete Element simulations of the density relaxation phenomenon is given.

1.2.2.1 Monte Carlo Simulation. Monte Carlo simulations applied to granular systems model the effects of collisions of particles by applying "random" displacements to the particles that are consistent with the physical process of the specific phenomenon under consideration. Since particle motions are not governed by Newtonian dynamics, there is no real time evolution; rather the goal is to find the equilibrium configuration that minimizes the energy. Perhaps one of the most interesting Monte Carlo studies was that of Rosato et al. [35] in 1986, who identified a geometric mechanism that occurs in size segregation promoted by tapping or vibrations - now known as the "Brazil Nuts model.

In 1988, Tobochnik [36] adapted the Metropolis approach [37, 38] to investigate rather complicated systems of two and three-dimesional hyperspheres with spherical boundary conditions. The maximum bulk solid fraction achieved for the random close packing system of 500 hyperspheres was ν=0.69. Obviously, the spherical boundary conditions caused a relatively large packing fraction as compared with that associated with a random close packing of spheres (i.e., ~ 0.63).

Later, Barker and Mehta [39] introduced a different Monte Carlo technique to induce the "shake" of the close-to-equilibrium system. In a series of consecutive papers [40, 41], they have considered a shaking cycle comprised of three phases:

1) Uniform vertical expansion of particles $y_i' = y_i \times (1+\varepsilon)$, with and without Gaussian randomly distributed lateral shifts $x_i' = x_i + \xi_x$, $z_i' = z_i + \xi_z$;
2) Monte Carlo procedure that incorporated random displacements of spheres in a neighborhood of radius *d*, i.e.,:

$$\boldsymbol{r}_i' = \boldsymbol{r}_i + \boldsymbol{a}d\,,$$

where $\boldsymbol{a}$ is a uniform random vector with components $a_x, a_y, a_z \in [-1;1]$, $\boldsymbol{r}_i$ is the position vector of the center of particle *i*, and a prime denotes the trial position.

3) A phase in which particles are allowed to 'roll' over supporting neighbors to stable configurations.

After a detailed analysis of the data, they suggested that the relaxation process involved both single particle and collective relaxation mechanisms. The dependence of packing fraction on a variety of expansion intensities ε in which the maximum number of shaking cycles was 100. It was suggested that the evolution of the solids fraction $\nu(t)$ could be modeled as the sum of two exponentials representing the individual and collective dynamics, given by

$$\nu(t) = \nu_f - \Delta\nu_{\text{ind}} \exp(-\frac{t}{\tau_{\text{ind}}}) - \Delta\nu_{\text{col}} \exp(-\frac{t}{\tau_{\text{col}}}) \qquad \textbf{(1.10)}$$

where ν_f is the final or equilibrium value, and τ_{ind} (τ_{col}) represent single particle (collective) relaxation times.

A series of studies of slow dynamics of granular compaction was performed by Nicodemi, Coniglio and Herrmann [42-51]. They applied the Monte Carlo technique to model the vertical shaking of the tilted two-dimensional periodic box filled with randomly located particles. The Hamiltonian of the particle-particle interaction was expressed by using the lattice gas Ising spin model. The density relaxation behavior corresponded to the logarithmic form by Knight given by Equation 1.8.

1.2.2.2 Discrete Element and Molecular Dynamics Modeling. As an outgrowth of conservative molecular dynamics methods used in the statistical physical community, the discrete element method (DEM) was originally developed in the 1971. The method has much use in modeling the behavior of bulk solids. In 1985, Williams, Hocking, and Mustoe [52] built up a theoretical basis for the DEM considering it as a generalized finite element method. The main idea of DEM involves the determination of the positions and velocities of the particles by numerical integration of Newton's equations, in which forces are governed by hard to soft sphere interactions. A key feature of the method is the inclusion of dissipation in the forces to model the energy loss that occurs in the collision of macroscopic particles. (For example see, Walton [53] and Schafer [54]).

DEM studies on the densification of granular matter have been report in the 1990's (eg., Luding [55], L.Liu [56], Cheng [57], G.Liu [58], Rosato [59]). In what follows, a brief review of the most recent studies appears.

In 2005, An et. al. [60] simulated the micromechanical response of a three-dimensional granular vessel of 2,000 spheres that was subject to a one-dimensional vertical vibration with amplitude $A = 0.1d$ and frequency f ranging from 8 to 32 Hz. They investigated the transition from initial random loose packing to random close

packing, where the densification process was seen involve to two different intrinsic mechanisms. The first of these mechanisms was termed jump filling, which occurs when inter-particle contacts are destroyed for high values of acceleration Γ, while the second was called push filling, where contacts are retained at low values of Γ. In subsequent simulations, they studied the packing behavior of cohesive wet particles [61]. Here, they identified three jamming regions depending on the force structure. For a system with loose packing $(\nu < 0.56)$, isolated force clusters were found; for the random close packing $(0.56 \le \nu < 0.64)$. continuous force networks were prevalent; and highly - jammed force networks were seen for dense configurations $(\nu > 0.64)$.

The formation of structural order for large vibration amplitudes was also confirmed by [62]. In this simulation, Remond and Galias investigated the behavior of 10,000 spherical particles within periodic parallelepiped container ($20d \times 20d \times 36.5d$). They investigated the effect of 500,000 cycles of "random vibration" with amplitude range varying from $0.005d$ to $0.065d$. Crystallization of systems was reported for the amplitudes $A \in [0.05; 0.065]$, at which solids fraction obtained was identical to those of packings having solids fraction in the range $[0.635; 0.66]$. Local structural ordering was observed in the radial distribution with a second neighbor (at $d\sqrt{2}$) corresponding to the face-centered cubic (fcc) or hexagonal-close packing (hcp).

A similar phenomenon of densification of granular matter through the application of continuous sinusoidal vibrations applied to a system of uniform spherical particles was reported by Zhang and Rosato [24]. The maximum solids fraction $\nu = 0.655$ was obtained for 8,000 spheres $\left(L/d = 25\right)$ with vibration amplitude $0.36d$. They also

observed a region in amplitude frequency space for which the highest solids fractions were obtained.

In 2006, Arsenovic et. al. [63] reported on the compaction dynamics of hard disks by using dissipative molecular dynamics methodology. The simulation was divided into two cycles. First, a packing of 1,000 disks experienced a linear vertical dilation and then the random velocities were set to all the particles. Second, the "event"-driven algorithm was implemented to model the parabolic trajectories two particles after collision (event). The dissipation of energy caused by the presence of Coulomb friction was used to equilibrate the packing. The evolution of solids fraction was fit to the Mittag-Leffler law:

$$\nu(t) = \nu_{\infty} - \Delta\nu \cdot E_{\alpha}\left[-\left(\frac{t}{\tau}\right)^{\alpha}\right], \quad 0 < \alpha < 1 \tag{1.11}$$

where

$$E_{\alpha}\left[-\left(\frac{t}{\tau}\right)^{\alpha}\right] = \sum_{n=0}^{\infty} \frac{\left(-(t/\tau)^{\alpha}\right)^{n}}{\Gamma(1+\alpha n)} \tag{1.12}$$

The authors also reported the dependence between time-scale τ and the tapping intensity Γ (K is a constant):

$$\tau = K\Gamma^{-1} \tag{1.13}$$

1.2.3 Theoretical Groundwork

The experiments performed by Knight were followed by several scientific publications attempting to build a fundamental theoretical basis of the evolution of the solids fraction evolution under tapping. It is easy to underline four major theoretical directions: free volume arguments initiated by Boutreux and de Gennes [64], the one-dimensional parking lot model of clusters of particles by Gavrilov [65], the stroboscopic decay model

of Linz [66], and the mesoscopic one-dimensional lattice model of Brey [67]. A description of each of these models now follows.

1.2.3.1 Free Volume Model. The "free volume model" for compaction of granular matter appeared in 1997 by Boutreux and de Gennes [64]. They assumed a Poisson distribution of holes (free volumes of voids between particles), and used a statistical mechanics approach to obtain a kinetic rate of compaction which led to an inverse logarithmic law (see Equation 1.8). Nowak in [31] expanded this theory by introducing of thermal fluctuations as an analogue to the experimental volume fluctuations; he stated that the evolution of the solids fraction is due to the reorganization of local volumes of particles. This idea was further developed by Head [68, 69], who found a similarity between the logarithmic compaction to the glass-transition phenomena of super-cooled liquid described by Adam and Gibbs [70]. He linked the vibration intensity parameter Γ to the "granular temperature" $\eta(\Gamma)$ and showed the intrinsic dependence of parameters B and τ on Γ. In 1998, Peng and Ohta [71] proposed one-dimensional model to simulate compaction of granular matter under vertical tapping. In particular, the continuity equation for density of particles was numerically solved by using discrete positions in a lattice. In addition, an analytical solution was asymptotically found to have an inverse logarithmic functional form.

1.2.3.2 Parking Lot Model. In 1998, Gavrilov [65] observed that the one-dimensional traffic flow model of randomly packed car clusters shows similarity to the behavior of packing voids undergoing vertical tapping. He assumed that the fragmentation parameter K, which physically represents the split of K individual particles from a cluster of j

particles during one vertical tap, was linearly dependent on the "dimensionless acceleration" Γ used by Knight. Gavrilov also assumed that the probability that a separate particle will join the group of j particles is the ratio of the number of groups with j particle clusters to the total number of clusters. This theory predicted the transition to crystalline state with maximum solids fraction and hexagonal structure of near neighbors and described the phenomenon of reversibility-irreversibility observed by Knight.

1.2.3.3 Stroboscopic Decay Theory. In 1996, Linz [66] introduced the stroboscopic decay law by using compaction ratio α_n (n is number of taps):

$$\alpha_n = \frac{\nu_n - \nu_\infty}{\nu_0 - \nu_\infty} \tag{1.14}$$

and applying the recurrent equation for the one-dimensional stroboscopic map:

$$\alpha_n = f(\alpha_{n-1}, n) = \frac{\alpha_{n-1}}{1 + h_n \alpha_{n-1}} \tag{1.15}$$

He derived the minimal relaxation law supported by Knight's inverse logarithmic law. He gave an explanation of the phenomenological nature of the compaction evolution as the process of two counteracting mechanisms: decompaction and recompaction of packings.

1.2.3.4 Stochastic Lattice Model. In 2001, Brey [72, 73] described the discrete compaction process by using a mesoscopic differential master equation:

$$\dot{\nu} = \frac{d\nu(t)}{dt} = f_1(\Gamma)\mu_1(t) - f_2(\Gamma)\mu_2(t) \tag{1.16}$$

where $f_1(\Gamma)$ and $f_2(\Gamma)$ are positive functions of Γ, and $\mu_1(t)$ and $\mu_2(t)$ are positive quantities depending on the configuration of the system. Applying the derivations to the

stochastic Markov process for one-dimensional lattice model, the evolution of linear response to the tapping small vibration intensity was obtained.

Table 1.1 below summarizes the literature that is most relevant to the density relaxation analysis that was considered in this section. Here, MC stands for results obtained by Monte-Carlo simulation, DEM - Discrete Element Method simulation, MD – Molecular Dynamics modeling.

Table 1.1 Density relaxation of solids fraction in the literature.

First Author	*Year*	*Methods*	*First Author*	*Year*	*Methods*
Stewart [19]	1951	Experiment	L. Liu [56]	1999	DEM
Macrae [25]	1957	Experiment	Head [68, 69]	1998/00	Theory
Round [74]	1963	MC	Cheng [57]	2000	DEM
Evans [20]	1964	Experiment	G. Liu [58]	2000	DEM
D'Apolonia [22]	1967	Experiment	Josserand [75]	2000	Experiment, Theory
Owe Berg [16]	1969	Experiment	Brey [72]	2001	Theory
Dobry [23]	1973	Experiment	Nicolas [33]	2002	Experiment
Tory [15]	1973	MC	Rosato [76]	2002	DEM
Powell [77]	1980	MC	Pouliquen [78]	2003	Experiment
Takahashi [26]	1986	Theory	Williams [79]	2003	MC
Rosato [35]	1987	MC	Abreu [80]	2003	MC
Tobochnik [36]	1988	MC	Coniglio [81]	2004	Theory
Mehta [39]	1991	MC	Silbert [82]	2004	MD
Walton [53]	1992	DEM	An [60]	2005	DEM
Barker [40, 41]	1992/93	MC	Brujic [83]	2005	Experiment
Luding [84]	1994	DEM	Ribiere [85-87]	2005	Experiment, MC
Knight [88]	1995	Experiment	Kim [89]	2005	Experiment
Schaffer [54]	1996	DEM	Budinski [90]	2005	MC
Jaeger [91]	1996	Experiment	Theuerkrauf [92]	2006	DEM
Nowak [31, 32]	1997/98	Experiment	Remond [62]	2006	DEM
Gavrilov [65]	1998	Theory	N. Zhang [24]	2006	Experiment, DEM
Linz [66, 93]	1996/9	Theory	Wouterse [94]	2006	Theory
Nicodemi [50, 51, 95]	1997/99	MC	Lumay [96]	2006	Experiment
Boutreux [64]	1997	Theory	Arsenovic [63]	2006	MC
McNamara [97]	1998	Theory	Ciamarra [98, 99]	2006/7	Theory, DEM

1.3 Microstructure Analysis of Spherical Arrangements

A quantitative characterization of geometrical properties of spherical particles has been a scientific goal for centuries. There are several global parameters used to insight into the structural geometry of the packings of spherical particles: Voronoï and Delaunay 'free volumes', coordination number, dihedral and solid angular distribution, radial distribution function, local orientation order, fabric tensor, etc.

Table 1.1 below lists several microstructure analysis studies in the literature. In this table, CRD represents coordination number distribution, RDF – radial distribution function, ADF – angular distribution function, Voronoi – analysis of Voronoi polyhedron distribution, Porosity – distribution of porosity, Phase – analysis of phase transition for different loose packings. In this dissertation, the focus will be on the coordination number and radial distribution function as well as introduce a new geometric measure – vertical center distribution.

Table 1.2 Microstructure analysis of spherical particles of solids fraction in the literature.

First Author	*Year*	*Quantity*	*First Author*	*Year*	*Quantity*
Smith [13]	1929	CRD	Pillai [100]	1977	Porosity
Bernal [5, 101]	1960/63	CRD, RDF	Powell [77]	1980	CRD
Scott [11, 102]	1962/69	CRD, RDF	Berryman [103]	1983	CRD
Haughey [104]	1966	CRD, RDF	Goodling [105]	1985	CRD
Mason [106]	1968	RDF	Onoda [10]	1990	Porosity
Tory [107]	1968	CRD	Nolan [108, 109]	1992/95	CRD, RDF,
Finney [110]	1970	CRD, RDF	Rosato [111]	1999	CRD,RDF
Cargill [112]	1970	RDF	Sederman [113]	2001	Porosity
Beresford [114]	1970	CRD	Torquato [115]	2000	Phase
Bennet [4]	1971	CRD, RDF	He [116]	2001	RDF
Adams [2]	1972	RDF	Liao [117]	2002	Voronoi
Gotoh [7, 118, 119]	1971/78	CRD, ADF	Wu [120]	2003	RDF, Voronoi
Iwata [121]	1974	CRD	Aste [1, 122]	2005	Overview
Matheson [123]	1974	RDF	Mueller [124]	2005	RDF
Dodds [125]	1975	CRD	Kumar [126, 127]	2005	Voronoi

1.3.1 Coordination Number

The coordination number describes the number of points of contacts between particles in a granular material. This measure was most likely originated in 1694 in a prominent dispute between Isaac Newton and David Gregory. These two famous scientists wanted to determine the number of three-dimensional monodisperse spheres in touch with one particular sphere (the so-called "kissing number"). Newton suggested that only 12 spheres may be in contact with a central sphere, on the other hand Gregory believed that there was enough space for 13. The first geometric proofs of Bender, Hoppe, and Günter were produced in 1874; they found that "though there is a significant amount of free

space left after packing 12 spheres around the central one, although it was not enough to put in a 13^{th} sphere".

An early study of irregular packings was completed by Smith et. al [13]. They carried out experiments where lead shot was poured into a large container, which was subsequently filled up with an acetic acid. After being drained of acid, the number of contacts for each particular lead shot (etched on the sphere surfaces) was simply counted. The assumption that packing consisted of only two possible arrangements (simple cubic and hexagonal) was a key in the derivation of the relationship between number of contacts and the porosity (and consequently solids fraction) of the random packing that was determined by following formula:

$$N_C = 26.484 - \frac{10.734}{\nu} \tag{1.17}$$

where N_C is the number of contacts and ν - the solids fraction of the spheres. Two limiting pairs of the Equation 1.17 correspond to the number of spheres in contact and solids fraction (6, 0.524) for simple cubic and (12, 0.7405) for hexagonal structures.

In 1960, Bernal and Mason [5, 101] shook 3,000 ball bearings enclosed in a box with an irregular floor. After the system equilibrated to the close packing, the container was filled with paint. Bernal analyzed the coordination number and found out that the random geometry of equal spheres formed by these shakes is highly different from the geometry of a crystal with fixed coordination. It was reported that two spheres within 5% of a diameter of each other have average coordination number about 6 (with the range of neighbors from 3 to 10). This peculiar feature was confirmed by independent observations by Scott [102] who measured the coordinates of 1,000 ball bearings; however he was not able to eliminate wall effects in his experiments.

The ensuing development of computational techniques has enabled the calculation of the geometry of random packings of equal spheres with a higher accuracy in comparison with experiments. The first use of Monte Carlo technique in granular science was by Metropolis [37] who analyzed the pair distribution function (radial distribution function) of two-dimensional system of particles. This approach was later extended to three dimensions by Rosenbluth and Rosenbluth [38]. The first analysis of two-dimensional coordination number distribution was done by Round in 1963 [74], followed by three-dimensional work of Levine and Chernick [128]. In the last paper, it was stated that, though the pattern of a global random bed structure was not distinguishable, the local structure could be clearly characterized by repeating volume unit cells of "polyhedrons created by touching points for each particular sphere".

The other approaches of finding the number of near neighbors were based on a variety of statistical methodologies. The first technique was used by Beresford [114] who studied the probability of readjustments of the random heaps of particles that occur during repeated random relocations of spheres. He observed a reasonable agreement between the probabilities to find a number of near neighbors that he calculated with the experimental results of Bernal and Scott [5, 102].

Using a binomial probability mechanism, Haughey and Beveridge [104] predicted the bell-like dependence of the probability distribution of a local mean voidage (fractional free volume in a local bed region) on the particular coordination number n. The summation of probabilities over all number of contacts provided the dependence of complete local mean distribution versus number of contacts. The dependence of mean voidage probability for different envelope radii ("search radii") was investigated as well.

Another statistical approach was used by Gotoh and Finney [119] who considered the formation of random packings as a combination of the tetrahedrons as the most probable "Voronoi polyhedrons". They also argued that the average coordination number in random packings is 6.0 and then infer the solids fraction packing density from that of the most probable tetrahedron.

Tory [15, 107] observed anisotropy in numerically simulated packings that were directed downwards under gravitational force in a system consisting of 297 equal spheres. The average number of contacts $\bar{N}_C \approx 6.1$ observed in simulations was deviating from at least four spheres in contact with an inner neighbor in experiments. This fact was explained by the creation of holes between spheres in real experiments.

An analysis of a random packing as the mixture of several known regular packings (cubic, orthorhombic, tetragonal-sphenoidal and rhombohedral) was performed by Gotoh [118]. The curve fit of coordination number $\bar{N}_C$ versus solids fraction ν was found to be:

$$\nu \cong 0.1947\bar{N}_C - 0.1301\bar{N}_C{}^2 + 0.05872\bar{N}_C{}^3 - 0.0128\bar{N}_C{}^4 \qquad \textbf{(1.18)}$$

The use of the combination of Monte Carlo simulation and statistical approach allowed Suzuki et. al. [129] to formulate the functional dependence of the number of neighbors with solids fraction as follows:

$$N_C = \frac{2.812}{\varsigma^2(1+\varsigma^2)\sqrt[3]{\nu}} \qquad \textbf{(1.19)}$$

where ς is an indeterminate coefficient which might be found from the derivation of the average inter-particle distance given by Gaussian error function (Erfc):

$$\frac{\bar{r}}{d} = \frac{1}{\sqrt[3]{\nu}} = \frac{1+\varsigma^2}{1+\varsigma \cdot e^{\varsigma^{-2}} \cdot \mathrm{Erfc}(1/\varsigma)} \tag{1.20}$$

The authors also compared the results obtained with those ones obtained by researchers in late 1950's - early 1970's the part of which is represented in Table 1.3 below.

Table 1.3 The functional relationship between the average coordination number $\bar{N}_C$ and solids fraction ν for random packings in the literature.

Author	*Relationship*
Smith [13]	$\bar{N}_C = 26.49 - \frac{10.73}{\nu}$
Rumpf [130]	$\bar{N}_C = \frac{3.1}{1-\nu}$
Meissner [131]	$\bar{N}_C = 2 \cdot e^{2.4\nu}$
Ridgway, Tarbuck [132]	$1-\nu = 1.072 - 0.1193\bar{N}_C + 0.0043\bar{N}_C^{\,2}$
Haughey, Beveridge [104]	$\bar{N}_C = 22.47 - 39.39(1-\nu)$
Nakagaki, Sunada [133]	$\bar{N}_C = 1.61 \cdot (1-\nu)^{-1.48}, \ \nu \geq 0.18$
Gotoh [118]	$\nu \cong 0.1947\bar{N}_C - 0.1301\bar{N}_C^{\,2} + O(\bar{N}_C^{\,3})$
Suzuki [129]	$\bar{N}_C = \frac{2.812}{\sqrt[3]{\nu}\left(1+\left(\frac{b}{d}\right)^2\right)}\left(\frac{d}{b}\right)^2$
Gotoh [119]	$\bar{N}_C = 20.7\nu - 4.35, \ \nu \in [0.47; 0.7]$
Ouchiyama [134]	$\bar{N}_C = \frac{32 \cdot (8\nu - 1)}{13}$
Aste [1]	$\bar{N}_C = 22.54\nu - 6.56, \ \nu \in [0.58; 0.64]$

The probability to have a particular number of contacts (frequency distribution) for a given random distribution of particles was found to possess a symmetrical bell-like silhouette which is depicted in Figure 1.1. The functional dependence is derived from statistical mechanical considerations in [135], this was modeled by considering x touching spheres around a central particle as a "gas" that may freely travel within an effective phase space confined by a solid angle $4\pi(1-\frac{x}{x^*})$, where x^* is the maximum number of contacts for one particle. Upon integration of the statistical free-volume partition function over all possible angular degrees of freedom, the probability or frequency distribution of the number of contacts x was found to be:

$$P(x)=\frac{(4\pi)^x\left(1-\frac{x}{x^*}\right)^x}{\sum_{x=1}^{12}(4\pi)^x\left(1-\frac{x}{x^*}\right)^x} \tag{1.21}$$

where $x^*=12.99$.

The aforementioned frequency distribution has also been validated by a series of experiments [5, 110] and numerical simulations [1, 15, 60, 77, 136, 137], in which a similar distribution was found in cylindrical packed bed [105]. As seen in [108], the average number of contacts for a random structure is 8, which is larger than the value of 6 obtained by Bernal [5]. Such a difference might be intuitively understood since random packings would hold different solids fraction. The shift of the peak of maximum frequency to the left represents the smaller average solids fraction (for instance, $\bar{\nu}=0.607$ [5]) while shift to the right is a peculiarity of packings with higher solids fraction.

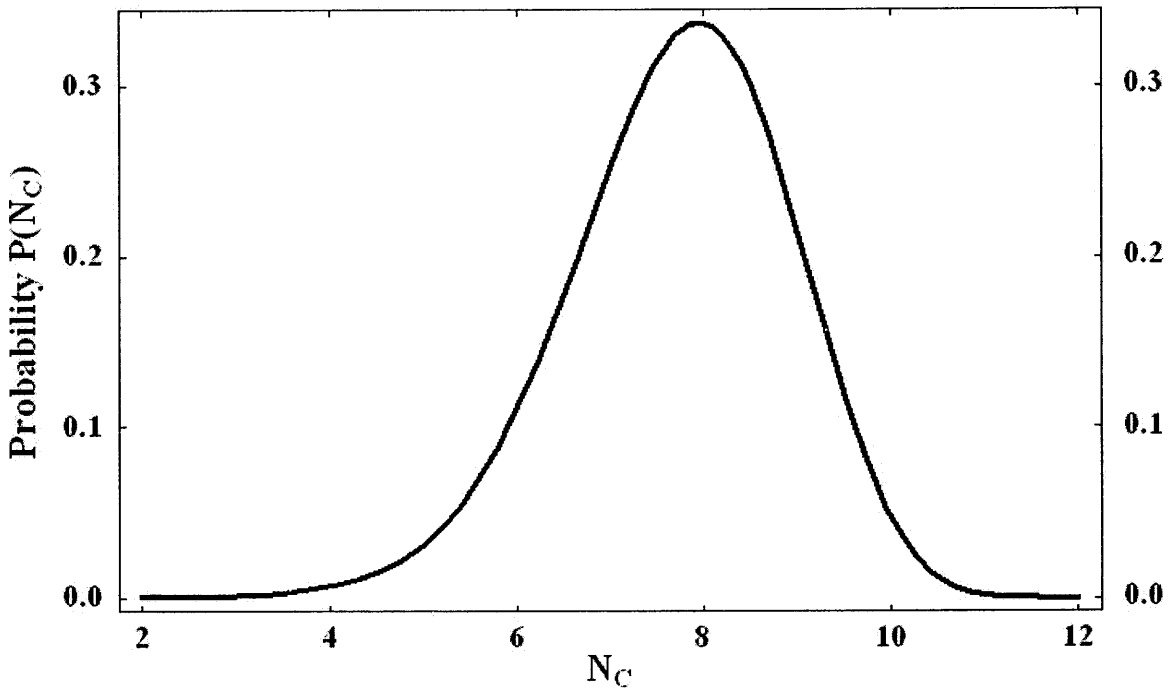

Figure 1.1 Bell-like dependence of the coordination number probability for random configurations

1.3.2 Radial Distribution Function

The radial distribution function (RDF) is the probability of finding one particle center at a given distance r from the center of a considered particle. Thus, the magnitude and position peaks of the radial distribution function may be regarded as a fairly reasonable indication of structured configuration formation.

The radial distribution can be written as

$$g(r) = \frac{n(r)}{4\pi r^2 \Delta r} \tag{1.22}$$

where $n(r)$ is the number of particle centers that are located inside a spherical layer of the thickness Δr and at a distance r from the center of a given sphere.

The radial distribution function is usually normalized by dividing by the bulk density. If ν denotes the bulk solids fraction and V_p the volume of a single particle, then

$$\bar{g}(r) = \frac{V_p}{\nu} g(r) = \frac{\pi d^3}{6\nu} g(r) \tag{1.23}$$

or

$$\bar{g}(x) = \frac{n(x)}{24\nu x^2 \Delta x}, \text{ where } x = \frac{r}{d} \text{ and } \Delta x = \frac{\Delta r}{d} \tag{1.24}$$

This normalization is reasonably useful in view of the fact that $\bar{g}\left(\frac{r}{d}\right) \to 1$, as $\frac{r}{d} \to 1$ as it was first observed by Scott [102]. This universal trait has been established for matter in fluid [138] and gaseous states [139] in contrast to the asymptotic linear behavior of atomic radial distribution functions [140].

This normalization is reasonably useful in view of the fact that $\bar{g}\left(\frac{r}{d}\right) \to 1$, as $\frac{r}{d} \to 1$. (See Scott [102]). This universal trait has been established for matter in fluid [138] and gaseous states [139] in contrast to the asymptotic linear behavior of atomic radial distribution functions [140].

The development of statistical mechanics in the 1930's brought in the recognition of radial distribution function (at that time, molecular pair distribution function [141]) as a very vital parameter of liquid solutions [142]. However, the first experimental analysis of this geometrical quantity for monodisperse granular matter was not done until 1962 by Scott [102], and later independently confirmed by Bernal [101], re-computed by Haughey [104], and summarized by Finney [110]. Bernal [101] noted that the magnitude of first peak, located at $r/d \approx 1.0$, represented the average coordination number. Recent

numerical computations have shown that the radial distribution function near r/d = 1.0 can approximated by power-law singularity [1, 12]

$$\overline{g}(r) \sim \frac{\text{const}}{r^{0.52}} \tag{1.25}$$

The second and third peaks corresponded to radial distances $r \sim d\sqrt{3}$ and $r = 2.0d$. These peaks implied that particles rearranged themselves into a structured order. It was suggested [1, 12] that the peak at $r \sim d\sqrt{3}$ was responsible for two coplanar tetrahedron bases formation while the peak at $r = 2.0d$ stood for the collineation of particles along the line.Later similar results were obtained by Mason who measured the Cartesian coordinates of 1,000 spheres and averaged 25 individual distribution functions of for each group of 25 spheres that were located in the center of the packing. Later these data were computationally analyzed for dense random packings ($\overline{\nu} = 0.637$) by Adams [2]. Similar observations were reported from experiments by Cargill [112] who for Ni-P non-crystalline alloys, subsequently computationally confirmed by Bennet [4]. Granular systems with modest random packings ($\overline{\nu} = 0.607$) were analyzed by Matheson [123].

1.4 Objective

In this dissertation, the effect of discrete taps applied to a vessel of granular material is modeled using two approaches, namely Monte Carlo and discrete element (also known as granular dynamics or dissipative 'molecular' dynamics) simulations, in which the granular material is modeled as uniform (monodisperse) spheres. The main

objective is to identify mechanisms responsible for the increase in density that has been reported in the experimental literature.

The simulation vessel itself consists of a rectangular parallelepiped having periodic boundary conditions in the lateral directions, a plan solid floor and an open top. For the Monte Carlo studies, the macroscopic solids fraction 'evolution' was determined via statistical analyses of ensemble averaged configurations. By applying the discrete Element Method (DEM), an investigation of the effects of the consecutive bumps or taps on the vessel was done in an attempt to establish a connection with the analogous Monte Carlo results. In the discrete element study, a tap to the assembly was done by imposing a half-since displacement to the plane floor for a time duration t_b at a frequency Ω. Further upward propagation of the energy through the system was produced via the inter-particle collisions that were characterized by the "soft sphere Hertzian model".

A systematic examination of geometrical topology of the microstructure of the configurations generated by Monte Carlo simualtions was performed using various local 'measurement' approaches, as well as through the computation of average global quantities, such as the radial distribution function and the coordination number. The results confirmed the formation of a dense configuration in the region adjacent to the floor, which propagated upwards towards the vessel surface as the number of taps increased. The development of the final dense packing of the system was essentially due to the ordered structure formation at bottom of the bed, as well as the rearrangement of spheres within a vessel subject to an external vertical tapping. The results show a possibility of formation of the configurations with a relatively higher solids fraction in comparison with those ones published previously in the literature. Both simulation

studies provided a clear picture of the dynamical process responsible for density relaxation, namely the upward progression of self-organized layers induced by the plane floor as the taps evolve. Its occurrence in both the MC and DMD simulations strongly suggests the universality of this mechanism in density relaxation.

1.5 Dissertation Outline

The remainder of this dissertation is organized as follows. Chapter 2 describes the Monte Carlo simulation method and how it is applied. Chapter 3 presents the results of Monte Carlo simulation with a detailed analysis of solids fraction and microstructure. Chapter 4 describes modifications that were made to an existing discrete element code in order to investigate the evolution of the solids fraction. Chapter 5 presents the results of the study of the microstructure propagation using the data from the Monte Carlo and Discrete Element simulations. Finally, Chapter 6 contains the conclusions and recommendations for further work.

CHAPTER 2

THE METHODOLOGY OF MONTE CARLO SIMULATION

2.1 Background

In 1946, Polish born mathematician Stanislaw Ulam developed a new computational technique which "solves the problem by generating suitable random numbers and observing that fraction of the numbers obeying some property or properties". Working with John von Neumann and Nicholas Metropolis, he further elaborated algorithms for computer implementations, as well as exploring means of transforming non-random problems into random forms that would facilitate their solution via statistical sampling. This new technique was given the name Monte Carlo by Metropolis as a reference to the world-known famous casino in Monaco [37].

Today Monte Carlo methods are exceptionally important in mathematics, computational physics [143], physical chemistry [144, 145], economics, and related applied fields. They are handy for the simulation of phenomena with a large number of coupled degrees of freedom [146], such as strongly coupled solids [147], liquids, and disordered materials (for instance granular particles), stochastic risk modeling, and integral differential equations of heat transfer. In granular science, the Monte Carlo technique is recognized for its role to imitate the compaction of granular solids. The Monte Carlo method is unlike molecular dynamics (MD) simulation in that it is stochastic in nature as opposed to the use of Newton's equations of motion in MD simulations governed by intermolecular forces.

2.2 Overview

The Monte Carlo code used in this dissertation utilizes the hard sphere models with the implementation of the Metropolis algorithm [37]. The basic of idea was taken from the early work on segregation using Monte Carlo modeling [35]. For the purpose of this dissertation, a new MC was written, that incorporates contact detection using the 'chaining-cell' method [148], as well as various criteria to determine completion to an equilibrium configuration. Analyses of the solids fraction and microstructure were performed using embedded subroutines and post-processing subroutines. The reader is referred to Appendix A for the details of these codes.

The Monte Carlo simulation is arranged as follows (See Figure 2.1):

0. Read the input file, initialize simulation parameters.
1. Assign particle positions (the code creates random poured assembly unless the computation is the continuation of previous simulation run).
2. Apply Metropolis algorithm which enables a series of random downward displacements of a single particle at a time (Monte Carlo Step).
3. Save coordinates of all particles for intermediate configuration and compute solids fraction for every million Monte Carlo steps. If the difference between two consecutive million Monte Carlo steps is less than 10^{-3} then terminate the Metropolis algorithm.

$$\left|\nu_{N+10^6} - \nu_N\right| \leq 0.001 \qquad \textbf{(2.1)}$$

4. Induce vertical tapping to the system (linear upward change of vertical coordinates).

5. Repeat from step 3. One tap corresponds to the red, green and blue arrows from Figure 2.1.
6. One realization is the simulation complete.
7. Statistical analysis of physical and geometrical properties for one case study is results from of the averaging over many realizations for the same set of paramteters.

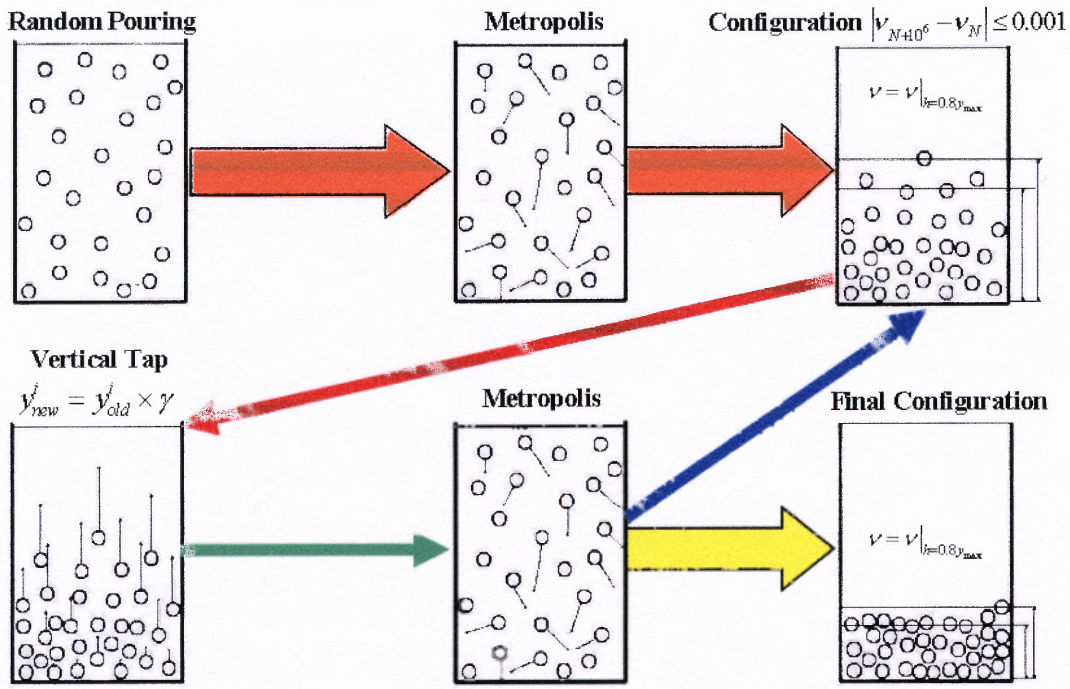

Figure 2.1 Scheme of Monte Carlo Methodology.

Hence, the Monte Carlo simulation has a strict hierarchy. The lowest element is a *Monte Carlo step* (random displacement of one particle at a time). A series of 15-20 million Monte Carlo steps restricted by criterion (2.1) completes one *tap*. Third hierarchical component is a *realization* which requires at least a few hundred to several

thousand taps to achieve equilibrium state for parameters considered in this dissertation. The top ladder of hierarchy is the *case* which is acquired when equilibrium state is achieved (supported by statistical averaging over a number of realizations which usually varies from 100 to 150 in this dissertation).

The flow chart of the FORTRAN subroutines is depicted on Figure 2.2.

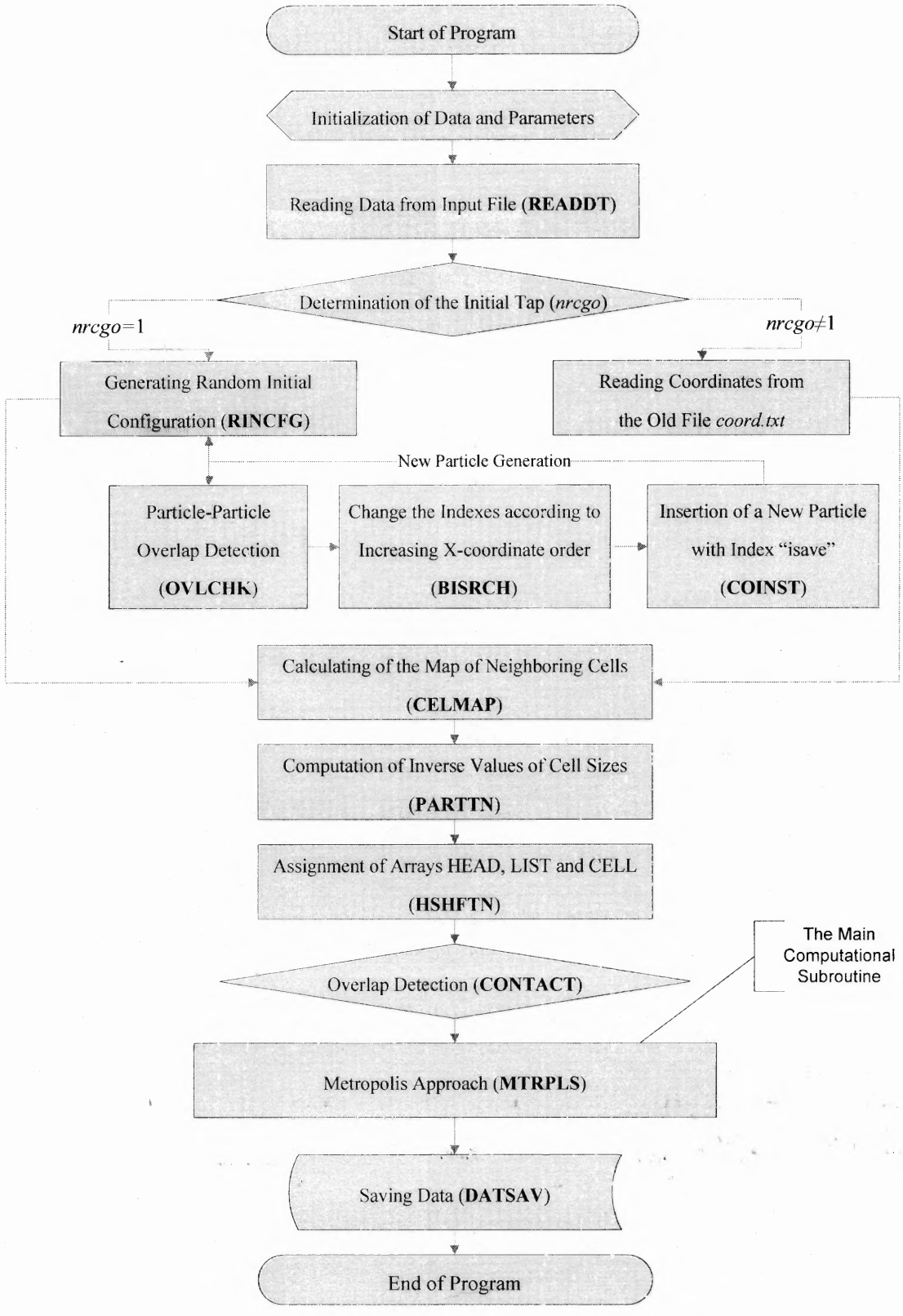

Figure 2.2 Flow Chart of the Monte Carlo Simulation.

The Monte Carlo program is structured by the main subroutine *mtcl1.f* which unites all other subroutines together. At the outset, the code initializes constants and parameters and opens old text files and generates new ones. Then, subroutine *READDT.f* reads data (the geometrical dimensions of a computational vessel, physical properties of particles, and global simulation parameters) from the input file *input.dat.* (A sample input file is shown in Appendix D). Note that all subroutines are described in Section 2.3 below). If specified in the input file (initial tap *nrcgo* $\neq$ 1) that the simulation is a restart of a previous run, then the coordinates of particles are read from the old file *coord.txt* that must be located in the same directory folder as the executable and the input files.

If the input file indicates that the simulation is a new one (*nrcgo* = 1) then a random initial configuration of particle center positions for all particles is generated by a subroutine *RINCFG.f.* Center coordinates of the particles are uniformly and randomly distributed within the computational box of given size. Note that the mechanism of initial contact detection and automatic application of periodic and hard boundaries is embedded in the code in all computational subroutines. The computational domain typically consists of a parallelepiped of dimensions $12d \times 24d \times 12d$ (d is the diameter of the sphere), with periodic boundaries in lateral directions (i.e. x and z directions). Further information about geometric sizes of the system of particles is given in Section 2.4. In addition, subroutine *RINCFG.f* calls in three supplementary subroutines *OVLCHK.f, BISRCH.f* and *COINST.f.* The subroutine *OVLCHK.f* carries out an overlap detection to ensure that a newly inserted (or trial) particle does not overlap existing ones. The penetration between two spheres takes place if the distance between their centers is less than the diameter of particle, d. If an overlap is found, then a new trial position for this particle is generated

until this particle does not overlap with particles or walls (in case of hard boundaries). The subroutines *BISRCH.f* and *COINST.f* determines the location of the trial particle according to an increasing order of x-coordinates of existing particles, and assigns the index of a new particle according to aforementioned order. The subroutine RAND (an embedded FORTRAN routine) is used to generate the random numbers. This routine was successfully tested by examining known problems of the random walk mean squared displacement and generation of number π using different integrating methods.

After the initial positions of the particles have been determined, subroutine *CELMAP.f* is called. The purpose of this subroutine is to store array *map* - a block of 27 memory locations, each containing the index of the neighboring cells of the cell having index (*imap*+27). Here, the term 'cell' refers to a single element of the partition of the computational box, i.e., the box is partitioned into cells. The subroutine *CELMAP.f* also accounts for boundary conditions of the box taken from subroutine *READDT.f*. If the floor, top, or rigid walls in x and z directions are specified, then the memory locations containing indexes of geometrically forbidden cells are assigned to the flag (*-99*). This flag will be frequently used in subsequent overlap detection subroutines *CONTACT.f* and *CNTMDF.f,* and this results in substantial decrease of computation time.

Subroutine *PARTTN.f* calculates and returns inverse values of cell sizes (for instance, *cellix*) using input parameters from subroutine *READDT.f*. If the edge length is too small, it is recomputed based on shortest allowable edge length. That is, the code calculates edge length based on the shortest dimension of the box, and then it scales the other sides so that there are an equal number of cells in each direction. It could be extended for the procedure of auto-calculation of *mdiv* by choosing a trial value for *mp*

based on maximum storage. In this case, the edge lengths are calculated based on this value. To reduce the computation time, the dependence of CPU time on the number of cells *mdiv* was analyzed, the results of which can be found in Appendix E. In addition, optimal parameters *mdiv* were found for various sizes of system (number of particles *np*).

The most time-consuming computational process of the Monte Carlo program is the overlap detection between two particles. To check that the central distances of all pairs of particles in the system are greater than diameter of particle takes at least $\frac{1}{2}np^2$ computational operations. A very powerful technique used to reduce CPU time is called the chain-cell search method [148]. The main idea of this method is to carry out overlap detection for a given particle with the particles that are located in the same cell as this particle, as well as with all the particles in the 27 neighboring cells. The heart of the chain-cell method appears in subroutine *CELMAP.f* when each cell is assigned to a 'map' of neighboring cells by using array *map*. Then, subroutine *HSHFTN.f* initializes arrays *HEAD*, *CELL* and *LIST*. Firstly, *HSHFTN.f* checks that all particle centers are positioned within the limits of the computational cell. If it is not the case then the subroutine calls error exit from the main code indicating the reason for the error. Afterwards, all the particles in the system are assigned to the cell corresponding to their center coordinates using hashing function *ICELLT*. Thus, the subroutine *HSHFTN.f* returns three arrays *HEAD*, *LIST* and *CELL* into the main code *mtcl1.f*. Details about the chain-cell search method may be found in Section 2.5.

Using arrays *HEAD*, *LIST* and *CELL* from chained-cells, an overlap detection routine *CONTACT.f* ensures that none of all particles in the system are overlapping each other or a boundary before the simulation starts. Subroutine *CONTACT.f* will return the

flag *ier* = 0 unless central distance between all the pairs of particles is less than diameter of particles; it this occurs, then *ier* is equal to -11, indicating a forbidden overlap of particles.

The core of the program, "Metropolis algorithm", is enclosed in the subroutine *MTRPLS.f*. This subroutine simulates the random displacement of one random trial particle at a time within a spherical neighborhood of diameter delta δ, checks overlap of a trial particle with neighboring particles and boundaries, and applies the Metropolis probabilistic approach to vertical displacement of a trial particle. To decrease computation time, *MTRPLS.f* contains several optimization criteria, which did not cause any significant statistical differences in the solids fraction results. More information about subroutine *MTRPLS.f* is given in Section 2.6. Besides Metropolis algorithm itself *MTRPLS.f* includes auxiliary subroutines *CNTMDF.f*, *CHANGE.f*, *GRAVPL.f*, *PACKPL.f*, *NEWCFG.f* and *DATSAV.f*.

CNTMDF.f checks the likelihood that one randomly selected particle with new trial coordinates *xmnew*, *ymnew*, *zmnew* and index "*imove*" will overlap with any of the particles in a new trial cell and any of the particles within its neighboring cells. To achieve this goal *CNTMDF.f* calls in the supplementary subroutine *CHANGE.f* which creates new modified arrays *CELLP*, *LISTP* and *HEADP* that symbolize a trial position of particle "imove". The forementioned modified arrays will become new arrays *CELL*, *LIST*, *HEAD* unless it is found that the trial displacement of this particle is forbidden due to the overlap with other particles. We remark that the designation of *CNTMDF.f* is completely different from that is used in previous overlap subroutines *OVLCHK.f* and *CONTACT.f* in view of the fact that during construction of the random initial

configuration, the routine *OVLCHK.f* verifies the permissible allocation of one new particle and existing ones (which might be less than the maximum number of particles in the system *np*), while *CONTACT.f* ensures that central distance between all the pairs of particles is greater than diameter of particles. Subroutine *GRAVPL.f* computes the total gravitational potential of the system of all particles for given vertical coordinates, density, and diameter of particles. Subroutine *NEWCFG.f* is responsible for the application of external disturbances to the system of particles. In this dissertation 'linear' and 'uniform lift' taps were used; however it is possible to apply other types of disturbances to the system in order to increases it potential energy. The reader is referred to Section 2.7 for detailed information about the vertical taps used in the simulations. Subroutine *PACKPL.f* is called to compute the bulk solids fraction of the current configuration. (See Section 2.9 for details). Lastly, after each tap, subroutine *DATSAV.f* writes the solids fraction for this particular tap into a file *pack.txt* and updates the file *coord.txt* with current coordinates of all particles so as to enable easy restarting of the code from the last tap if necessary. After the desired number of taps has been completed, *MTRPLS.f* is halted, and control is returned to the main code. At this point, *CONTACT.f* verifies that there are no forbidden overlaps of the particles in the final configuration.

For the sake of completeness, the two post-processing programs should be mentioned: microstructure analysis and study of solids fraction statistics. These programs are independent of *mtcl1.f* subroutine albeit they post-process output files *pack.txt* and *coord.txt* produced by Monte Carlo code.

Characterization of the global microstructure is facilitated by computations of the radial distribution function (*RADDST.f*), the coordination number (*CRDNMB.f*) and

fabric tensor (*FABRIC.f*). The reader is referred to Section 2.10 for more information about these quantities. It is noted that it is possible to also determine the Voronoi structure of the system from which dihedral and solid angular contact distributions can be obtained. The sample of FORTRAN file *ave.f* which endows with statistics of solids fraction is shown in Appendix K.

The remaining Sections of Chapter 2 are arranged in following order: Section 2.3 Description of Subroutines, 2.4 Geometry of System, 2.5 - Chain-Cell Method, 2.6 - Metropolis Algorithm, 2.7 - Vertical Tapping, 2.8 - Equilibrium Bulk Solids Fraction, 2.9 - Solids Fraction and lastly 2.10 - Microstructure Analysis.

2.3 Description of Subroutines

The following subroutines are the building blocks for the Monte Carlo code and post-processing programs.

- *ave.f*

  ave.f post-processes an evaluation of the average and the standard deviation of solids fraction from output files *pack.txt* for many realizations.

- *BISRCH.f*

  BISRCH.f finds the place for a new particle in *RINCFG.f* according to increasing order of x-coordinate (part of *RINCFG.f*).

- *CELMAP.f*

  CELMAP.f creates a map of neighboring cells.

- *CHANGE.f*

  CHANGE.f is used to assign tryout arrays *CELLP*, *HEADP* and *LISTP* for overlap detection *CNTMDF.f*.

- *CNTMDF.f*

  CNTMDF.f produces overlap detection during Metropolis displacement.

- *COINST.f*

  COINST.f inserts a trial particle into a position defined by *BISRCH.f* (part of *RINCFG.f*).

- *CONTACT.f*

  CONTACT.f ensures that none of two particle pairs overlap each other.

- *CRDNMB.f*

  CRDNMB.f computes the number of spheres in contact with a given particle (part of microstructure analysis).

- *DATSAV.f*

  DATSAV.f stores solids fraction in output file *pack.txt* and coordinates of all particles in *coord.txt* after each Metropolis tap.

- *FABRIC.f*

  FABRIC.f computes the average fabric tensor for all particles in the system (part of microstructure analysis).

- *GRAVPL.f*

  GRAVPL.f evaluates the total gravitational potential of the system.

- *HSHFTN.f*

  HSHFTN.f assigns array *HEAD* for all cells and arrays *CELL* and *LIST* for all spheres in the system.

- *mtcl1.f*

  mtcl1.f is the main code of Monte Carlo program, unites all subroutines together.

- *MTRPLS.f*

MTRPLS.f simulates a specified number of taps, each of them consists a number of Monte Carlo steps (random displacement of one particle at a time) that correspond to restricting criteria.

- *NEWCFG.f*

  NEWCFG.f recalculates vertical coordinates of all particles i.e. performs the vertical iifting.

- *OVLCHK.f*

  OVLCHK.f confirms the permissible allocation of one new particle and existing ones (part of *RINCFG.f*).

- *PACKPL.f*

  PACKPL.f computes bulk solids fraction.

- *PARTTN.f*

  PARTTN.f is used to calculate inverse values of cell sizes.

- *RADDST.f*

  RADDST.f is employed to find radial distribution function (part of microstructure analysis).

- *READDT.f*

  READDT.f reads incoming data from *input.dat* file.

- *RINCFG.f*

  RINCFG.f creates random initial configuration of particles.

2.4 System Geometry

The density relaxation process occurs as a result of a series of discrete taps applied to a 'box' containing N_p spherical particles of diameter d. The computational domain (i.e. the

'box') is a rectangular parallelepiped having periodic boundary conditions in the lateral direction, which is denoted here as x and z. The box has a rigid square base ($12d$ x $12d$) floor that does not allow particles to drop below the bottom, or mathematically saying the vertical position of the particle can never be less than the radius of a sphere. At the top the box isn't constrained by a physical "roof". The vertical size of the box ($24d$) is chosen to optimize CPU time. Two typical geometrical configurations is represented on Figure 2.7. The first arrangement is obtained by a random deposition in all coordinates of the number of particles (N_p) into a box with aforementioned sizes. The second configuration is obtained by allowing particles to fall downwards under the gravity which is performed by Metropolis Algorithm that is described later in Section 2.6. The simulation results for this particular system size are given in the Chapter 3.

The analysis of larger and smaller systems with square-base floor is provided in the Chapter 5. Higher systems ($36d$ and $48d$) with the same floor size ($12d$ x $12d$) were taken to observe the effect of the flat bottom that is responsible for the formation of ordered configuration at the lower layers. The Monte Carlo Simulation was also extended to the systems with a floor size ($10d$ x $10d$). The Discrete Element Method study was performed only for the rectangular vessel with the base of ($12d$ x $12d$) and a series of aspect ratios of the height to the base size.

2.5 Chain-Cell Method

The most important part of the current Monte Carlo technique is the contact detection subroutine, since the particles of the system are considered to be hard spheres. The hard

spheres cannot overlap; i.e. the distance between the centers of two particles is always greater or equal to the diameter of a sphere. Contact detection is performed by three subroutines that check the mutual geometrical position of each pair of particles.

Regardless of the simplicity of the detection subroutine, the overlap check becomes very computationally expensive if the contact check has to be performed for each possible pair of particles. Simple analysis shows that this routine requires about N_p^2 computations (~10^6 contact checks) per each Monte Carlo step. In general one realization from a computational study consists of the billions of accepted Monte Carlo steps; as a result, the completion of even one simulation becomes very computationally expensive thereby indicating the importance of the use of some auxiliary technique.

The chain cell method implemented into this Monte Carlo code was first proposed by Allen and Tildesley in [149]. The main idea is to impose a grid of cells of a given dimension on the geometrical configuration, determine the initial positions, and keep permanent track of all the particles by assigning arrays *HEAD*, *LIST* and *CELL*. Thus, for each particle the subroutine finds the indexes of all the neighboring particles in the cell where it is located as well as of all the particles in the neighboring cells. The neighboring cells are preliminarily arranged by array *MAP* by taking into account boundary (periodic or hard wall) conditions. Qualitative analysis shows that when using this method, the contact detection subroutine requires approximately N_p^2/N_c operations where N_p is the number of particles and N_c is the total number of cells.

The comparative analysis of the dependence of CPU time usage on the number of cells N_c is given in Appendix E. Detailed information about the chain cell method can be found in [148].

2.6 Metropolis Algorithm

The simulation is initiated by randomly placing within the box N spheres that are subsequently allowed to collapse vertically under gravity to generate a configuration corresponding to a loose ('poured') assembly. The spheres are 'hard'; that is, in order to avoid overlap of the spheres, for each $i \neq j$, the distance $|\vec{r}_i - \vec{r}_j|$ between the centers $\vec{r}_i = (x_i, y_i, z_i)$ and $\vec{r}_j = (x_j, y_j, z_j)$ of particles is always greater than $d + \varepsilon$, where $\varepsilon = 10^{-4} d$. The Metropolis [37] algorithm is then used to advance the system to a stable configuration. A single Monte Carlo (MC) step in the Metropolis algorithm consists of the random selection of a particle (x_i, y_i, z_i), followed by its assignment to a trial position in accordance to the prescription,

$$\begin{cases} x_i' = x_i + \delta(1 - 2\xi_x) \\ y_i' = y_i + \delta(1 - 2\xi_y) \\ z_i' = z_i + \delta(1 - 2\xi_z) \end{cases} \tag{2.2}$$

Here, ξ_x, ξ_y, ξ_z are random numbers sampled from a uniform distribution on [0,1], and δ is the maximum allowed displacement. The trial position is accepted unconditionally as the new center coordinate if the change in the system potential energy is negative, i.e., $\Delta E \equiv mg \sum_{i=1}^{N} (y_i' - y_i) < 0$. Otherwise, $(\Delta E \geq 0)$ the trial position is accepted with probability $e^{-\beta \Delta E}$. For the macroscopic particles that we are studying, β is very large [35] so that for all practical purposes, only downward displacements are allowed. Another particle is then selected at random, and this procedure is repeated.

As the process described above advances through many hundreds of MC steps, the space between adjacent particles is reduced and the bulk density increases. If the

maximum allowed displacement δ were set to a small fixed value $\delta/d << 1$ at the outset, the evolution of the system to a local equilibrium would be prohibitively slow. The situation would be the same if $\delta/d \sim 1$, since the percentage of accepted steps would be drastically reduced as the system density increases. In order to prevent this from taking place, we dynamically change δ from a maximum value $\delta = d$ at the beginning of the process to a minimum $\delta = 10^{-3} d$ by monitoring the accepted fraction of steps every 10^4 MC steps. If more than half of the MC steps have been accepted, δ remains unchanged; otherwise δ is modified as follows: $\delta' = 0.995\delta$. While other algorithms in the literature may be more computationally efficient [150, 151], this approach has a great deal of virtue in its simplicity.

The change in the bulk solids fraction is computed every one million MC steps and the Metropolis algorithm is terminated when

$$\left|\nu(n;\gamma) - \nu(n-10^6;\gamma)\right| < 0.001 \qquad \textbf{(2.3)}$$

where $\nu(n;\gamma)$ is the bulk solids fraction at number of Monte Carlo steps n and lift intensity γ. To ensure that this stopping criterion did not cause premature termination, in many test runs we required the criterion in Equation 2.3 to be satisfied twice before ending the process. In none of these instances was a premature termination observed, allowing us to satisfy Equation 2.3 only once for many of the results presented below. In all of the case studies reported in this dissertation, the initial random assembly collapsed to a loose configuration having a bulk solids fraction in the range 0.56 to 0.58. In general, the poured assemblies filled the box to a height $H/d \cong 11$. The detailed flow chart of Metropolis algorithm is shown on Figure 2.6.

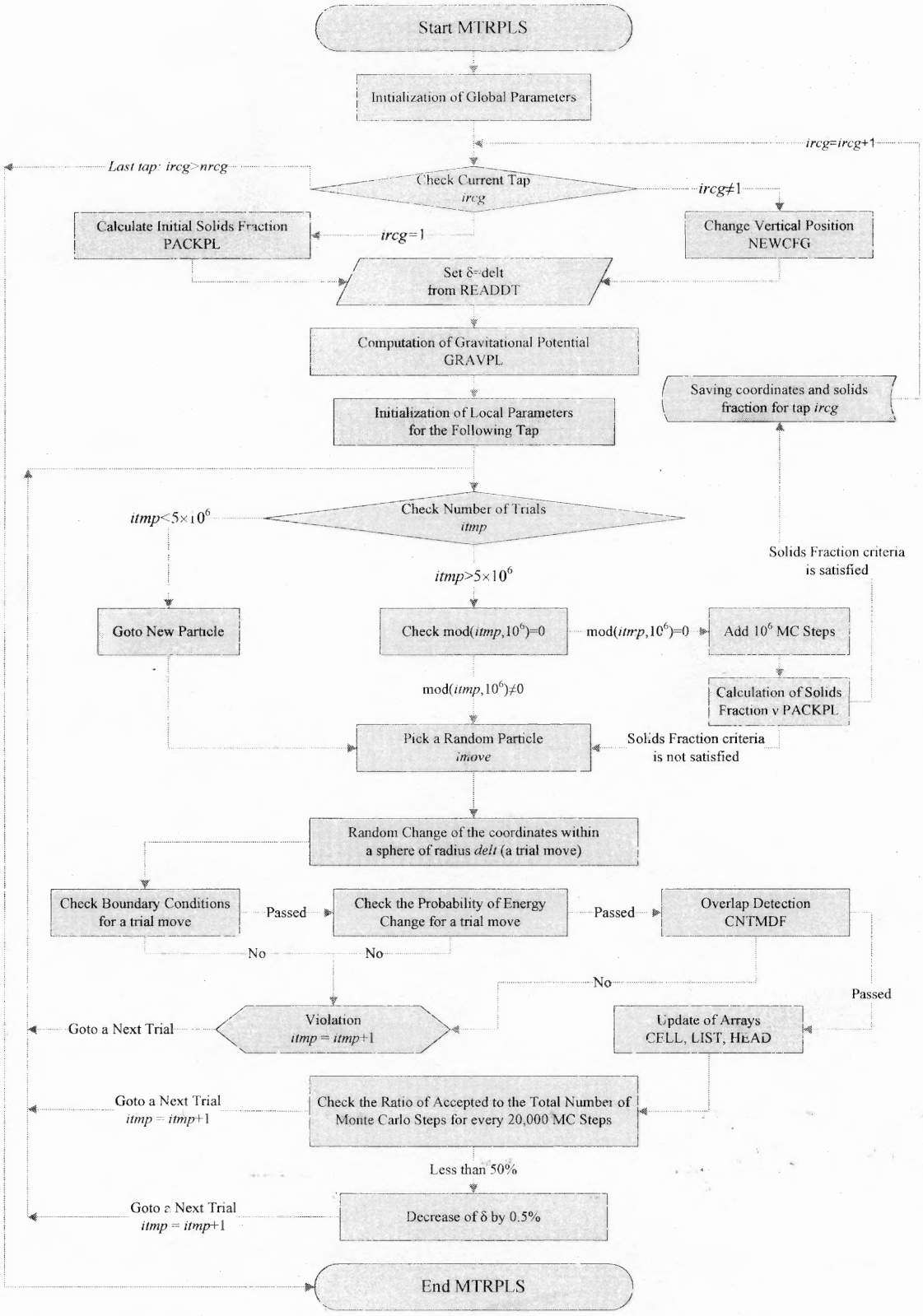

Figure 2.3 Flow Chart of the Metropolis Subroutine (**MTRPLS**).

2.7 Vertical Tapping

The poured assembly is dislodged from its local energy minimum by applying vertical position dependent displacements to each particle in accordance to

$$y_i^{new} = y_i^{old} \times \gamma . \tag{2.4}$$

The factor γ represents the effect of a single tap so that in a qualitative sense, a greater impulse applied to the container corresponds to a larger value of γ. We remark that the form Equation 2.4 for vertical displacements is equivalent to that used by Barker and Mehta [40], who also imposed random lateral displacements on the particles at each tap. The influence of applying this additional lateral displacement on the equilibrium solids fraction is considered later in this dissertation. After expanding the vertical coordinates using (2.4), the system is allowed to settle using the Metropolis algorithm as described in the previous section. Satisfaction of the stopping criterion (Equation 2.3) to signal completion of a single 'tap' applied to the system typically required 17 to 20 million MC steps (~ 40 CPU seconds on our computers). Figure 2.4 shows a sequence of configurations, starting from the initial random placement, the 'poured assembly', its expansion via a single tap (2.4), and its state in accordance with the criterion (2.3).

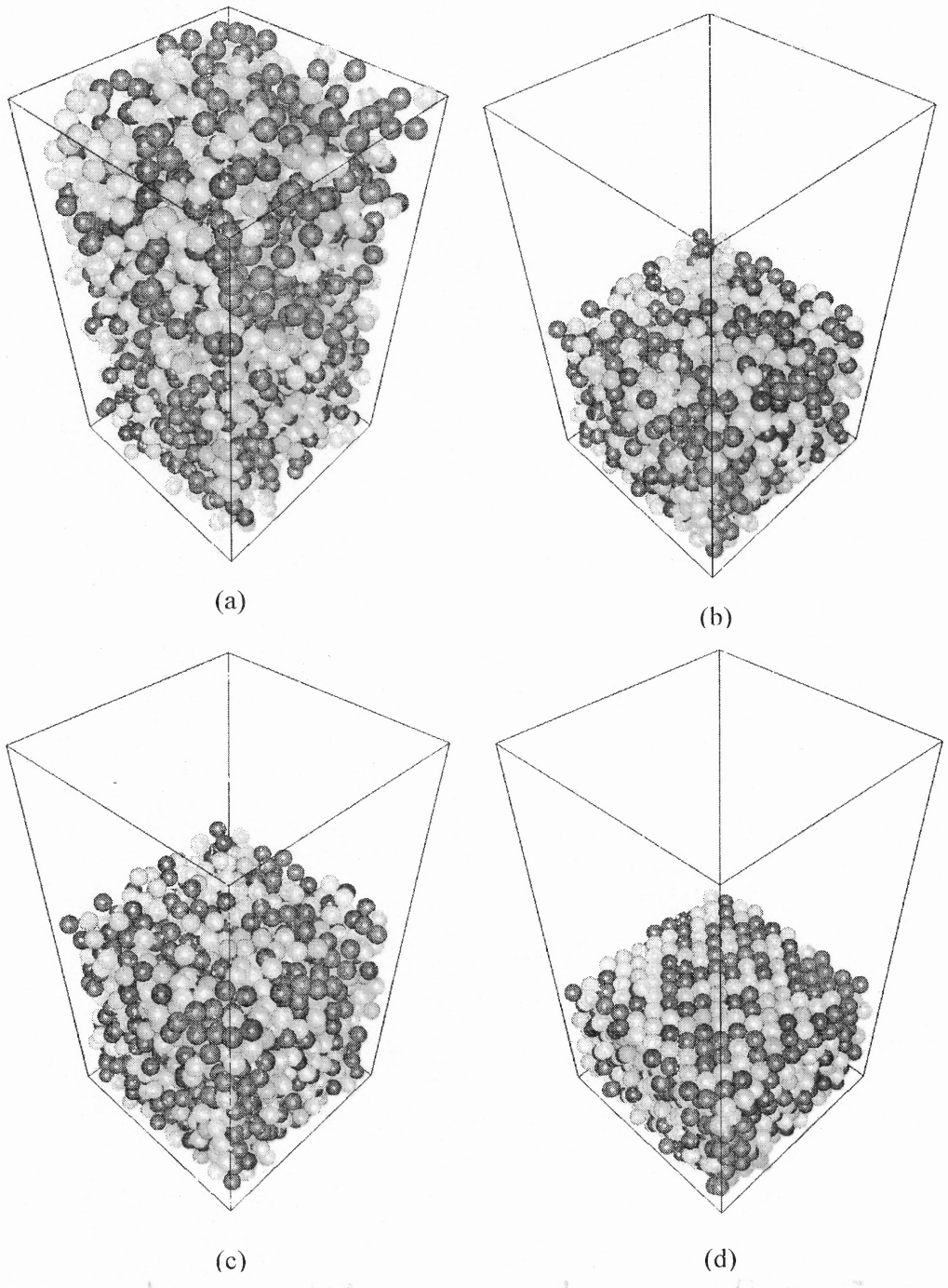

Figure 2.4 Snapshots of system: (a) Initial random configuration, (b) Poured assembly (ν=0.568), (c) Configuration after applying one tap, and (d) Final configuration at 1000 taps. Note that particles are shaded only for the purpose of visualization.

2.8 Equilibrium Bulk Solids Fraction

A tapping cycle is initiated with the poured particle assembly as described in previous Section 2.6. A single experiment (or realization) consists of a sequence of individual taps (Section 2.7). As used here and henceforth, the term 'tap' refers to the expansion by Equation 2.4, and subsequent relaxation. Each realization is carried out using a fixed lift intensity γ; the total number of taps to obtain equilibrium depends on γ. For smaller values of γ, more taps are needed to reach an equilibrium solids fraction, which is intuitively reasonable since each such tap is less effective in rearranging the locations of the particles. However, as will be seen later, our results suggest that there is a value of γ that optimizes the evolution of the system to equilibrium. Typical plots of bulk solids fraction against the number of taps N_T are shown in Figure 2.5 for two different realizations at $\gamma = 1.25$. The graphs exhibit an overall increase in the solids fraction with the number of taps, a general trend that was evident in all realizations. The convergence to the equilibrium configuration also exhibited dependence upon the choice of γ, which will be demonstrated in subsequent figures.

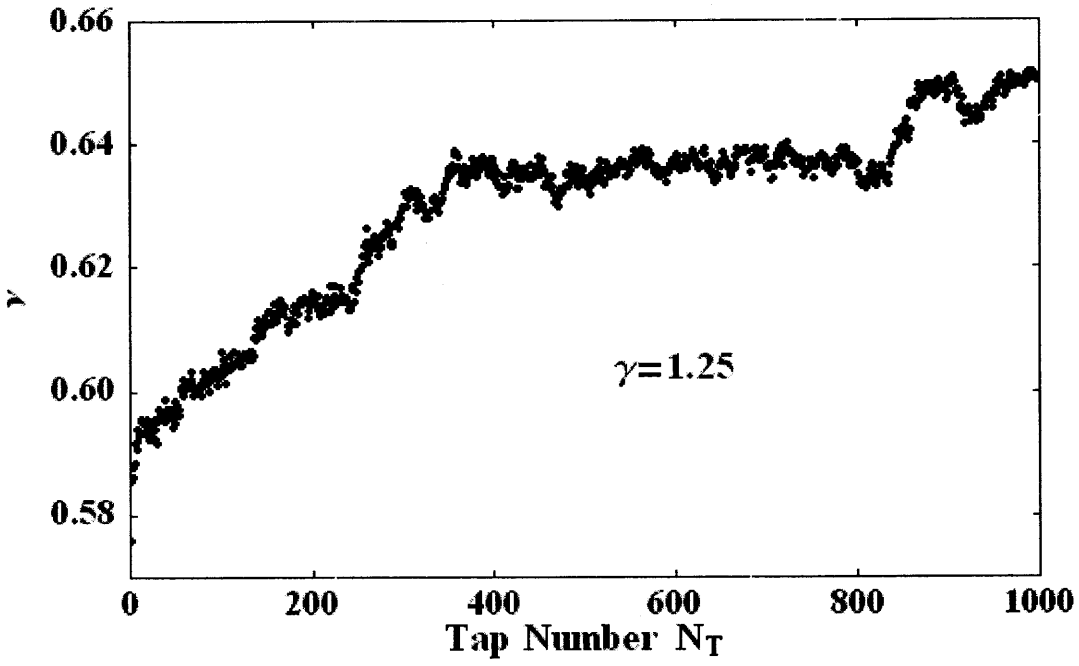

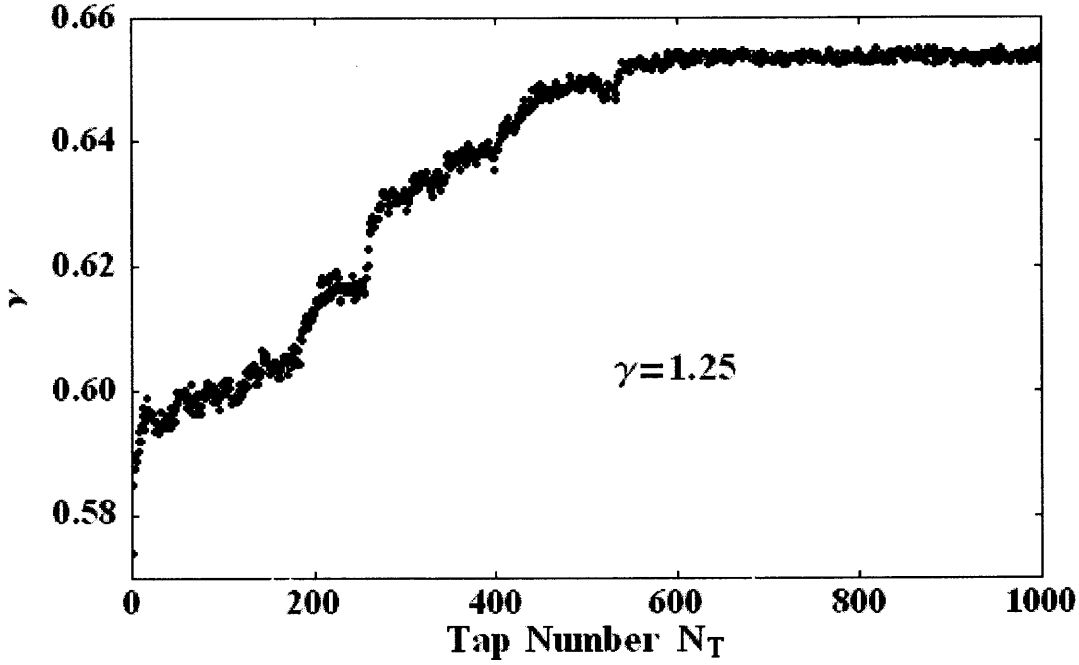

Figure 2.5 Bulk solids fraction ν versus tap number N_T for two independent realizations at tap intensity $\gamma = 1.25$. These plots show the typical evolution of the system.

The ensemble averaged bulk solids fraction $\langle \nu(n;\gamma) \rangle$ was computed over M realizations. In order to identify the minimum number of realizations M so that a statistically correct equilibrium value was obtained, the standard deviation $\langle \sigma(n;\gamma) \rangle$ as a function of the tap number n was determined as

$$\langle \sigma(n;\gamma) \rangle^2 = \frac{1}{M} \sum_{k=1}^{M} \left[\nu_k(n;\gamma) - \langle \nu(n;\gamma) \rangle \right]^2 \tag{2.5}$$

where

$$\langle \nu(n;\gamma) \rangle = \frac{1}{M} \sum_{k=1}^{M} \nu_k(n;\gamma) \tag{2.6}$$

The behavior of $\langle \sigma(n;\gamma) \rangle$ was monitored by increasing the number of realizations M until, over a sufficient number of taps N_T,

$$\langle \sigma(N_T;\gamma) \rangle \quad < 0.001 \tag{2.7}$$

which essentially defines equilibrium in the simulations. The behavior of the standard deviation $\langle \sigma(N_T;1.25) \rangle$ depicted in Figure 2.6 demonstrates that criterion (2.7) is reached when of $N_T \sim 800$ for this value of γ. The ensemble averaged solids fraction as a function of M is shown in Figure 2.7 for the same case when $N_T = 1000$. The vertical lines in the figure denote error bars in the ensemble averaged solids fraction. In general, it was found that $M \cong 100$ realizations were adequate to satisfy the criterion in

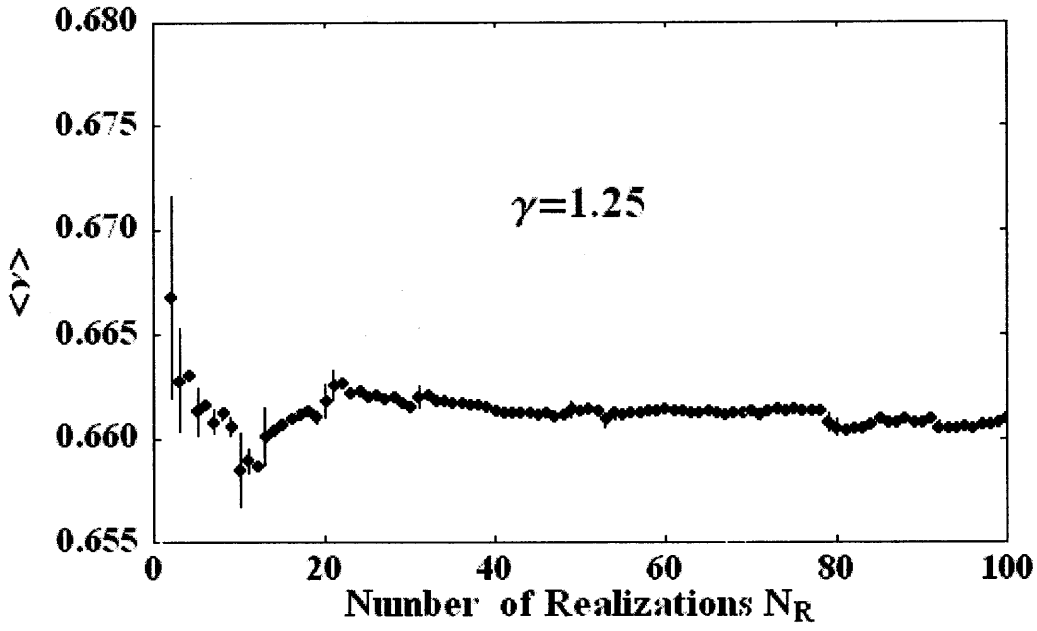

Figure 2.6 Standard deviation of the bulk solids fraction $\langle \sigma(n;\gamma) \rangle$ versus tap number N_T at tap intensity $\gamma = 1.25$ for 100 realizations. This demonstrates the convergence properties of the methodology.

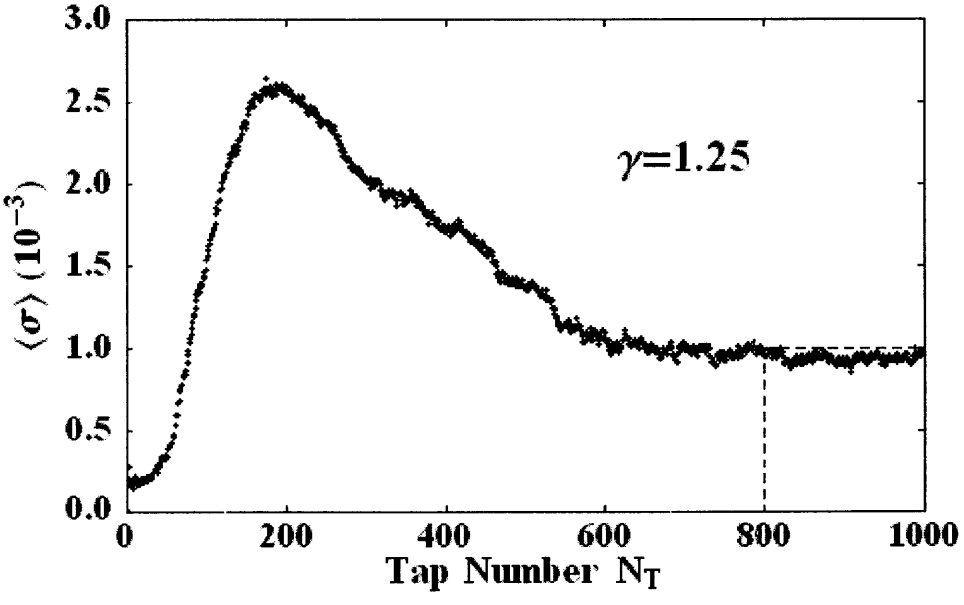

Figure 2.7 Dependence of the ensembled-averaged bulk solids fraction $\langle \nu(1000;\gamma) \rangle$ on the number of realizations at tap intensity $\gamma = 1.25$ to exhibit the sensitivity of the system to the ensemble size. The vertical lines through the points are error bars.

2.9 Computation of Solids Fraction

The solids fraction is defined as the volume ratio of solid particles to the total volume within which the particles are enclosed. The complete description of four different approaches used to define the structural and evolutional behavior of the solids fraction of the granular matter is incorporated in this section. Figure 2.8-2.8 show all the possible segmentations of the spheres by a sampling layer. The geometric conditions of these segmentations are classified depending on the locations of the particle centers. For each classification, the exact formula to determine the contributions to the volume that is occupied by the spheres inside a sample layer are tabulated in the Table 2.1.

The first technique (named "low eighty") involves the computation of the total volume of particle segments for the lower 80% of the height of the granular stack. The elimination of the volumes of the particles from the top was performed to avoid the "top effect" that is responsible for the random loose rearrangement of the particles on the top of the stack. This technique was embedded into the code as a subroutine *PACKFR.f* that was called after the last Monte Carlo step for each discrete tap. The outcome of the computation was the solids fraction ν that was stored in output data file *pack.txt*. Afterward the evolution of solids fraction $\langle\nu\rangle$ versus tap number was provided by the statistical analysis of the solids fraction averaged over the ensemble of discrete realizations for each individual tap. The details of this analysis are provided in Chapter 3. It is clear that for the "low eighty" approach the total volume of spheres below the top 20% of the stack could be determined by the summation of the contributions of the spheres that are prescribed in these three cases: spherical center lies *above* the layer top

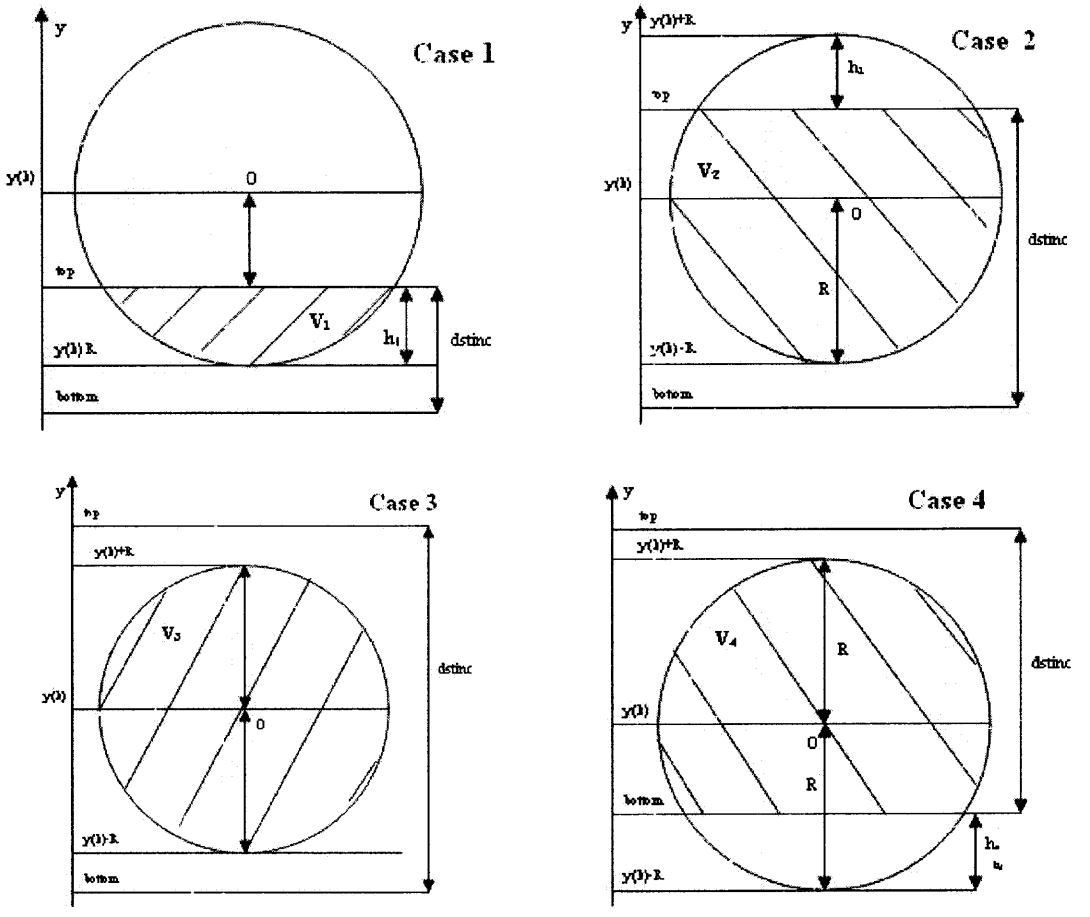

Figure 2.8 The volume occupied computation by the spheres inside a sample layer: case 1 – spherical center lies *above* the layer top, case 2 – spherical center is located *below* the layer top, but the spherical bottom is situated *above* the layer bottom, case 3 - sphere is *entirely inside* the layer, case 4 – spherical center is positioned *below* the layer top and *above* the layer bottom, while the spherical bottom is *below* the layer bottom.

(case 1), spherical center is located *below* the layer top, but the spherical bottom is situated *above* the layer bottom (case 2), and sphere is *entirely inside* the layer.

The second solids fraction approach used was so-called "slice method", which produces the profile of the solids fraction along the height of the packing. This vertical

distribution of the solids fraction in the vertical vessel is computed by summation of the volume of the pieces of spheres within layers or slices to the volume of that layer (i.e., product of the area of the square base and thickness of the layer denoted by *dstinc*). In essence, by selecting very thin layers, it is possible to determine the solids fraction profile – as a function of y/d. It is easy to see that with increasing of the thickness of the sample layer, the generated number of data points ν(y/d) decreases so that the resolution of the solids fraction profile becomes coarser. However, the analysis of the integral behavior of the solids fraction ν using a layer thickness of one sphere diameter (*dstinc=d*) is especially important, because the curve with this resolution represents a complete profile of the solids fraction at this moment. The slice method may require all eight possible bisections of the particles that are tabulated in Table 2.1 (especially for the layer with a thickness *dstinc* less than spherical diameter). While "lower eighty" is basically used for the evolution of solids fraction versus increasing number of taps, the slice method is used to obtain some insight into the vertical distribution of the solids fraction for a particular tap. The analysis of the modified vertical expansion of the system which is fundamentally built on the slice method is presented in Chapter 5.

There are two additional approaches to analyze the height dependence of solids fraction. The first technique considered in this dissertation called "fixed bottom – moving top") calculates the solids fraction as the ratio of the volume occupied of the particles to the total volume constrained by two horizontal planes: the bottom of the bed and one that is restricted by an imaginary line y_{top}. This imaginary line moves upwards to the maximum vertical position of the particles (y_{max}) with a step of 1% of the diameter of the particle ($0.01d$). This method was performed by calling the subroutine *PACKBT.f.*

The second approach *PACKTP.f* was named as "fixed top – moving bottom". In contrast to the previous technique, this method computes the contributions of the partial solids fractions of particles inside a box that is constrained by the planes of the maximum vertical position of the particles y_{max} and the imaginary bottom y_{bot}, which moves starting from the floor with the same increment of 1% of the diameter of the particle ($0.01d$) up to the maximum vertical position of all particles. Thus, the solids fraction vertical profile is "scanned" from the top to the bottom with a very high precision. Both techniques are computationally expensive for the same aforementioned reason as in slice method; therefore they were not embedded into the Monte-Carlo code but rather were executed in a post-processing stage. For both subroutines, the bisecting cases 6, 7, and 8 (Table 2.1) were excluded from the search of the solids fraction since the sample layer could not possibly split the sphere into three parts based on the definition of methods. Simulation results when using both techniques are given in Chapter 3.

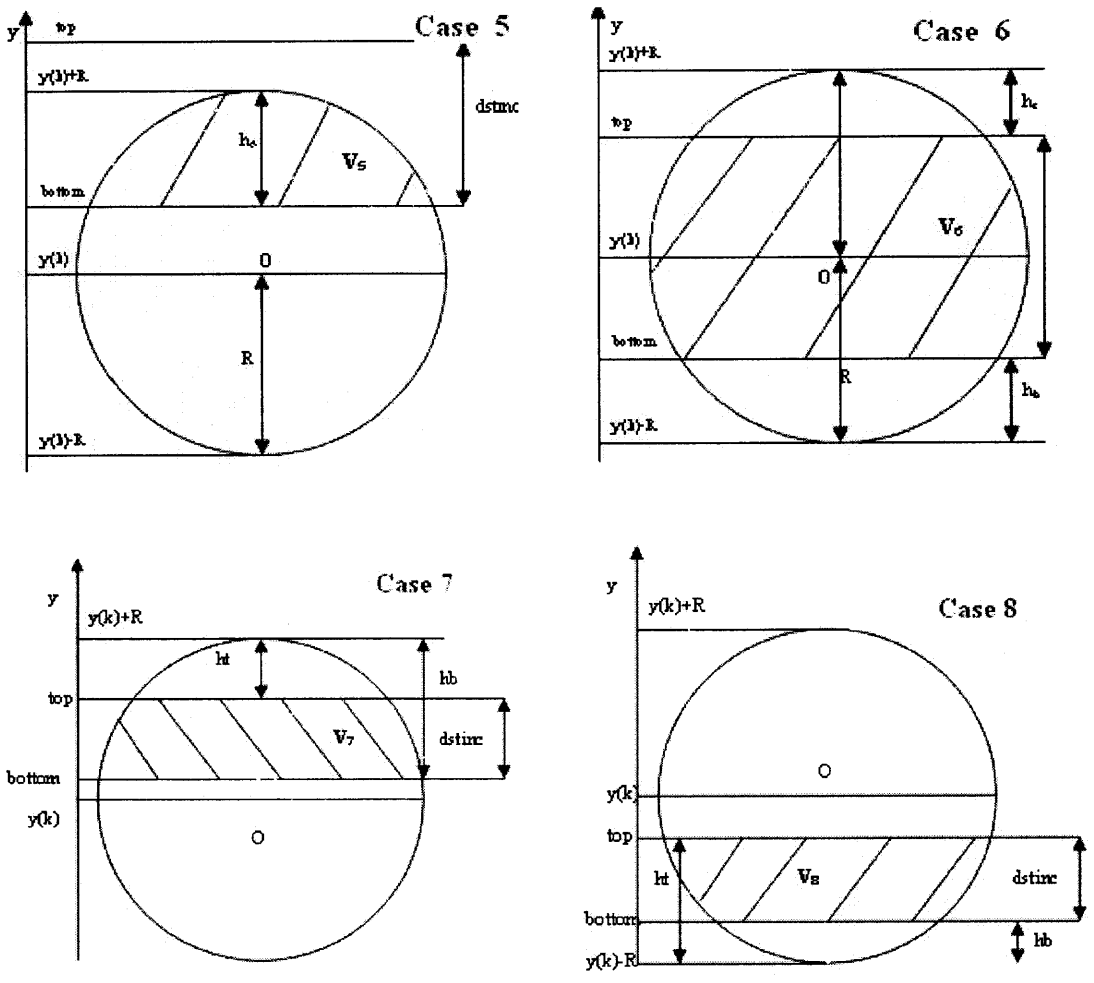

Figure 2.9 The volume occupied computation by the spheres inside a sample layer: case 5 – spherical center is *below* the layer bottom, while the spherical top is located *above* than the layer bottom, case 6 – the sphere is *divided by three parts*, and the spherical center lies *between* the planes of layer top and bottom, case 7 - the sphere is *divided on three parts*, while both planes of the layer top and bottom are situated *above* than the center of the sphere, case 8 - Sphere is *divided on three parts*, while both planes of the layer top and bottom are located *below* than the center of the sphere.

The volumes that are computed in Table 2.1 bring into play the known expressions for volume of sphere and the volume of spherical caps that are formed as the cut off by the appropriate planes of a layer ("bottom" and "top"). The thickness of the cap was defined

Table 2.1 Computation of the volume occupied by spherical particles (sum of the segments of spheres) inside of a sample layer for the all possible bisections

$\text{Case 1}: \begin{cases} top < y(k) \le top + R \\ y(k) > bottom + R \end{cases}$ $h_1 = top - (y(k) - R)$ $Volume: V_1 = \frac{\pi}{3} h_1^2 (3R - h_1)$	$\text{Case 2}: \begin{cases} top - R < y(k) \le top \\ y(k) > bottom + R \end{cases}$ $h_2 = y(k) + R - top$ $Volume: V_2 = \frac{4\pi}{3} R^3 - \frac{\pi}{3} h_2^2 (3R - h_2)$
$\text{Case 3}: \begin{cases} y(k) > bottom + R \\ y(k) \le top - R \end{cases}$ $Volume: V_3 = \frac{4\pi}{3} R^3$	$\text{Case 4}: \begin{cases} bottom < y(k) \le top - R \\ y(k) \le bottom + R \end{cases}$ $h_4 = bottom - (y(k) - R)$ $Volume: V_4 = \frac{4\pi}{3} R^3 - \frac{\pi}{3} h_4^2 (3R - h_4)$
$\text{Case 5}: \begin{cases} y(k) > bottom - R \\ y(k) \le bottom \end{cases}$ $h_5 = y(k) + R - bottom$ $Volume: V_5 = \frac{\pi}{3} h_5^2 (3R - h_5)$	$\text{Case 6}: \begin{cases} y(k) > top - R \\ y(k) \le bottom + R \end{cases}$ $h_t = (y(k) + R) - top$ $h_b = bottom - (y(k) - R)$ $Volume: V_6 = \frac{4\pi}{3} R^3 - \frac{\pi}{3} h_t^2 (3R - h_t) -$ $- \frac{\pi}{3} h_b^2 (3R - h_b)$
$\text{Case 7}: \begin{cases} y(k) < top \\ y(k) < bottom \end{cases}$ $h_t = (y(k) + R) - top$ $h_b = (y(k) + R) - bottom$ $Volume: V_6 = \frac{\pi}{3} h_b^2 (3R - h_b) -$ $- \frac{\pi}{3} h_t^2 (3R - h_t)$	$\text{Case 8}: \begin{cases} y(k) > top \\ y(k) > bottom \end{cases}$ $h_t = top - (y(k) - R)$ $h_b = bottom - (y(k) - R)$ $Volume: V_8 = \frac{\pi}{3} h_t^2 (3R - h_t) -$ $- \frac{\pi}{3} h_b^2 (3R - h_b)$

by the mutual vertical coordinates of the spherical center *y(k)*, top *y(k)+R* and bottom *y(k)-R* and the vertical positions of cutting planes of the sample layers "top" and "bottom".

2.10 Microstructure Analysis

There are several global parameters that provide insight of the structural geometry of the packings of spherical particles: Voronoï and Delaunay 'free volumes', coordination number, dihedral and solid angular distribution, radial distribution function, local orientation order, fabric tensor etc. In this dissertation, a geometrical characterization of packing configurations was performed by monitoring following measures: coordination number and radial distribution function. Both topological quantities were computed for the lower 80% of the packing to have consistency with solids fraction computation and avoid the "top effect" described in the previous section.

2.10.1 Coordination Number

The coordination number represents the number of particles in contact with a given particle. It is one the most frequently used geometrical quantities which provides significant description of the local and global configurations of granular packings.

The definition of contact is highly dependent on the distance between the centers of two spheres. A detailed analysis of the influence of central distance on coordination number was done by Aste [122]. In the current work, the criterion for a sphere to be in contact with another is that the distance between their centers is less than or equal to 1.05 sphere diameters. This computation was performed by generating bins for the integer number of contacts, and then counting all number of spheres having the specified number of contacts.

2.10.2 Radial Distribution Function

The radial distribution function (RDF) is the probability of finding one particle center at a given distance r from the center of a considered particle. The first analysis of this geometrical parameter for granular matter was done by Bernal [5] who showed that the magnitude and position peaks of radial distribution function are a good indications of the formation of structured configuration.

The master equation for radial distribution is defined by:

$$g(r) = \frac{n(r)}{4\pi r^2 \Delta r} \tag{2.8}$$

where $n(r)$ is the number of particle centers that are located inside a spherical layer of the thickness Δr and at a distance r from the center of a given sphere. In this dissertation, the thickness of the layer was set at a constant value 0.01 of the particle diameter throughout all the calculations.

CHAPTER 3

MONTE CARLO SIMULATION OF VERTICAL TAPPING

3.1 Introduction

In this chapter the results of Monte Carlo Simulation are given. First, the solids fraction evolution versus tap number is discussed. Then, the model fitting analysis of solids fraction evolution was done using hyperbolic tangent, inverse logarithmic, stretched exponential and reciprocal linear functions. Also we carried out the studies of system microstructure via coordination number and radial distribution function. Finally, we discuss the necessity of the modified and uniform expansions of the bed for higher systems of particles and analyze the results obtained.

3.2 Evolution of the Solids Fraction

The value of the equilibrium bulk solids fraction depends on the lift intensity γ, which, in a physical experiment, is analogous to changing the intensity of the taps on the containment vessel. As will be seen, the results demonstrate that it is possible to obtain a rather wide range of equilibrium solids fractions, from loosely packed assemblies to rather dense configurations whose radial distribution functions contains peaks associated with the presence of crystalline structures.

For the pouring phase of the simulation, we obtained 'poured' solids fractions in the range 0.560 to 0.580, corresponding to a random loose structures reported in the literature [10, 31, 85, 88].

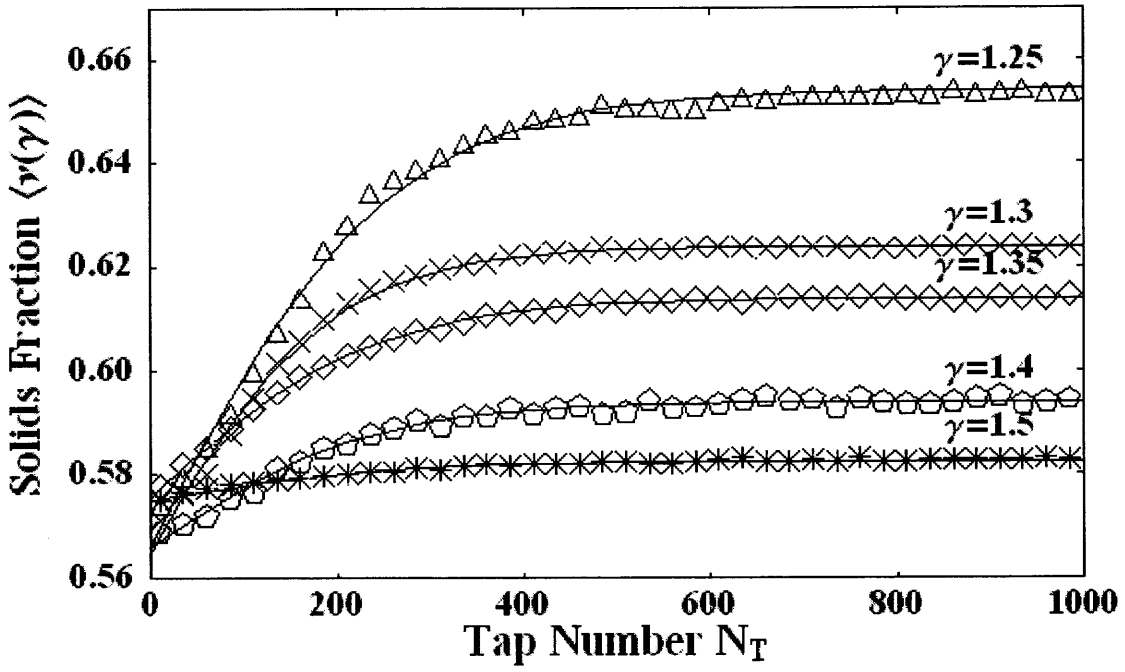

Figure 3.1 Evolution of the ensemble-averaged bulk solids fraction $\langle \nu(n;\gamma) \rangle$ for tap intensity γ = 1.25 (Δ), 1.3 (X), 1.35 (◊), 1.4 (⬠), 1.50 (*). This demonstrates the effect of increasing γ on $\langle \nu(n;\gamma) \rangle$.

Starting from the poured structure, taps are applied to the system following the procedure described in Sections 2.2 and 2.6. The ensemble-averaged bulk solids fraction $\langle \nu(n;\gamma) \rangle$ for lift intensities γ between 1.25 and 1.50 as a function of the tap number is shown in Figure 3.1.

For the purpose of clarity, only every twentieth data point is plotted; here each symbol represents the average bulk solids fraction over 100 realizations. It can be seen in the figure that taps of smaller intensity eventually yield larger equilibrium bulk densities. Simulations were also performed at $\gamma = 1.2$; however these results were not included in Figure 3.1 because of the larger number of taps ($N_T \geq 2{,}000$) required to reach equilibrium. In fact, for $\gamma = 1.15$, we carried out 10,000 taps, which were not sufficient to

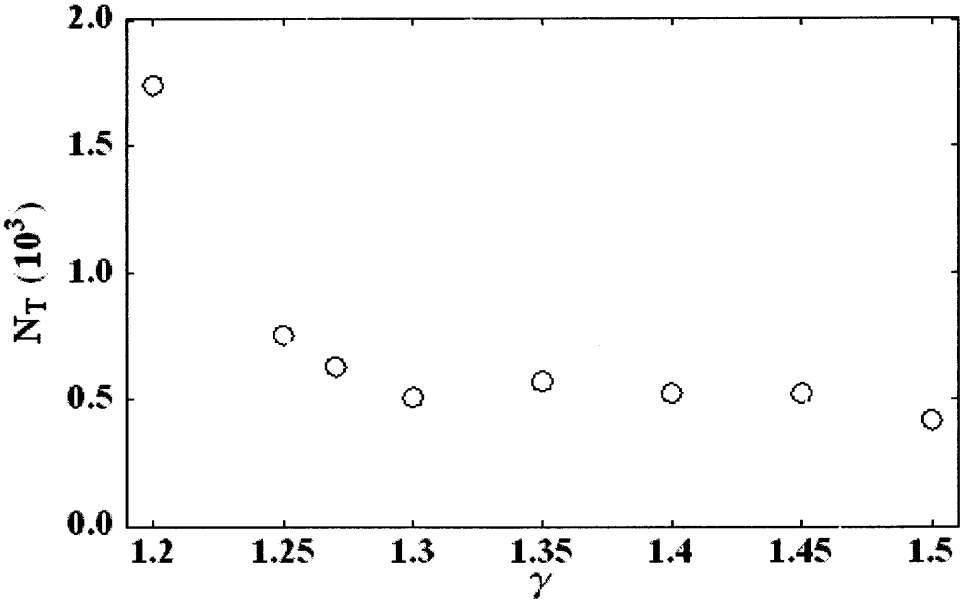

Figure 3.2 The number of taps required to attain 99.5% of equilibrium bulk solids fraction versus the tap intensity γ. A reduction of γ results in a greater number of taps to reach equilibrium.

satisfy the equilibrium criterion in Equation 2.7. This is not unexpected given the trend shown in Figure 3.2 for the number of taps required to reach 99.5% of the equilibrium solids fraction.

The deviations (equations 2.5 and 2.6) for $\gamma = 1.25$, 1.35 and 1.50 as a function of the tap number in Figure 3.3 exhibit a clear-cut dependence on lift intensity γ. The peak observed in the $\gamma = 1.25$ case was observed to be a characteristic feature at small values of the intensity.

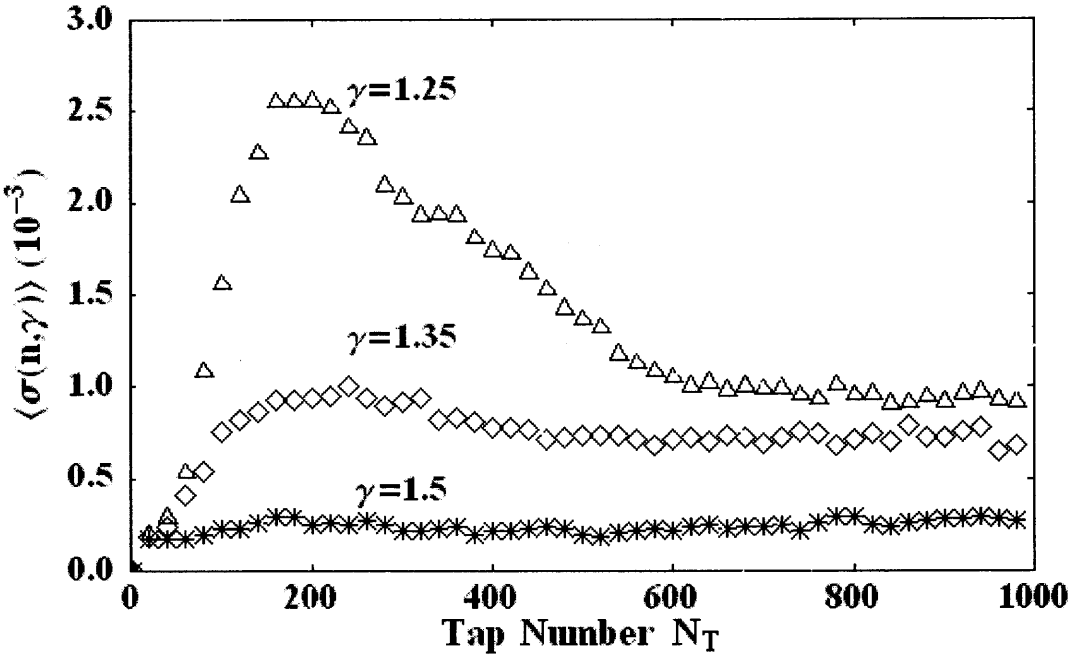

Figure 3.3 The standard deviation of bulk solids fraction $\langle\sigma(n;\gamma)\rangle$ versus tap number N_T for tap intensity γ = 1.25 (Δ), 1.35 (◊) and 1.50 (*). Smaller values of γ yield higher variances.

However, as the lift intensity became smaller, the peak in the deviation grew so that it required significantly more taps to satisfy criterion (Equation 2.7). At the smaller intensities γ considered here, the system tends to visit a greater portion of the phase space in approaching its final lower energy state. However, preliminary results have indicated that for much smaller values of γ than are considered in this dissertation, the system remains at local energy minima without extensive exploration of the phase space.

In order to determine if random lateral displacements of the particles in sync with vertical taps would significantly change the equilibrium bulk solids fraction, we modified our Monte Carlo procedure by incorporating this feature of Mehta et al.'s algorithm [40]. That is, in conjunction with the vertical motion prescribed by (Equation 2.4), each particle is assigned a random lateral displacement within a disk of radius ρ given by,

$$x' = x + \rho(1 - 2\xi_x), \qquad z' = z + \rho(1 - 2\xi_z) \tag{3.1}$$

where ξ_x and ξ_z are uniformly distributed random numbers $\in [0;1]$.

The parameter ρ is computed at each tap as the average (over N_p particles) of the minimum near-neighbor lateral distance,

$$\rho = \frac{1}{N_p} \sum_{k=1}^{N_p} r_k^{\min} \tag{3.2}$$

Here, $r_k^{\min} \equiv \min_{j \neq k} \left\{ \sqrt{(x_k - x_j)^2 + (y_k - y_j)^2} \right\}$, where the minimum is taken over all particles j whose centers are within two diameters from particle k. In Figure 3.4 below, we compare the bulk solids fraction versus tap number at lift intensity $\gamma = 1.25$ with and without application of the random lateral displacements given by Equation 3.1.

The trends of the two graphs are very similar, and we observed steady-state values of the solids fraction that were statistically equivalent. A further check was done by introducing lateral displacements in a system that had equilibrated without them in order to determine if it would return to the same equilibrium solids fraction. In the results of this study, it was observed that random lateral displacements did not move the system out of equilibrium.

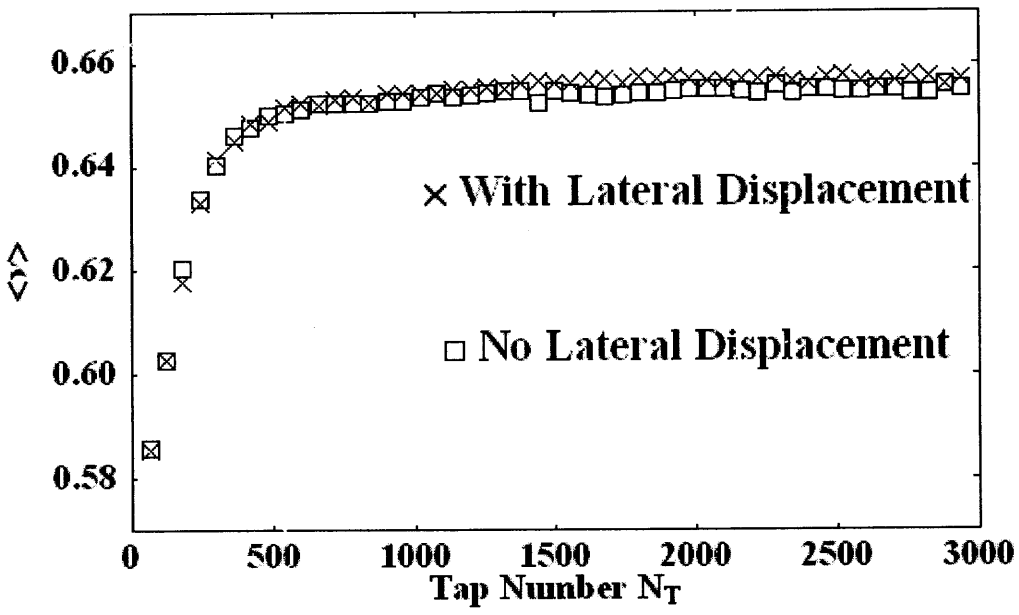

Figure 3.4 Comparison of the evolution of the ensemble-averaged bulk solids fraction at intensity $\gamma = 1.25$ with (X) and without (□) the application of random lateral displacements. The results with and without these displacements are statistically indistinguishable.

3.3 Fitting Analysis of the Solids Fraction

The simulation data could be fit to a hyperbolic tangent model (solid lines in Figure 3.1) of the form,

$$\nu(n;\gamma) = \nu_0(\gamma) + [\nu_\infty(\gamma) - \nu_0(\gamma)]\tanh(A(\gamma)n) \tag{3.3}$$

where $\nu_0(\gamma)$ and $\nu_\infty(\gamma)$ are its initial and equilibrium values, respectively and $A(\gamma)$ is the controlling rate constant. The use of Equation 3.3 is motivated in part by the rate law $\frac{d\rho(t)}{dt} = -\beta\rho$, the solution of which suggests a difference equation of the form,

$$\rho_n - \rho_{n-1} = Ce^{-\beta n}. \tag{3.4}$$

Table 3.1 Fitting parameters for hyperbolic tangent law

γ	ν_0	ν_∞	A×10-3
1.2	0.5699	0.6592	2.57
1.25	0.5663	0.6542	3.91
1.3	0.5651	0.6238	5.18
1.35	0.5759	0.6139	4.22
1.4	0.5666	0.5939	4.34
1.5	0.5721	0.5825	3.94

The general solution of this difference equation is given by

$$\rho_n = B + \frac{C}{1-e^{\beta}} e^{-\beta n}. \tag{3.5}$$

By expressing the model in Equation 3.3 in terms of Linz's [66] compaction ratio $\rho_n \equiv \frac{\nu_n - \nu_\infty}{\nu_o - \nu_\infty}$, it becomes

$$\rho_n = 1 - \tanh(An). \tag{3.6}$$

It can be noted that the solution of Equation 3.5 with $B=1$, $\beta = 2A$ and $C = 2\left(1-e^{2A}\right)$ is seen to be the first two terms of the asymptotic expansion of Equation 3.6.

Parameters determined from the least-squares fit to Equation 3.3 using the simulation results appear in Table 3.1 for $\gamma \geq 1.2$. Recall that these parameters are the initial and final solids fractions $\nu_0(\gamma)$ and $\nu_\infty(\gamma)$, respectively, and the rate constant $A(\gamma)$.

Observe that the initial solids fractions $\nu_0(\gamma)$ from the fit fall within the range 0.560 to 0.580 generated by the simulation and that the plot of the rate A versus γ in Figure 3.5 suggests that there may be a value of the lift intensity that optimizes the

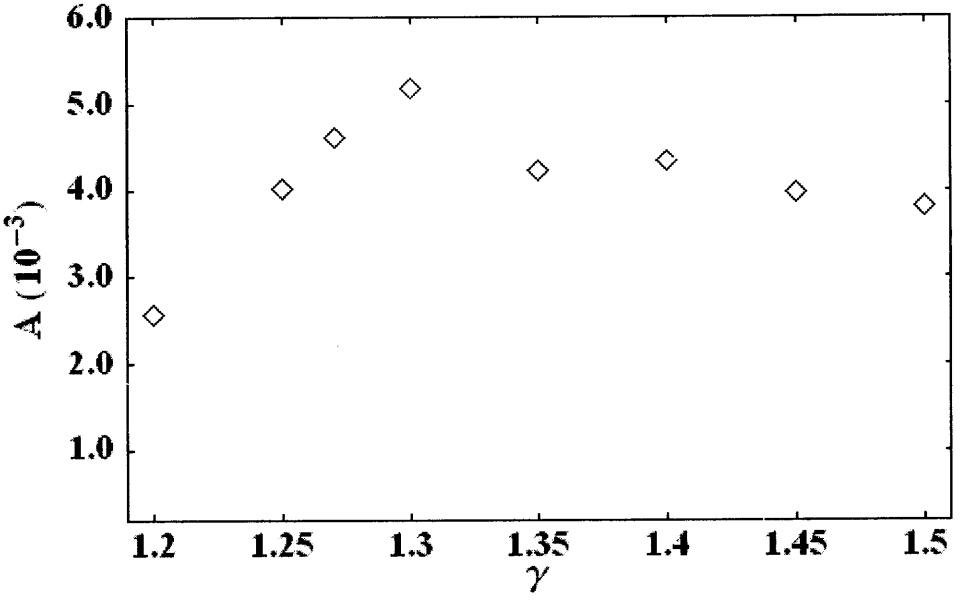

Figure 3.5 Behavior of the rate constant A versus intensity γ from fits of the data to the hyperbolic tangent model $\nu(n;\gamma) = \nu_0(\gamma) + [\nu_\infty(\gamma) - \nu_0(\gamma)]\tanh(A(\gamma)n)$.

densification rate. Although it is premature to be more definitive on this point, recent discrete element simulations and experiments [24] would appear to support this conjecture.

The graph of $\nu_\infty(\gamma)$ versus γ in Figure 3.6 shows that a reduction in the lift intensity results in the creation of a more dense system, but at the expense of an increasingly growing number of taps (see Figure 3.2) to reach equilibrium via criterion given by Equation 2.7. Values of $\nu_\infty(\gamma)$ from the fit closely matched that obtained from the simulation for $\gamma \geq 1.2$.

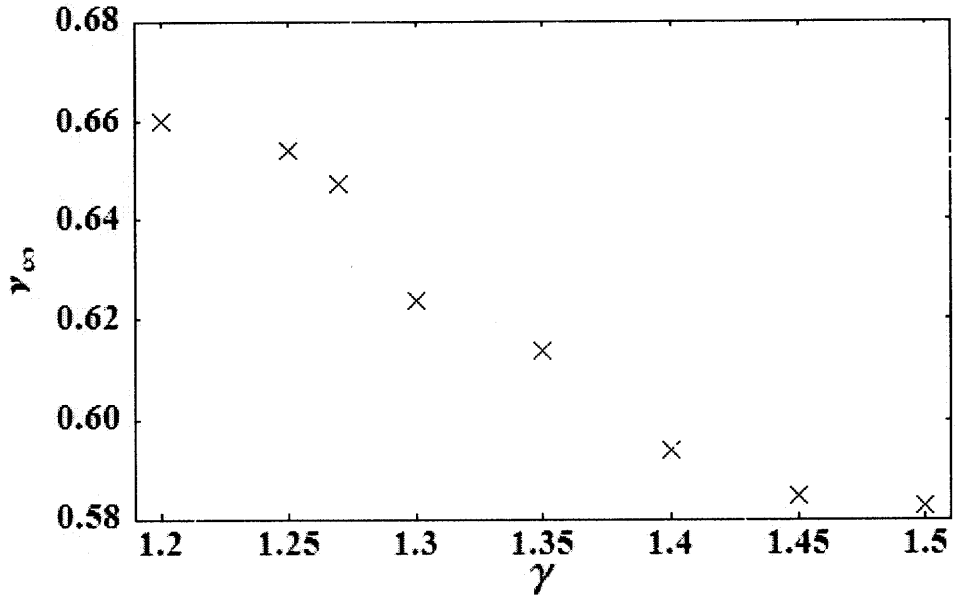

Figure 3.6 Behavior of the equilibrium solids fraction ν_∞ obtained from the fit of the data to the hyperbolic tangent model $(\nu(n;\gamma)=\nu_0(\gamma)+[\nu_\infty(\gamma)-\nu_0(\gamma)]\tanh(A(\gamma)n))$ versus intensity γ. Smaller tap intensities yield more dense configurations.

Furthermore, the model displayed rather good agreement with the progression of the data with tap number n, although (as expected) less than perfect conformity was found at the onset of the densification process.

However, the hyperbolic tangent function was not observed fit the lower intensity data (at $\gamma=1.1$ and 1.15) as well since computational limitations precluded the generation of a data set of sufficient size in the sense of being close to equilibrium. In fact, a crude backward extrapolation of the data in Figure 3.2 suggested that for lift intensity $\gamma=1.1$ upwards of 40,000 taps may be required.

For the sake of completeness, we have also considered fits of the simulation data to other models in the literature.

Table 3.2 Fitting parameters for stretched exponential law

γ	ν_0	ν_∞	τ	β
1.2	0.564	0.658	246	0.85
1.25	0.569	0.654	196	1.29
1.3	0.568	0.623	152	1.40
1.35	0.575	0.614	174	1.17
1.4	0.564	0.593	176	1.30
1.5	0.572	0.583	133	0.60

In particular, comparisons were done with the stretched exponential [152, 153], and the inverse log law [88]. The stretched exponential takes the form

$$\nu(n) = \nu_\infty - (\nu_\infty - \nu_0)\, e^{-(n/\tau)^\beta}. \tag{3.7}$$

There are four parameters in this model, corresponding to the initial solids fraction ν_o, the equilibrium solids fraction ν_∞, the Monte Carlo time scale τ and the stretching exponent β [152]. The fits to the data appear in Table 3.2 from those cases in which equilibrium was attained in accordance with Equation 2.7; these fits do not reveal a consistent value or a trend in the stretching exponent β. Furthermore, neither τ nor τ^β revealed a decrease with intensity γ, as would be expected for a time scale measure. Despite these issues, the fits matched the data for the tap intensities considered in this study.

The inverse log model is given by

$$\nu(n) = \nu_\infty - \frac{\nu_\infty - \nu_o}{1 + B\log(1 + n/\tau)} \tag{3.8}$$

where the four parameters are the initial and equilibrium solids fractions ν_o and ν_∞, respectively, the Monte Carlo time scale τ and an amplification factor B. For tap

Table 3.3 Fitting parameters for inverse logarithmic law

γ	N_T	ν_0	ν_∞	$B/\tau \times 10\text{-}3$
1.1	4,000	0.5920	0.6723	1.44
	6,000	0.5915	0.6714	1.51
	8,000	0.5919	0.6728	1.45
	10,000	0.5914	0.6822	1.37
1.15	4,000	0.5920	0.6723	4.11
	6,000	0.5750	0.6702	3.93
	8,000	0.5748	0.6748	3.84
	10,000	0.5747	0.6756	3.85

intensities $\gamma \geq 1.2$, poor correlation between this model and the simulation data was found since equilibrium was attained more rapidly than could be accommodated by the form of Equation 3.8. In the lower tap intensity regime (i.e., $\gamma = 1.1$ and 1.15), Table 3.3 shows that nearly constant values of the ratio B/τ were obtained as a function of the number of taps, with the value of this ratio being dependent on γ.

The possibility that B/τ is a relevant parameter for low tap intensities is also suggested by the experimental data in Fig. 5 of Knight et al. [88]. An exact correlation between γ in the Monte Carlo simulations and the bed's response to the sinusoidal taps, as in the experiments of Knight et al., is a matter of further research. However, rough scaling arguments (done by equating the normalized average bed expansion in the simulations with the experimental tap amplitude a) suggest that the lower intensities ($\gamma = 1.1$ and 1.15) correspond to accelerations $\Gamma \equiv a\omega^2/g$ greater than the experimental values, but within the same order of magnitude. A similar fit analysis of the data to (14) for $\gamma \geq 1.2$ revealed that B/τ was not constant as a function of the number of taps; for example, the ratio increased monotonically by an order of magnitude for $\gamma = 1.25$ when $600 \leq N_T \leq 3000$.

Table 3.4 Fitting parameters for reciprocal linear law

γ	N_T	ν_0	ν_∞	D×10-3
1.1	4,000	0.5920	0.6723	1.43
	6,000	0.5915	0.6714	1.50
	8,000	0.5919	0.6728	1.47
	10,000	0.5925	0.6725	1.40
1.15	4,000	0.5746	0.6684	4.11
	6,000	0.5751	0.6686	4.00
	8,000	0.5759	0.6693	3.84
	10,000	0.5763	0.6696	3.75

Further exploration of the significance of B/τ was carried out by fitting the low intensity data ($\gamma = 1.1$ and 1.15) to the functional form

$$\nu = \nu_\infty - \frac{\nu_\infty - \nu_0}{1 + Dn} \quad . \tag{3.9}$$

The results are given in Table 3.4, where it is observed that the values of D are close to B/τ obtained from the inverse log fits (Table 3.3). Furthermore, the increase of D with γ is in line with the expected behavior of a time scale parameter. These findings suggest the ratio is an important factor that captures the evolution of the data as a function of Monte Carlo time (i.e., tap number n). Note that Equation 3.8 is simply the first order approximation to the denominator of Equation 3.9 with the identification that $D \equiv B/\tau$.

3.4 Characterization of the Microstructure

The dependence of the configuration microstructure was examined by computing the ensemble-averaged (i.e., equilibrium) distribution of near-neighbor contacts as well as the radial distribution function. These computations were done for a variety of lift intensities. Distribution functions were determined by averaging on configurations in which the

upper 20% of the particles was removed from the data so as to minimize the influence of the top surface and to simplify (without a loss in accuracy) the numerical procedure.

Spheres were defined as being in contact if the distance between their centers is less than or equal to $1.05d$. The number of nearest neighbors is commonly referred to as the coordination number. Figure 3.7 shows the expected result that the near-neighbor contact distributions shift to the right corresponding to an increase in mean coordination number $\langle N_C \rangle$ with bulk solids fraction ν_∞ as determined from the fit to Equation 3.3.

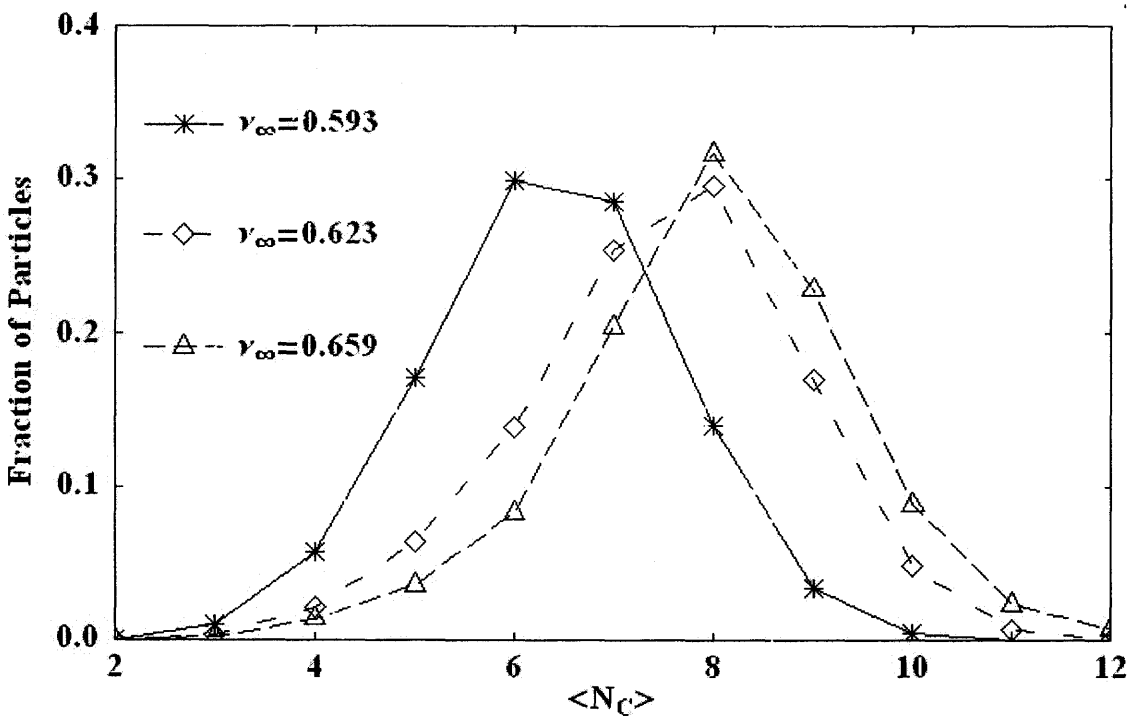

Figure 3.7 Mean coordination number (i.e., fraction of particles with mean number of nearest contacts $\langle N_C \rangle$) for equilibrium bulk solids fraction values (and associated tap intensity γ) $\nu_\infty = 0.593$ ($\gamma = 1.4$) (*); $\nu_\infty = 0.623$ ($\gamma = 1.3$) (◊); $\nu_\infty = 0.659$ ($\gamma = 1.2$) (♦). As expected, systems which are more tightly packed have, on the average, more contacts per particle.

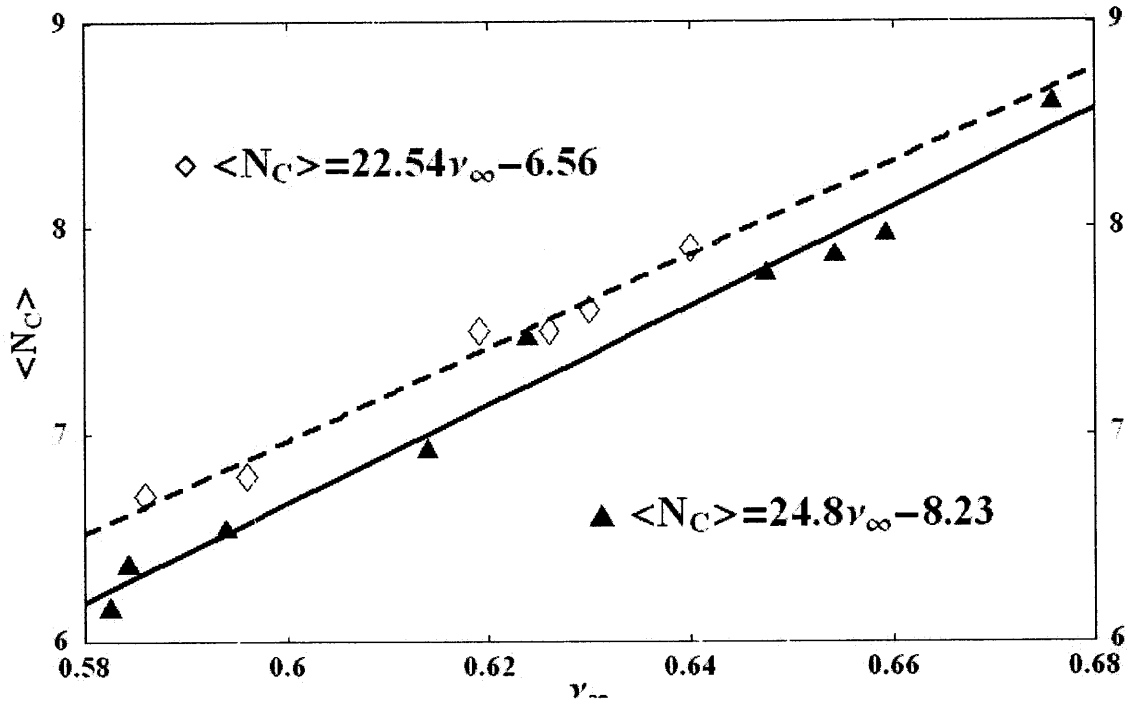

Figure 3.8 Mean coordination number $\langle N_C \rangle$ versus ν_∞ from the simulation results (▲) and experimental measurements (◊) of Aste et al. [1]. This comparison with the experimental data shows good agreement.

A comparison of the simulated values $\langle N_C \rangle$ as a function of ν_∞ with the experimental measurements of Aste et al.[1] is shown in Figure 3.8, where the simulation results are denoted by solid triangles. Here, good agreement is observed with the trend of the data, as indicated by the linear regression fits appearing in the figure and a quantitative comparison of the data with the reported experimental averages.

The radial distribution function [154] is given by:

$$\bar{g}(r) = \frac{1}{\rho N_p} \left\langle \sum_{i}^{N} \sum_{j<i}^{N} \delta\left[r - r_{ij} \right] \right\rangle \tag{3.10}$$

where N_p is the number of particles, ν is the bulk density (i.e., number of particles per unit volume where $\nu = \rho \pi d^3 / 6$), r_{ij} is the distance between the centers of particles i and

j, and δ is the standard delta distribution. Thus, $\bar{g}(r)$ may be considered as that quantity which, when multiplied by the bulk density, yields the local density. Computationally, $\bar{g}(r)$ is approximated as an ensemble-average quantity taken at the last Monte Carlo time step (or tap).

$$\langle \bar{g}(r/d) \rangle \cong \frac{\langle N(r) \rangle}{24 \langle \nu \rangle (r/d)^2 (\Delta r/d)} \tag{3.11}$$

where $\langle \cdot \rangle$ represents the ensemble average, $N(r)$ is the number of sphere centers within a spherical shell of radius r and thickness Δr , and ν is the bulk solids fraction. Due to limited computational facilities, more refined 'time' and ensemble averaging was not possible over the range of tap intensities considered in this study. However, several preliminary calculations indicated little difference in the radial distribution results when 'time' averaging was included.

Figure 3.9 shows $\langle \bar{g}(r/d) \rangle$ of the initial configuration and the result of three tap intensities ($\gamma = 1.15$, 1.3, and 1.45) corresponding to decreasing solids fractions ν_∞. As the density increases, observe that the peaks in the distribution function become more pronounced. For $\gamma = 1.15$, a power-law singularity at $r = d$ of the form

$$\bar{g}(r) \approx c_0 |r - r_0|^{-\alpha} \tag{3.12}$$

was found. The least-squares fit to Equation 3.12 yielded $\alpha \approx 0.528$, in agreement with the value reported in the molecular dynamics studies of Silbert et al. [12] and later experiments of Aste [122]. The second and third peaks in the distribution appear at $r/d \sim \sqrt{2}$ and $\sqrt{3}$, which correspond to those in a hexagonal-close packing lattice.

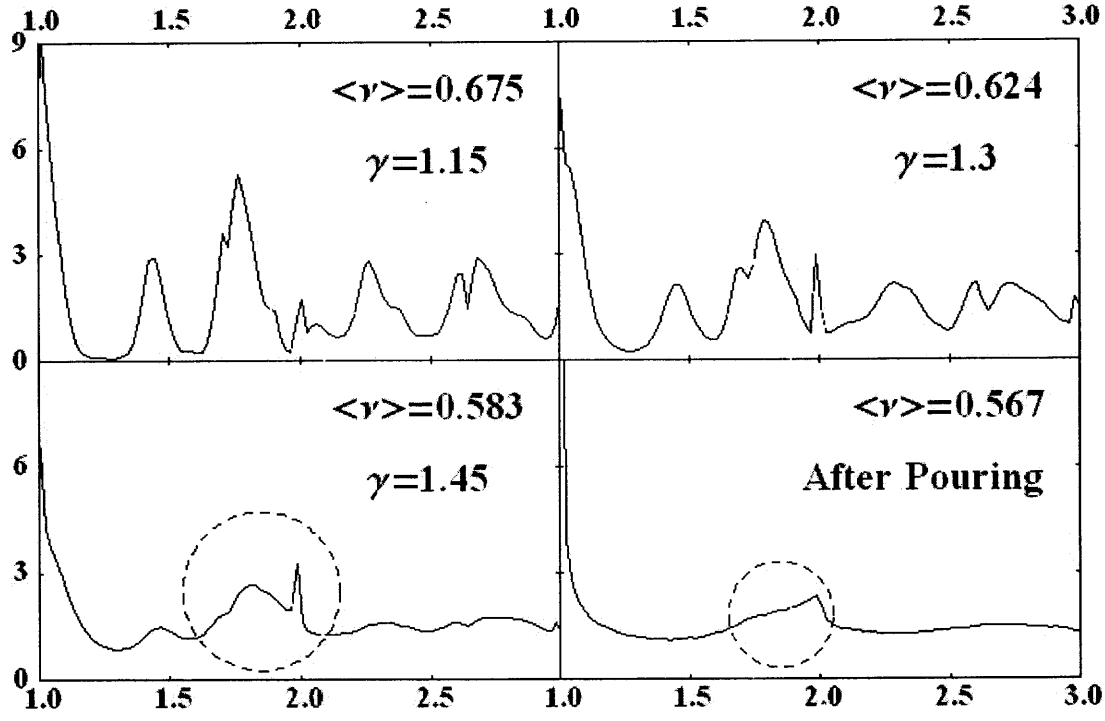

Figure 3.9 Radial distribution function for a poured assembly and for various equilibrium bulk solids fractions ν_∞ with their associated intensities γ shown. The higher ν_∞ results reveal local crystalline structure, while systems with smaller ν_∞ exhibit features observed in experiments.

This result suggests that the low intensity taps tend to induce local crystalline order in the system that resembles a hexagonal-close packing structure. At the lowest tapped solids fraction (circled in Figure 3.9, for $\nu_\infty = 0.583$), it is observed that the two peaks at $r/d \sim 1.8$ and 2.0 provide evidence of a local structural arrangement similar to the experimental results of Aste [122]. This structure does not appear in the poured assembly $\nu_0 = 0.567$ as seen in the plot at the lower right hand corner of Figure 3.9. We remark that this local arrangement differs from that seen by Nicolas et al. [33], who observed hexagonal close-packed structures resulting from the application of horizontal cyclic shearing.

3.5 Study of the Uniform Lifting of the Vessel

In previous sections of this dissertation we have established the formation of the ordered microstructure for the system of 1,728 monodisperse particles which were located inside the granular container of dimensions $12d \times 12d \times 12d$. Unfortunately, the number of particles chosen might technically limit the geometry of possible configurations to those ones enclosed in a cube having dimensions $12d \times 12d \times 12d$. Because the fill height is approximately the same as the lateral dimension of the box, this causes very fast densification and a high compaction. Consequently, in this section, results on deeper systems are presented.

A system of 3,456 identical particles was chosen, in which the cross-section area of the box is identical to the previous study ($12d \times 12d$), but is now twice as high ($24d$) as previous case, so that the dimensions are $12d \times 24d \times 12d$. Typical configurations of random initial configurations and poured assemblies for 3,456 particles are shown on Figure 3.10. The fill height H for such systems generally varies from 22 to 24 diameters.

For the deeper system, the linear expansion method as described in Section 2.7 in caused a very substantial displacement of the particles in the upper layers. For instance, following Equation 2.4, the displacement corresponding to the linear expansion with $\gamma = 1.25$ of the particles at the top $(y \sim 20d)$ could reach 5 particle diameters, which correlates to a relatively high input of potential energy into the system. This physically unrealistic upward movement causes the effect of particles in the upper layers to "forget" the positions of previous configurations.

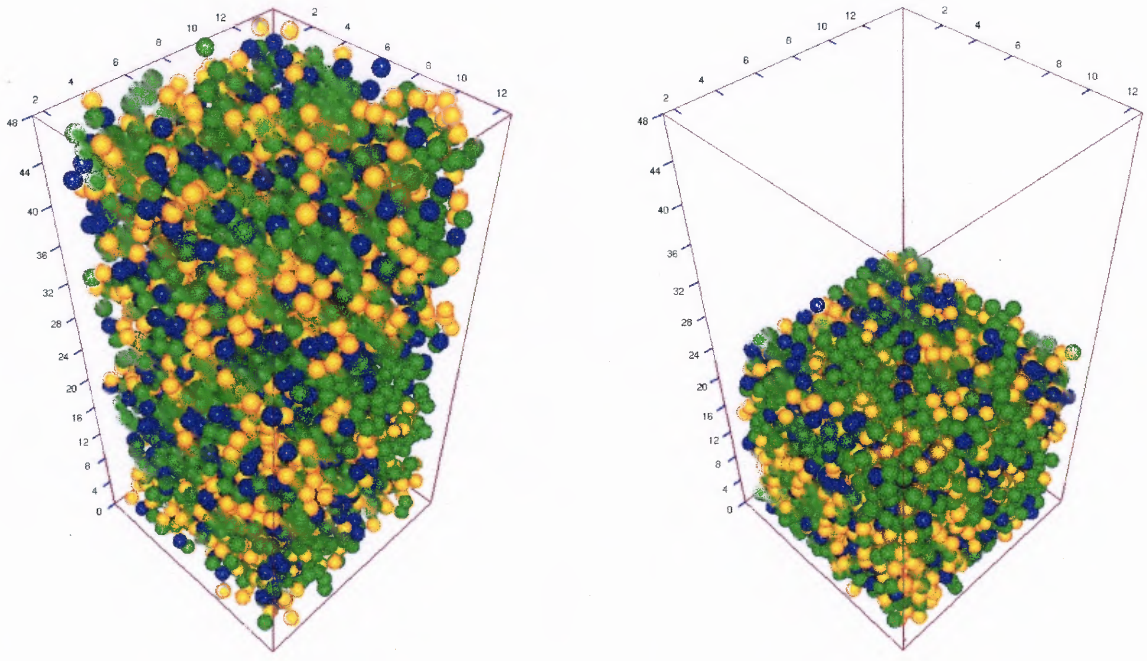

Figure 3.10 Snapshots of system of 3,456 particles: random initial configuration (picture to the left) and poured assembly with fill height H/d~22 (picture to the right).

To verify the "memory loss" that takes place at the upper layers, simulations were carried out in which the tapping of the system was modified. The tapping of the system is carried out so that the lower layers (up to fixed y_C) were expanded proportionally to their vertical positions expressed by Equation 2.4, while the particles in the top layers that are higher than y_C were uniformly lifted by an equal amount λ corresponding to the value of the lift at y_C. The particle vertical displacement of the modified expansion is defined as follows:

$$\frac{\Delta y^i}{d} = \begin{cases} y^i_{old} \cdot (\gamma - 1); \; y < y_C \\ \lambda, \text{ if } \; y \geq y_C \end{cases} \tag{3.13}$$

To avoid the possibility of a forbidden particle overlap, a condition of continuity was imposed so that the uniform lift intensity λ is given by expression $\lambda = (\gamma - 1) \cdot y_C$.

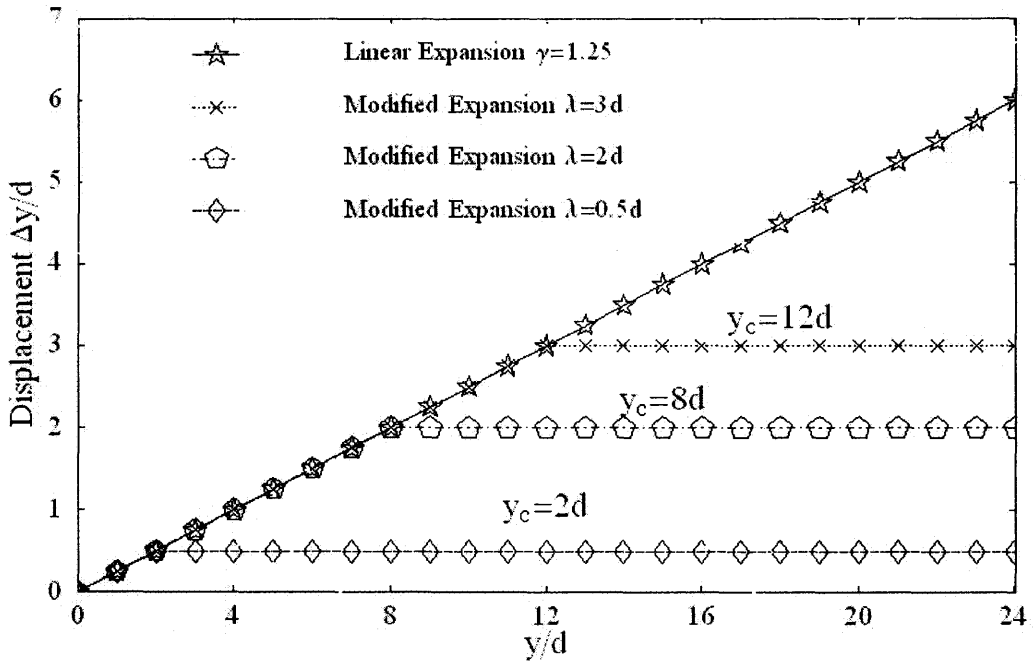

Figure 3.11 Vertical displacement of linear and modified expansions with different stationary points y_C and different λ values.

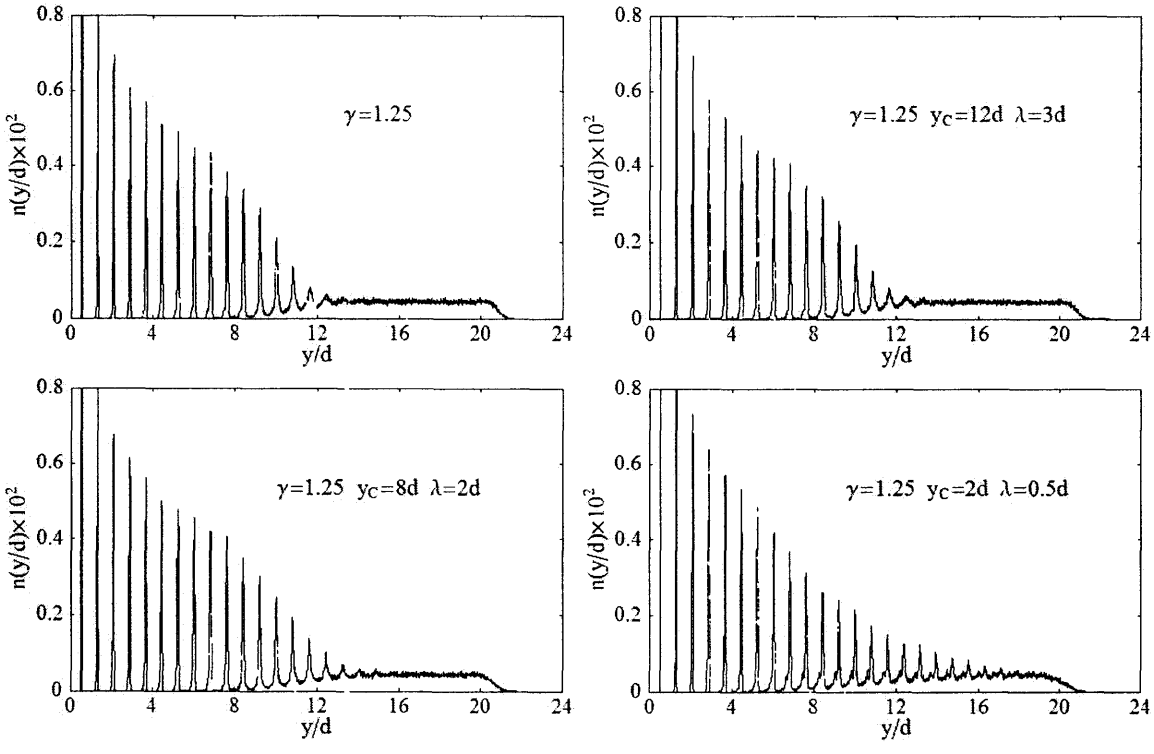

Figure 3.12 Vertical center distribution for modified expansions by Monte Carlo method.

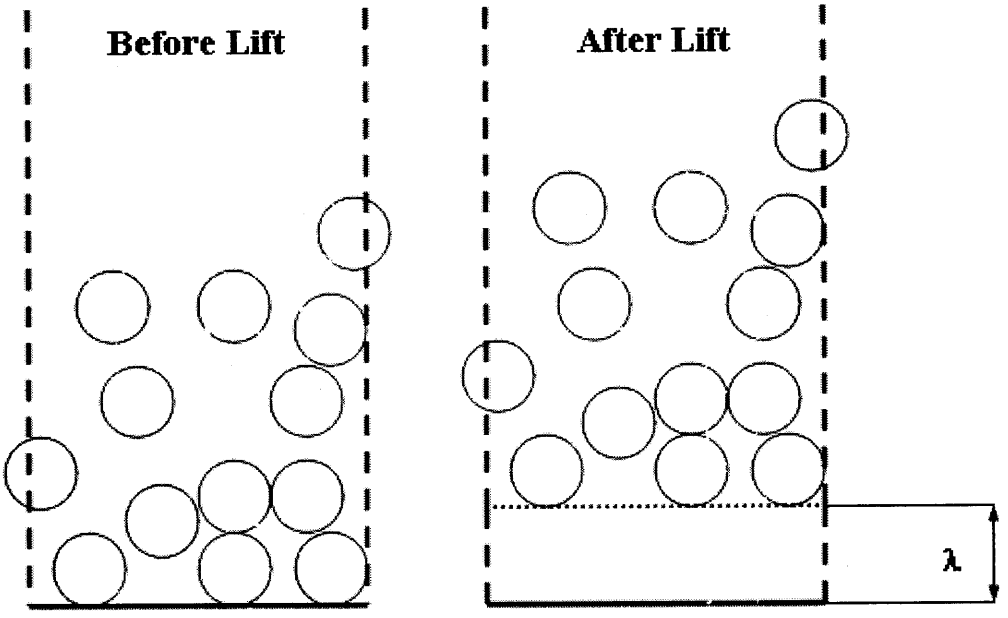

Figure 3.13 Graphic representation of uniform lift of system particles on lift intensity λ.

The distribution of centers along the height of the bed, (details of the calculations appear in Chapter 5), provides the evidence of a physically unrealistic lift. As seen from Figure 3.12, very intensive energy inputs of top layers for linear and modified expansions with $y_C = 12d$ causes the top of system to remain in a very loose state. On the other hand, smaller values of $y_C = 2d$ at $\lambda = 0.5d$ leads to perceptible advance of crystallization into the top layers. This observation indicates the importance of the nature of the energy input mechanism on further crystallization progress.

Thus, in subsequent computations, the system was tapped by lifting all particles by the same vertical displacement regardless of their vertical positions during the tap (referred to as a 'uniform lift'). Hence,

$$y^i_{new} = y^i_{old} + \lambda \qquad \textbf{(3.14)}$$

All other simulation routines remain the same as described in Chapter 2 for linear expansion. The effect of uniform lift on the vertical coordinates of system particles is schematically represented on Figure 3.13. Segments of particles that are shown located outside of the box represent the periodic boundary conditions in lateral directions.

A characteristic ensemble average solids fraction evolution for several uniform lift intensities is given in Figure 3.14. Here, lift intensities varying from $\lambda = 0.1d$ to $\lambda = 0.35d$ are used. On this plot each point represents the average solids fraction (average over 100 realizations via the procedures described in Section 2.8) at every 500 taps. This figure clearly demonstrates the effect of lift intensity on the solids fraction evolution.

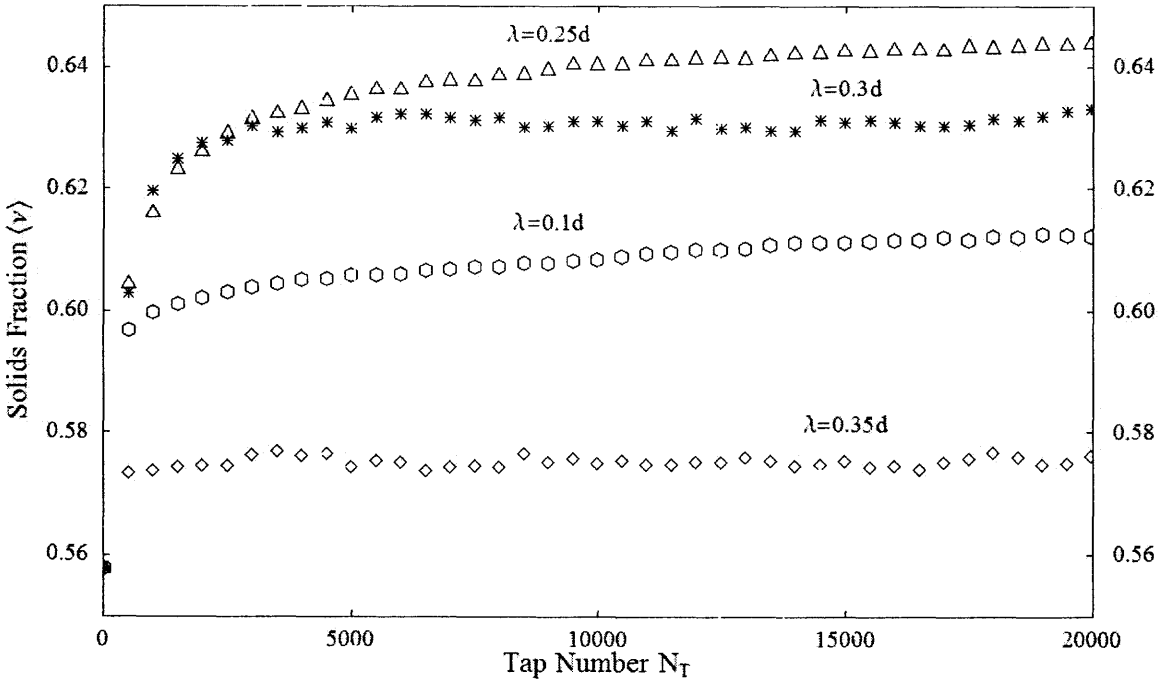

Figure 3.14 Ensemble average solids fraction ν versus tap number N_T for different lift intensities. The plot shows the typical evolution of the solids fraction for uniform expansion of the system.

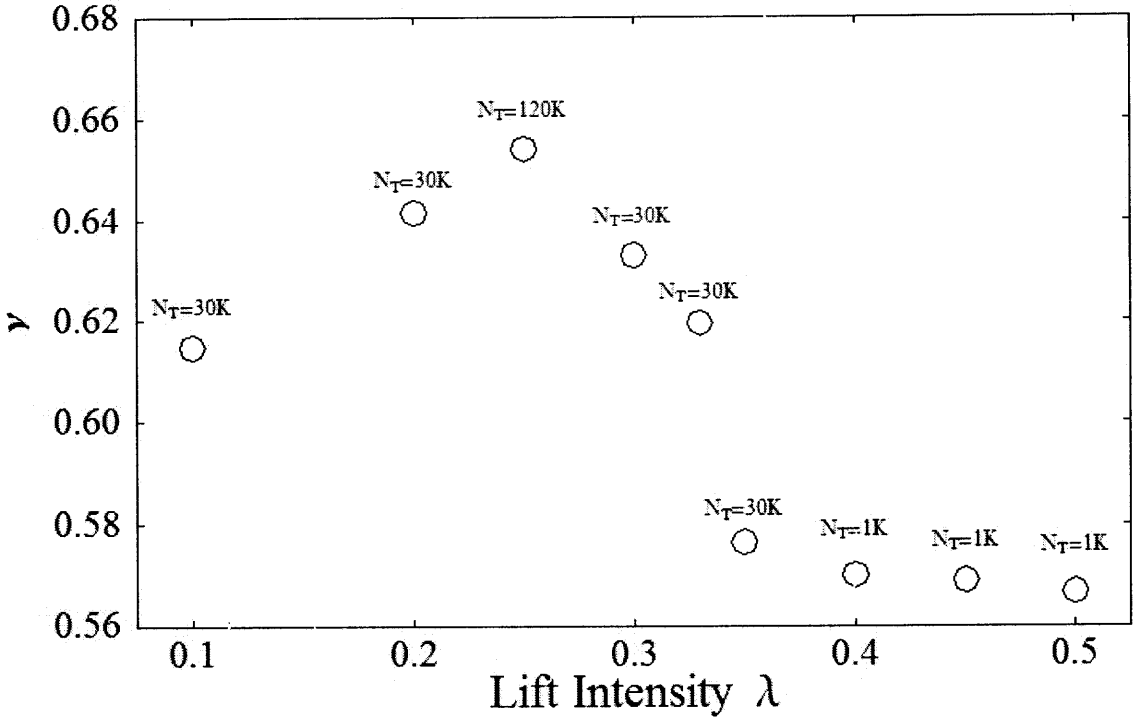

Figure 3.15 Solids fraction attained at final tap N_T for different lift intensities λ.

Figure 3.15 depicts the results of solids fraction obtained for different lift intensities. Note that each data point represents the solids fraction for the particular number of taps shown with the symbol. At the larger lift intensities ($\lambda > 0.35d$), no significant increase in bulk density from the initial poured configuration was observed. However, the results shows a large improvement in solids fraction at $(\lambda = 0.25d)$. Although not all of the points shown in Fig. 3.15 were at equilibrium, it is hypothesized that there may be a critical intensity at which the solids fraction is optimized.

CHAPTER 4

DESCRIPTION OF DISCRETE ELEMENT MODEL

4.1 Introduction

This chapter contains a description of the Discrete Element simulation, beginning with a concise background on the method itself and the force models used. This is followed by introducing the physical properties of system. Details of the modifications made to an existing discrete element code are described, consisting of how discrete taps were implemented. Finally, the analyses of the particle layer responses to the taps via maximum displacements are provided.

4.2 Background

In the discrete element method, the positions and velocities of the particles are determined by integrating the equations of motion governed by Newton's second law. This approach was introduced in the 1970's by Cundall and Strack [18] to describe the mechanical behavior of spheres and discs. The principles of discrete element method are very similar to those that are used in molecular dynamics (MD) modeling. The key difference between these two methods is that the motion of molecules is determined by molecular forces that are conservative, while the collisional (or contact) forces for macroscopic particles in discrete element simulations are dissipative.

The discrete element code that was modified for the purpose of this dissertation was originally written by Walton and Braun [53] to study flows of monodisperse,

frictional, inelastic spheres subjected to uniform shear. This code was subsequently modified by Zhang [24] to investigate the densification behavior of granular systems within a rectangular box, in which the floor was a piston that periodically oscillated up and down. Subsequent to this, the code was code was modified to analyze segregation and migration in granular Couette shear flows, and to study the floor pressure in a cylindrical vessel loaded with particles.

This version of the code employs a partial-latching spring model that was developed by Walton [155]. The energy of independent particles dissipates during their collision for both normal and tangential directions. The normal direction is parallel to the line connecting the centers of two spheres, and the tangential direction is perpendicular to the normal one. Along the normal direction, the dissipation mechanism is described by a linear spring model which involves a loading with stiffness K_1, and unloading with a spring stiffness K_2, such that $K_1 > K_2$. The energy loss along tangential direction is simulated by applying Mindlin-Deresiewicz's theory [156].

The physical properties of the system particles were as follows: restitution coefficient $\varepsilon_{elast} = 0.9$, friction coefficient $\mu = 0.1$, density of the system particles $dens = 1.2 \, g/cm^3$, normal force loading stiffness $K_1 = 2.8 \times 10^5$, unloading stiffness $K_2 = 10^5$, and tangential to normal stiffness coefficient ratio of 0.8.

4.3 Modifications to DEM code

For this dissertation, the DEM code was modified to simulate the response of the particles in a rectangular vessel whose floor was subjected to harmonic vertical taps. Tapping is provided by the half-period of sine displacement (or half-period of cosine velocity) that are applied to the floor. In the code, the floor is represented by a "floor particle", which is located one radius below the level y_f, and it has a "virtual" radius equal to the radius of system particle. Thus it is simply an "image particle" whose role is to mimic the effect of the floor. The governing equation for the floor motion is given by:

$$v_f(t) = v_{amp} \cdot \cos\left(\Omega\left(t - t_p + (ir-1)t_C\right)\right) \tag{4.1}$$

where v_{amp} is the maximum velocity "amplitude" of the floor oscillation, Ω is the cyclic frequency of oscillation which is equal to $2\pi f$, f is the frequency of oscillation, t_p is the relaxation time, t_C is the time of one cycle, (equal to the sum of "tapping" time t_b and the "relaxation" time t_p), and *ir* is the tap number. The relationship between tapping time and frequency is given as:

$$t_b = \frac{1}{2f} \tag{4.2}$$

During the tapping, the impulse (energy input) that is experienced by the floor is transmitted to the particles through collisional impulses. As the tapping period of time is completed, the floor returns to its initial zero level and stays motionless there for the duration of the relaxation time t_p, thereby allowing the system particles to settle down to a configuration for minimal kinetic energy. A schematic illustration of the floor motion is depicted in Figure 4.1.

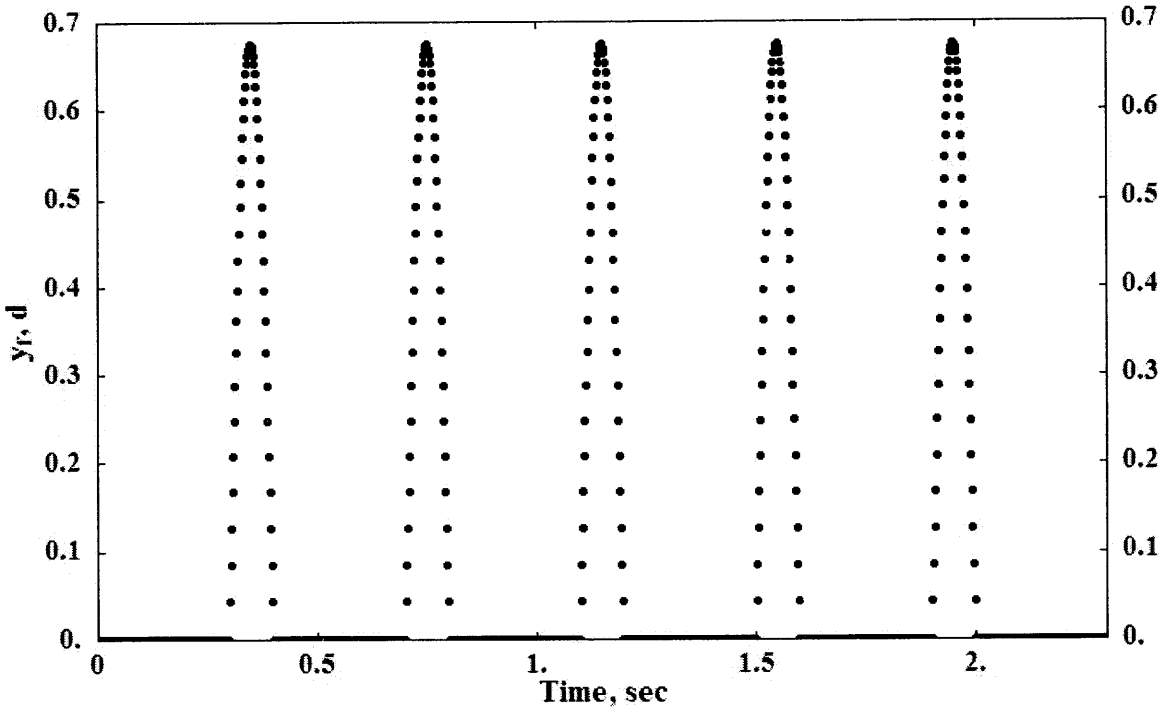

Figure 4.1 The vertical location of the floor level y_f as the tapping occurs. The floor particle is positioned below y_f at one particle radius.

In this particular case, the frequency of oscillation was 5 Hz, t_b = 0.1 sec, time of tapping is 0.1 sec, t_p = 0.3 sec and time of one cycle (t_C) is 0.4 sec (or, in other words, 5 complete cycles for 2 seconds).

4.4 Response of the System to the Discontinuous Tapping

The subroutine *avezon.f* was created to examine internal response of the particles to tapping. This subroutine finds the maximum vertical displacement of a particle during a tap. For this purpose, the computational cell was partitioned into vertical layers or 'zones' of thickness equal to one particle diameter.

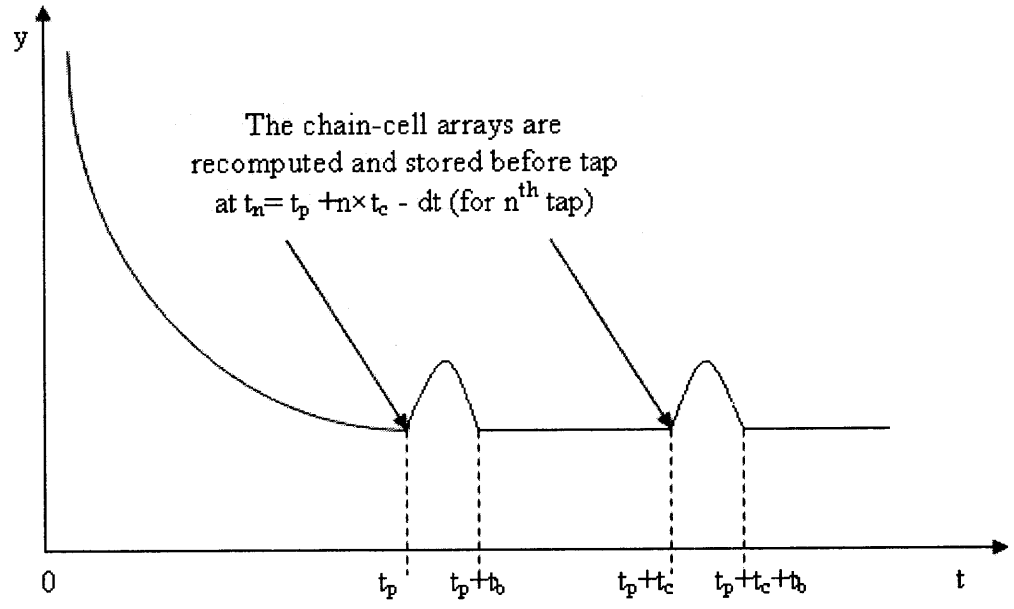

Figure 4.2 The time at which arrays ZONE, LIST and HEAD are being computed.

Before the tap, spheres were assigned to the related chain-cell arrays according to their vertical positions (see Figure 4.2). Subsequently, the vertical coordinates of the particles in a zone are traced by following the corresponding sphere indices and then averaging their maximum vertical positions over the number of spheres within the layer. For a graphic visualization of the response of seven layers to the harmonic tapping described above, the reader is referred to Figure 4.3.

The maximum vertical displacement for a layer is computed as the difference between the maximum and minimum values of the average vertical positions, that is,

$$\Delta y / d = \frac{\overline{y}_{max} - \overline{y}_{min}}{d} \tag{4.3}$$

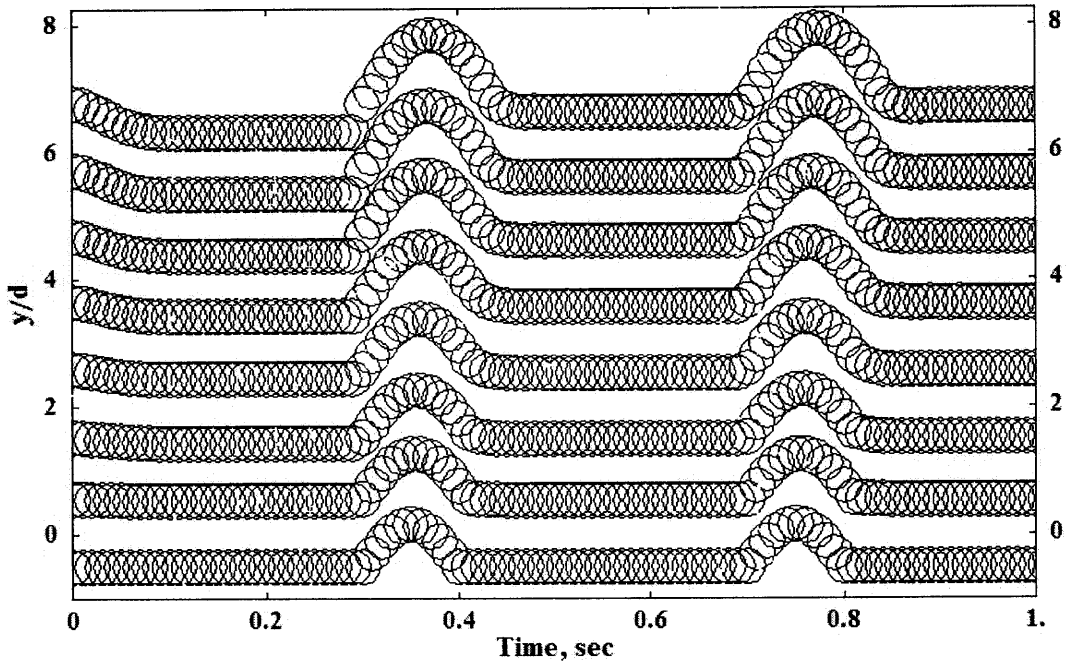

Figure 4.3 The schematic response in time of multiple layers (7 zones) of spheres to the floor tapping. The positions of the floor particle are shown as the dynamics of the lowest layer of spheres.

Generally, a minimum vertical average is reached right at the moment when the tracing arrays were recomputed (i.e. the time-step before tapping is initiated). This moment is also characterized by the minimum potential energy of particles in the layer for a particular tap number. On the other hand, a maximum vertical average is attained within a short period of time after the middle of the tapping period. This is related to the wave nature of signal propagation in granular matter that has been reported in the literature [157-159].

Another helpful parameter used was the expansion factor γ, which is the ratio of maximum to minimum vertical average $\left(\gamma = \overline{y}_{\max} / \overline{y}_{\min}\right)$. The use of this quantity was motivated by the desire to identify a connection between two Monte Carlo and Discrete Element results.

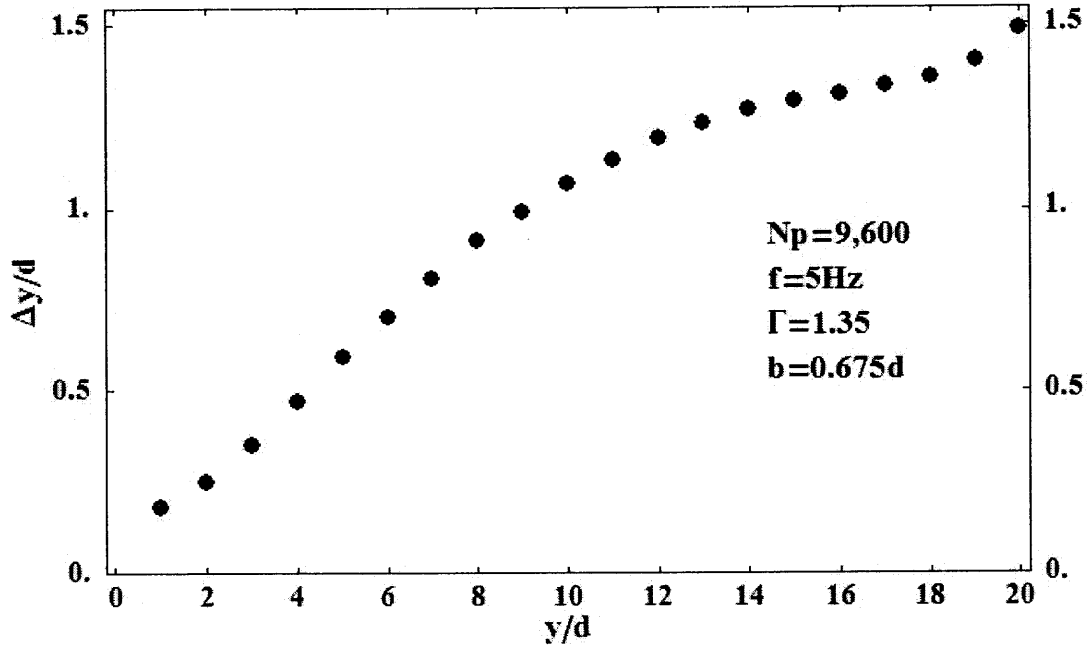

Figure 4.4 Maximum vertical displacement of the vertical layer average as the response to the floor tapping.

Figure 4.4 illustrates the maximum vertical displacement in terms of layer height location (y/d) for the case f = 5 Hz, Γ = 1.35, and displacement amplitude b/d = 0.675. It is clear that the response of the particles to harmonic oscillation of the floor has nonlinear behavior which is in contrast to the Monte Carlo linear expansion given by Equation 2.4.

For the Discrete Element Method we calculate the parameter γ which is an equivalent to the linear expansion parameter from Monte Carlo simulation as described in Section 2.7:

$$\gamma^i = \frac{y^i_{new}}{y^i_{old}} \tag{4.4}$$

where y^i_{old} is the average vertical coordinate for a layer i (usually the smallest one), y^i_{new} is its maximum vertical coordinate after a tap.

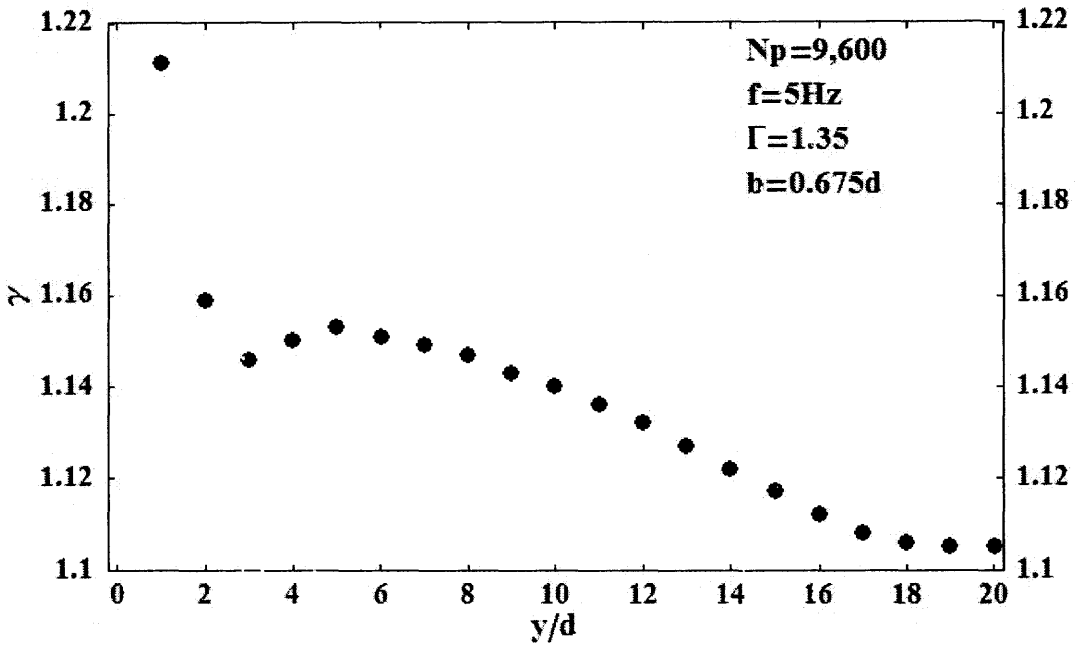

Figure 4.5 DEM expansion factor γ of the vertical layer average as the response of granular matter to the floor tapping.

As seen from the Figure 4.5, the expansion factor varies within a relatively narrow interval $[1.1;1.16]$, except for the particles of the first layer that lie on the floor and have a small value of $\overline{y}_{\min}$. For the case presented in Fig. 4.5, the range of expansion factors obtained for in the discrete element simulations lies in a region which corresponds to the low-energetic linear expansion tapping of the Monte Carlo simulation.

The results seen in Fig. 4.5 cannot be said to be characteristic of the expansions fact as it was done for only a single set of vibration parameter Although beyond the scope of this dissertation, it is clear that a complete parameter study should be done to characterize the behavior of the expansion factor as a function of amplitude, frequency and acceleration.

CHAPTER 5

FORMATION AND DEVELOPMENT OF ORDERED MICROSTRUCTURE IN GRANULAR MATTER

5.1 Introduction

In this chapter the formation and development of ordered microstructure in a tapped configuration of spheres is discussed. For this purpose, a local geometric measure is introduced that quantifies the distribution of centers along the height of the box. Characteristic features of the vertical center distributions are explained for both the random initial and poured configurations, as well as for the evolving system as the taps progress. These results are used to more clearly interpret the analogous effect that was observed in Monte Carlo technique results presented in Chapter 3.

5.2 Motivation of Analysis

How does a random, loose assembly of spheres subjected to tapping develop an 'ordered' microstructure? To find an answer for this question, scientists have developed a variety of geometrical structure analysis tools that were discussed in previous chapters. Unfortunately, most of these techniques (coordination number, radial distribution function, fabric tensor etc.) are global geometrical measures, and as a result they do not provide a clear picture of the evolution of interior structure. In this study, the propagation of the ordered configuration is quantified by using the vertical distribution of particle centers. This idea was inspired by the use of local area fraction for one-

dimensional theory of fluidized suspensions of spheres by P. Singh et. al. [160, 161]. The outcome of the vertical distribution analysis and conclusions drawn from it follow.

5.3 Vertical Center Distribution for Monte-Carlo Simulation

Vertical distribuuon analyses for the both Monte Carlo and Discrete Element simulation results are done via post-processing using the positions of the sphere centers (stored in file *coord.txt*). The box is partitioned (see Fig. 5.1) into layers of thickness $(\delta H = y_i - y_{i-1} = 0.01d)$ and the number of sphere centers (x_k, y_k, z_k) within this layer is summed, the result of which is divided by the number of particles (N_p) in the system. Thus,

$$n(y,\delta H) = \frac{1}{N_p}\sum_{k=1}^{N_p}\delta(y - y_k)\delta H \tag{5.1}$$

This distribution describes the allocation of particle centers along the height of the box. The vertical thickness equal to 1% of the particle diameter was identified as optimal after performing a series of tests using thicknesses d, $0.5d$, $0.25d$, $0.1d$, $0.05d$ and $0.001d$. For a relatively large thickness $0.1d$ the evolution picture was rough and rather inaccurate. On the other hand, implementation of the "precise" thickness $0.001d$ provides relatively noisy pattern because the vertical center distribution would reflect every minute detail of the microstructure.

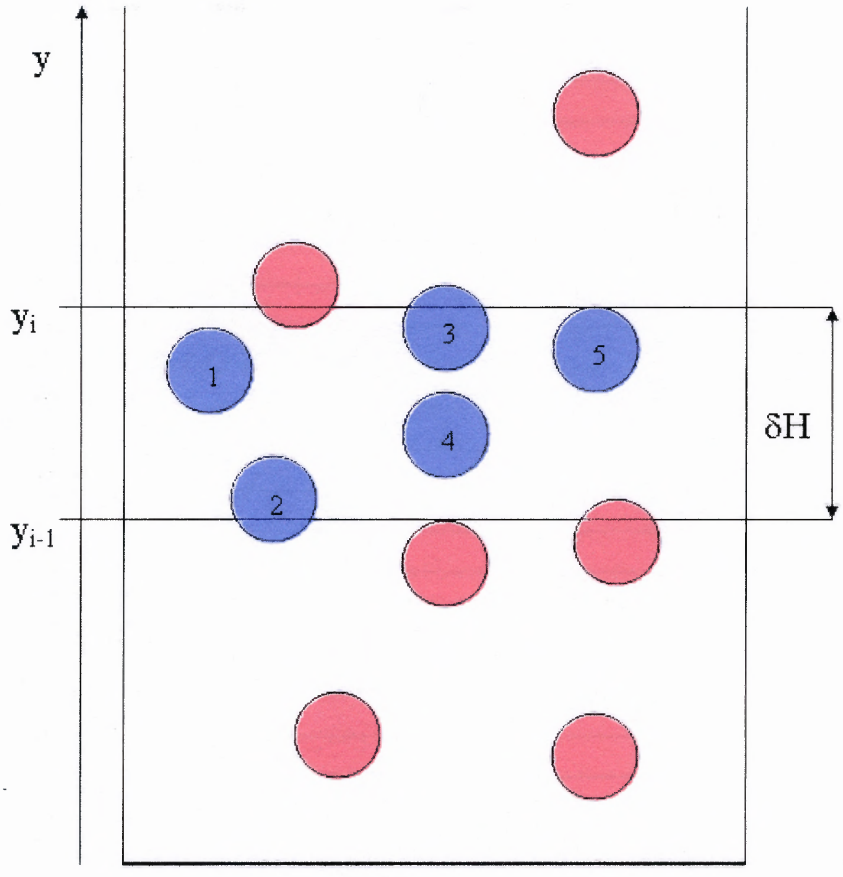

Figure 5.1 Schematic representation of the inspection layer of thickness δH. Blue spheres are counted for vertical center distribution.

Now we consider the outcome of vertical center distribution analysis. The first spherical arrangement of the system of 3,456 particles stored for Monte Carlo simulation is a random initial configuration generated by subroutine *RINCFG.f* (see Figure 2.4 a for snapshots). For this system, the vertical coordinates vary from 0.5*d* to 36 *d*, and the total number of layers equals to 3,550 (corresponding to 0.973 centers per layer and $n\left(y/d\right) \approx 2.7\times10^{-4}$). For this configuration, a relatively low peak in the vertical center distribution was observed near the floor, followed by a uniform distribution of centers up to the vessel surface (see Figure 5.2). The small peak at the floor can be explained by

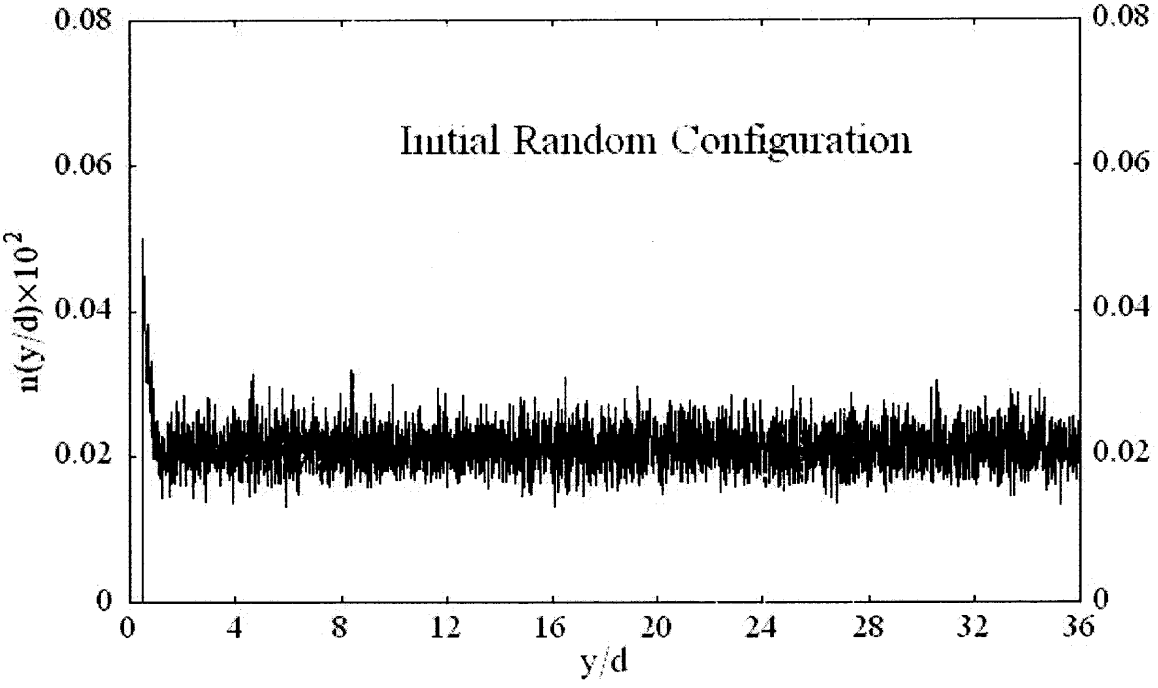

Figure 5.2 Vertical center distribution for random initial configuration from Monte Carlo simulation.

physical limitation that no particles could be placed lower than 0.5 *d*. A mean value $\bar{n}\left(y/d\right)=2.5\times10^{-4}$ corresponds approximately to the average number of of particles per layer for uniform initial distribution.

Following the Monte Carlo procedure described in Section 2.6, particles settled down to poured state (see Figure 2.4 b). The vertical center distribution of the poured state is shown in Figure 5.3. The highest particle is now located at $y_{\max}=22.3d$ in contrast to $y_{\max}=36d$ for random initial configuration, which reflects that the system has settled. The vertical center distribution contains a rather high peak near the floor, followed by three smaller peaks, all of which are characteristic of the local ordering effect of the plane floor. Although not reported in this dissertation, the formation of

hexagonal-close packing geometry was also seen from two-dimensional analysis of the layer of particles adjacent to the floor. For subsequent layers upwards from the 1st near the floor, (for instance, second and third), there is a weakly developed hexagonal structure, which was found experimentally and reported in 1969 by [16, 17]. Finally, the layers above $3.5d$ have a slightly noisy uniform distribution similar to that seen for random initial configuration. However, the mean value of vertical distribution $\overline{n}\left(y/d\right) \approx 4.5\times10^{-4}$ is significantly higher than the mean value of the random initial configuration since the particles were packed closer to each other.

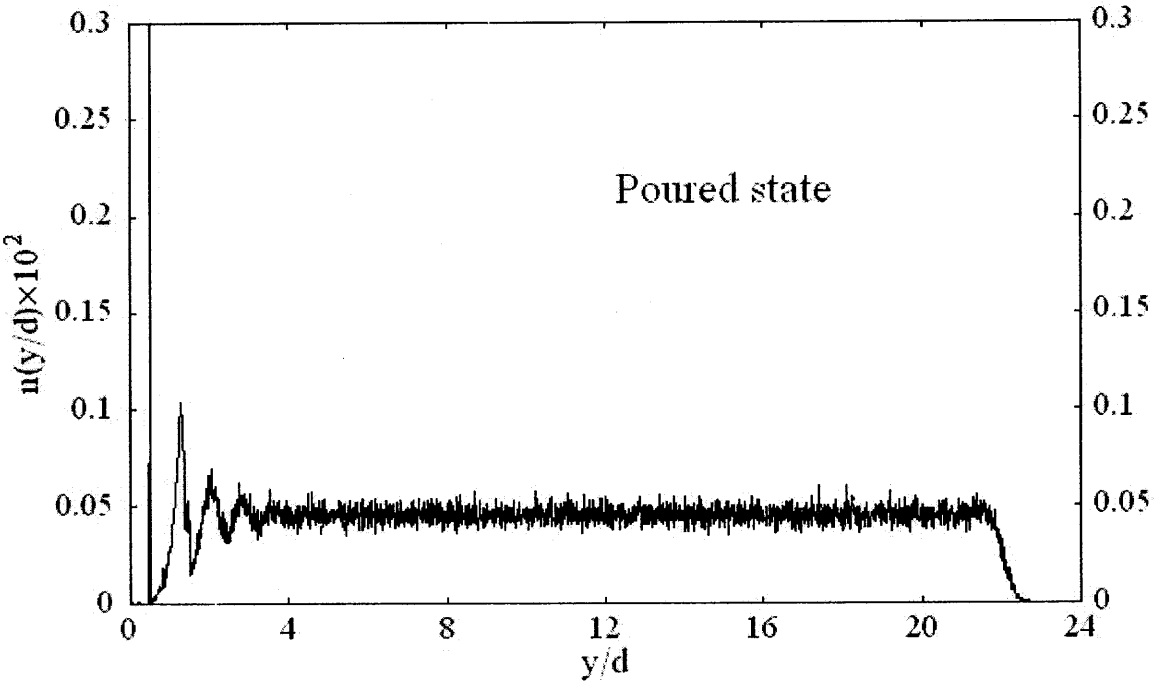

Figure 5.3 Vertical center distribution for a poured configuration for the system of 3,456 spheres.

As the tapping proceeds, the geometry of the bulk configurations becomes more and more organized and the vertical crystallization advances from the floor into the middle of the container. For the analysis that follows, Monte Carlo taps were done using a uniform lift equal to $0.25d$.

Two states of crystallization level are labeled - intermediate and ultimate. The intermediate state is characterized by the creation and slow progression of new peaks in vertical center distribution, which indicates the formation of newly ordered layers of particles at higher positions above the floor. As can be readily observed from Figure 5.4, for $N_T = 50, \langle \nu \rangle = 0.579$, four ordered layers near to the floor are in the process of being formed, while a disordered structure can be seen at the level roughly equal to four diameters. At $N_T = 250, \langle \nu \rangle = 0.597$, the particle arrangement shows evidence of the

formation of at least eight ordered layers and the disordered loose state "retreats" to 7.8 *d*. It is worth noticing that the magnitude of peaks is constantly growing which clearly indicates the "filling up" of the open spaces to establish a hexagonal-close packing geometry. The bulk solids fraction of this configuration is very close to the lower limit of random loose packings. At $N_T = 1000, \langle \nu \rangle = 0.617$ is identified as the beginning point of a transitional phase to the ordered microstructure for the entire bulk vessel. Here, we discern at least nineteen layers in which some ordered is evident, while the disordered state remains for heights from 14.5*d* to 21 *d* above the floor.

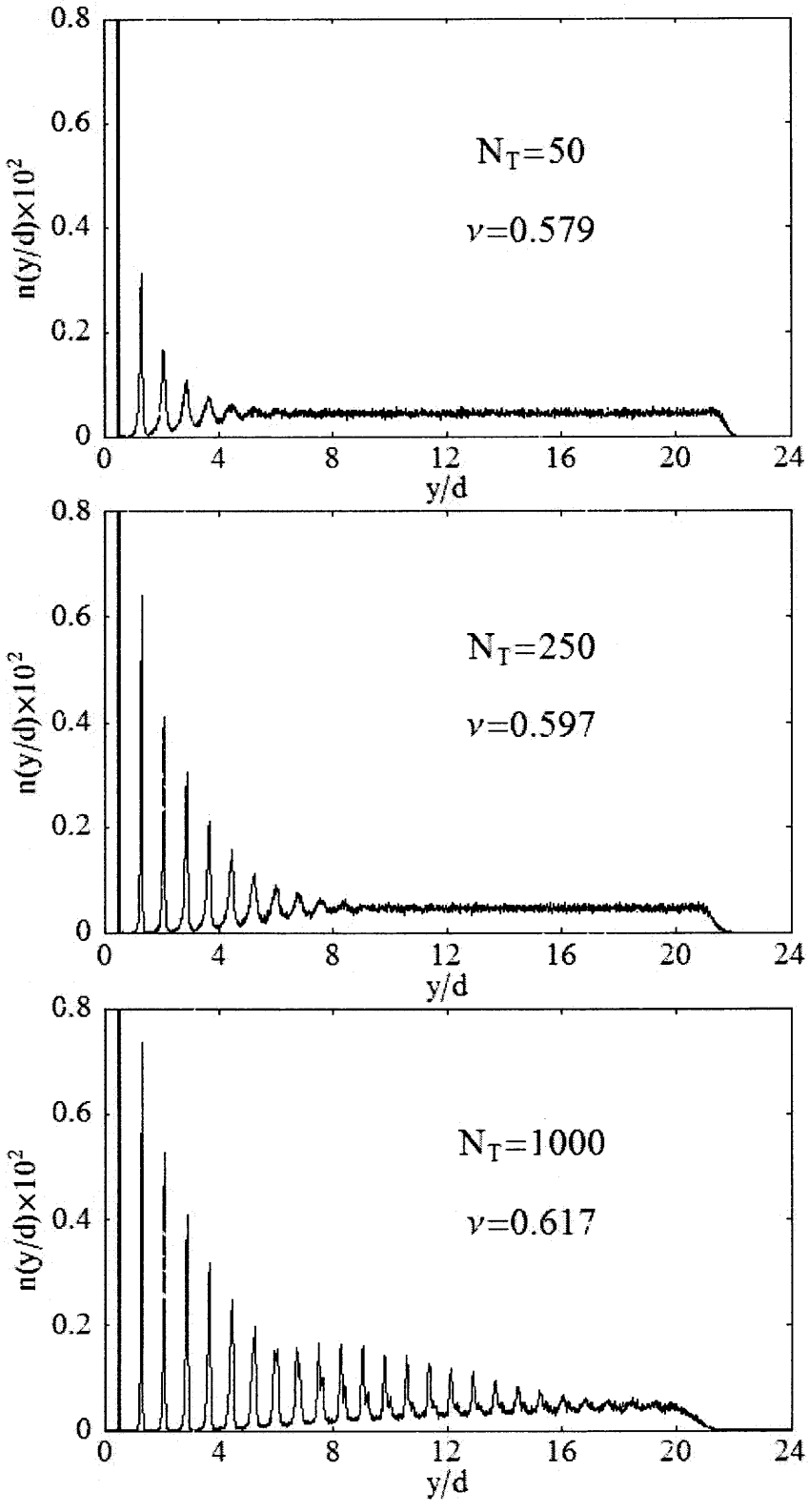

Figure 5.4 Progress of crystallization at the intermediate level of the tapping process.

The evolution of the vertical center distribution at the later stages in the simulation is shown in Figure 5.5. Here, the evolution could be characterized by the vanishing of the disordered layers from one side, and an expansion of the ordered structure into the bulk from the other side. For $N_T = 7,000, \langle \nu \rangle = 0.638$ the arrangement of spheres is largely associated with an ordered state. Higher peaks near the bottom (up to the height $6d$ from the floor) give very clear evidence that ordered layers are almost completely shaped and, an increase of the peak magnitude supports the idea that the last open holes are being filled up by spheres from upper layers; this organization proceeds further to the top with small divergence for the set of secondary peaks that are isolated from the primary peaks and are slightly lower in magnitude than the primary peaks. The emergence of the secondary peaks starting from $7d$ from the floor could be explained by the formation and development of secondary ordered configuration, the nature of which is yet unknown. As tapping further proceeds and the granular vessel tends to relatively dense ordered configurations at $N_T = 90,000, \langle \nu \rangle = 0.654$, the final geometry of the primary peaks becomes well-organized with intervals without intermediate layers of spheres (vertical center distribution is equivalent to zero). The secondary peaks become smaller and the secondary ordered geometry starts to vanish.

The evolution of the bulk solids fraction is given in Figure 5.6 and Figure 5.7. This shows the attainment of the microstructure development from random loose packing to a random close packing with a transition to the intensification of dense ordered configurations (as depicted on Figure 5.7). A fit of the bulk solids fraction as a function of tap to the slow inverse logarithmic law [88] is included in Figure 5.7.

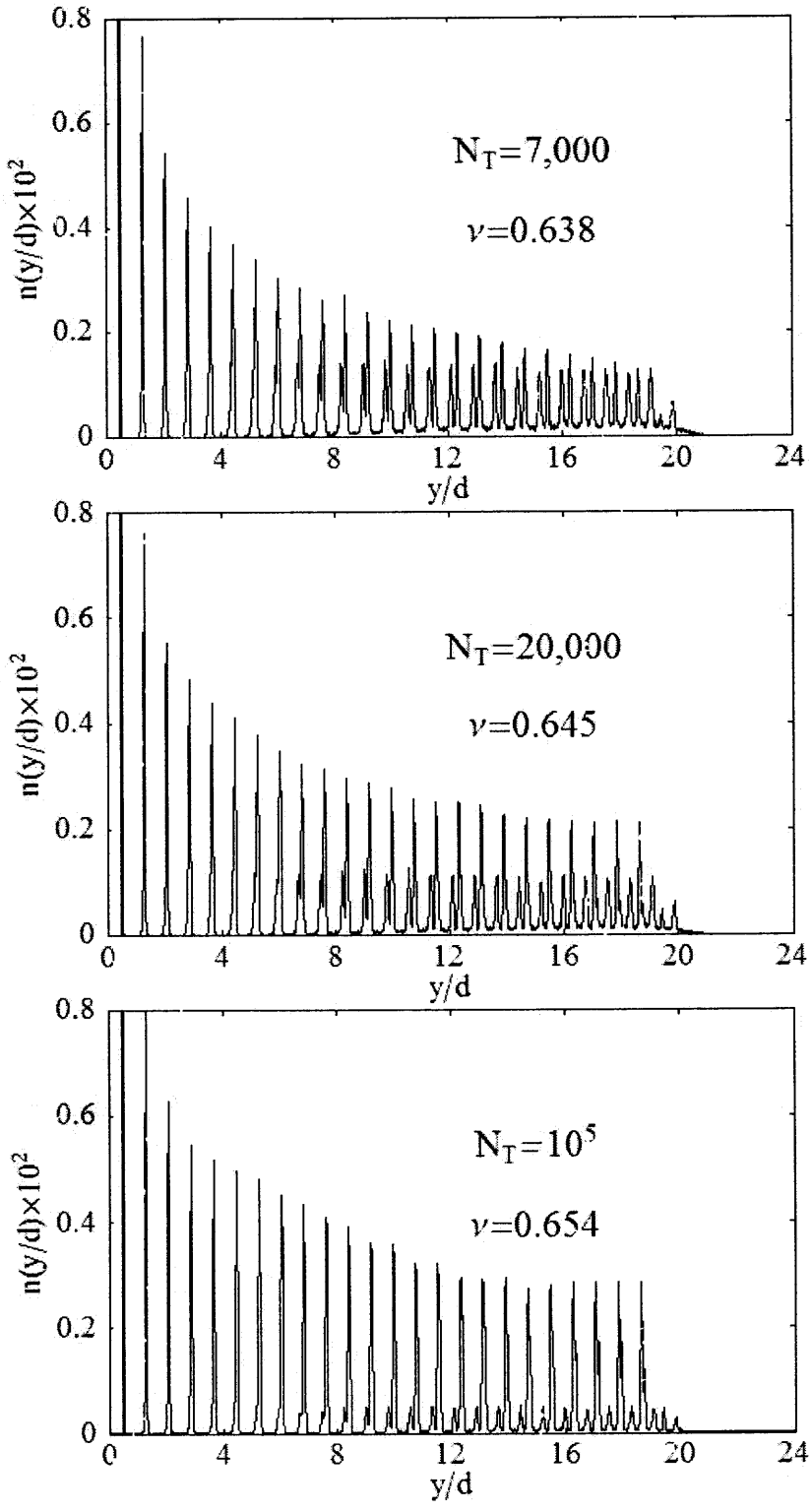

Figure 5.5 Progress of crystallization at the ultimate level of the tapping process.

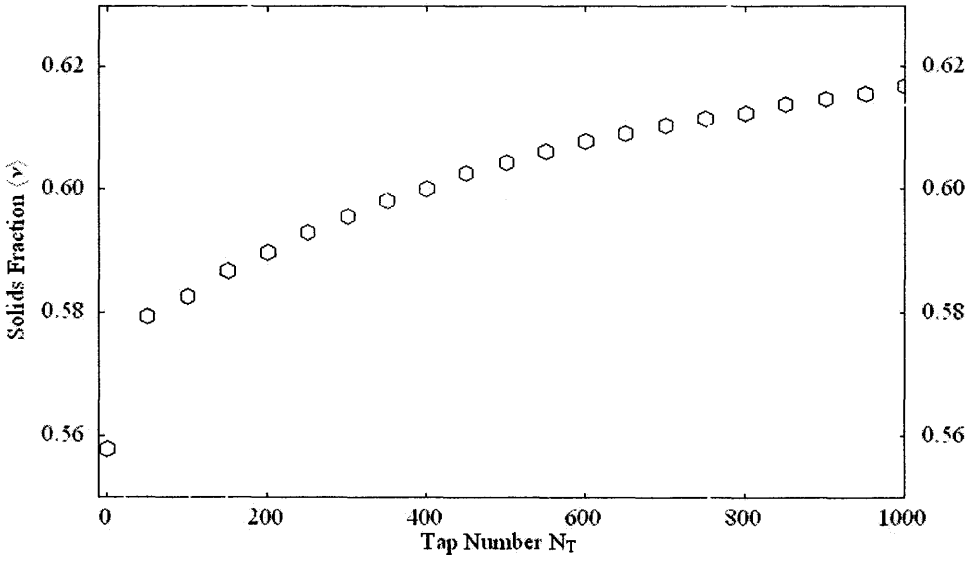

Figure 5.6 Evolution of the ensemble-averaged bulk solids fraction $\langle \nu(n) \rangle$ for lift intensity $\lambda = 0.25d$ for intermediate tap numbers $N_T = 1,000$. Each circle stands for the solids fraction at every 50 taps.

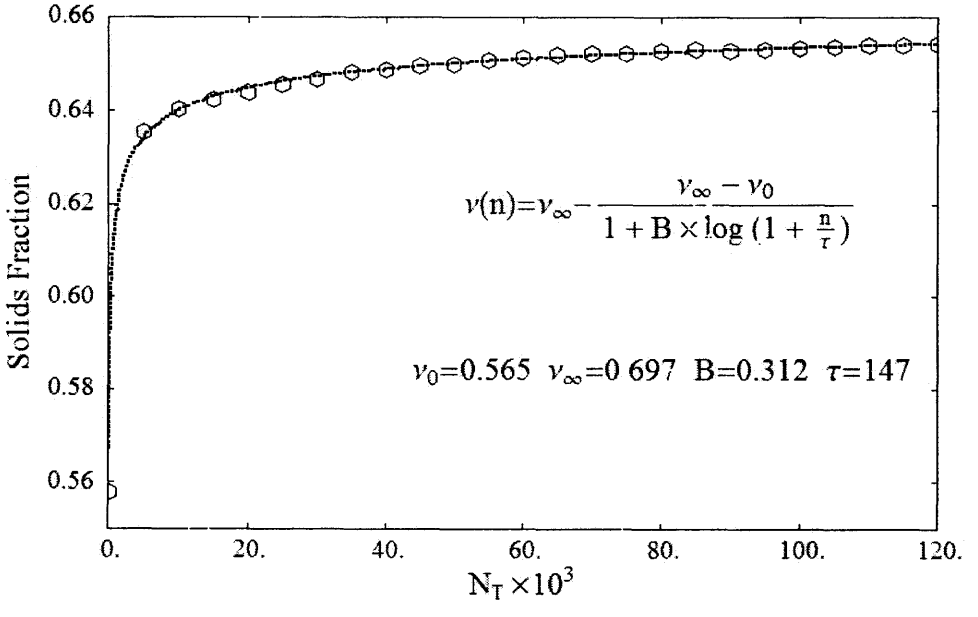

Figure 5.7 Evolution of the ensemble-averaged bulk solids fraction $\langle \nu(n) \rangle$ for lift intensity $\lambda = 0.25d$ for ultimate tap numbers $N_T = 120,000$. Each circle stands for the solids fraction at every 5,000 taps.

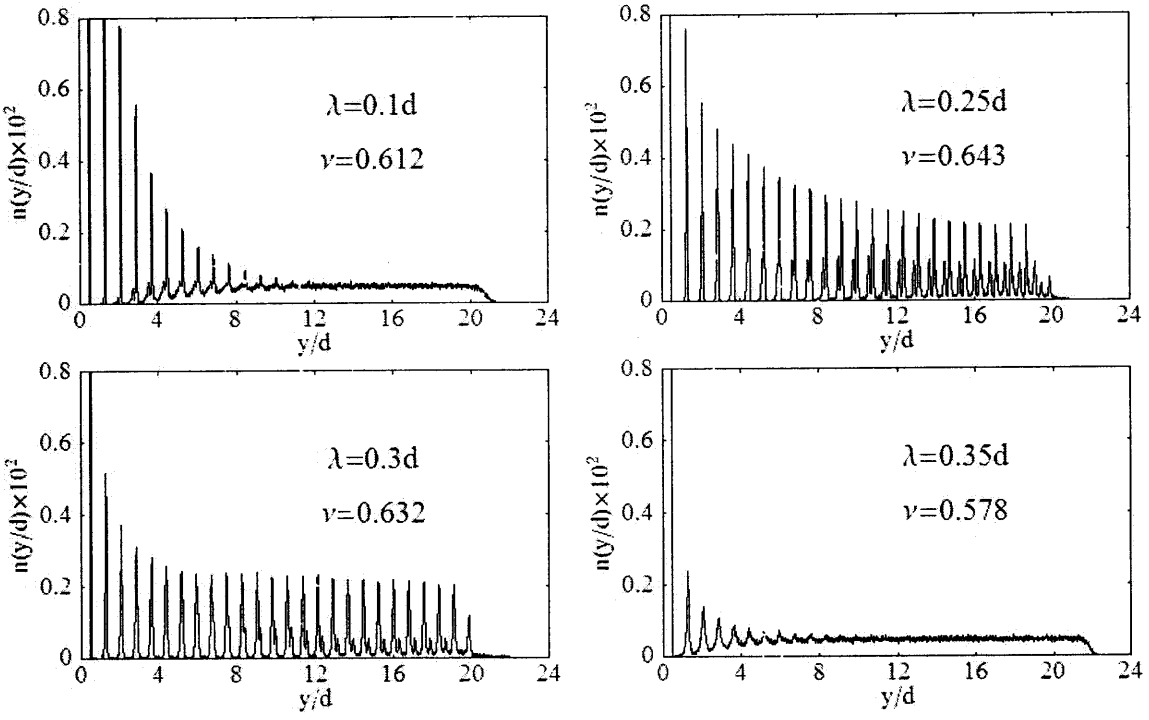

Figure 5.8 Vertical center distribution for various lift intensities at tap $N_T = 20{,}000$. Different lift intensities cause different crystal structure development.

In Figure 5.8 above, the influence of the energy input mechanism on crystallization progress is considered for different lift intensities (λ). As seen from the plot, crystal structure develops starting from the bottom to the top of vessel for modest $\lambda = 0.25d$ and $0.3d$, slowly propagates for small λ = $0.1d$, and almost stalls for an 'energetic' value λ = $0.35d$, for which a loose packing occupies most of the box.

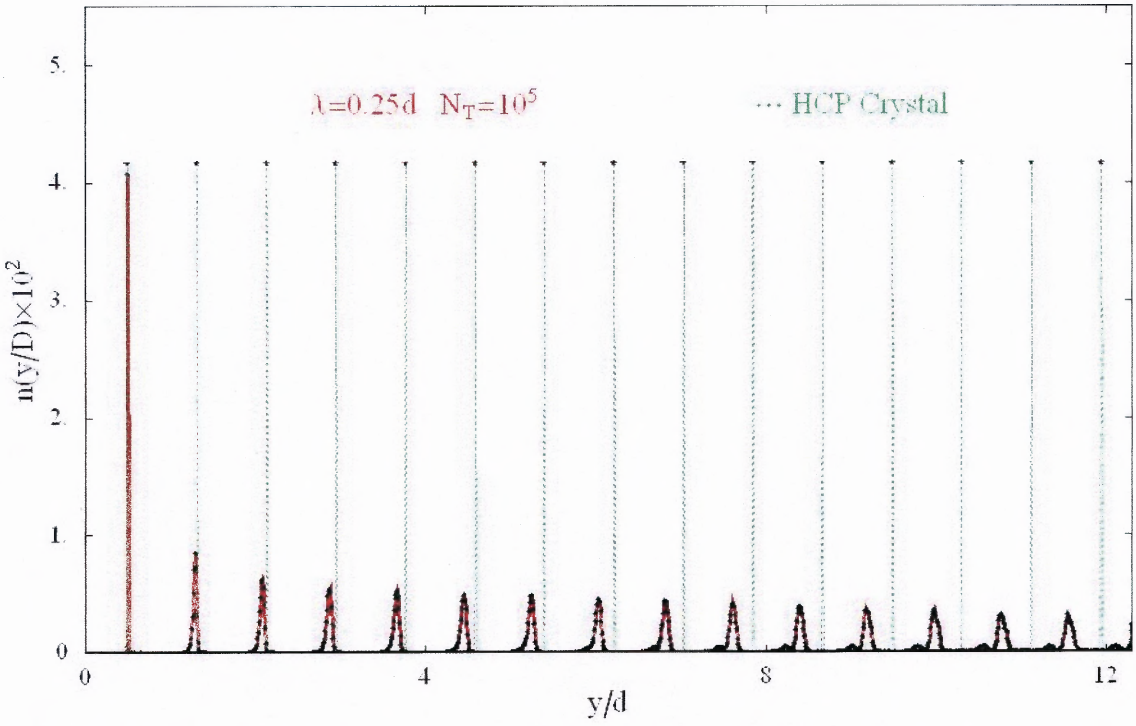

Figure 5.9 The comparison of the vertical center distribution for the MC configuration at $N_T = 10^5$ (plotted by thick red lines) and the hexagonal-close crystal packing (marked out by dash-dotted green lines). Both systems enclose 3,456 independent particles.

Figure 5.9 demonstrates the vertical center distribution from the Monte Carlo configuration at the final stage of the tapping process, i.e. at $N_T = 10^5$ and that of a hexagonal-close crystal structure (green lines). The positions of the vertical center distribution peaks of the bottom layers supports the existence of a HCP-like geometry of the ordered layers located near the floor. The magnitude of the peaks gradually diminishes for higher layers, which may be due to voidage between the layers. The nature of the further divergence of the MC configurations from hexagonal close-packing which occurs for the layers that are located higher than 4*d* from the floor remains a matter of further exploration.

Table 5.1 Summary of the energy input effect on crystallization propagation and solids fraction evolution for Monte Carlo method using uniform lift of the system.

Energy Input	Low	Moderate	High
Range of Lift Intensity λ/d	$0.1 \leq \lambda/d \leq 0.2$	$0.2 \leq \lambda/d \leq 0.33$	$\lambda/d > 0.33$
Solids Fraction Evolution	Very Slow densification $0.6 \leq \nu_{\infty} \leq 0.63$	Moderate densification $0.63 \leq \nu_{\infty} \leq 0.69$	Little compaction found $0.56 \leq \nu_{\infty} \leq 0.58$
Crystal Structure Propagation	Several layers adjoining to floor are "ordered"	All layers of the system are "ordered"	A few layers adjoining to floor are "ordered"
Loose Packing (LP)	LP slowly "retreats" to the top of the vessel, as tapping proceeds	LP is not found after $N_T > 20{,}000$	Most of the system layers have LP features

Table 5.1 summarizes the effect of different lift intensities λ on developed of structure in the system, in which three separate regions of the energy input are identified, depending on the lift intensity λ.

5.4 Vertical Center Distribution for Discrete Element Method

In this section we consider the vertical center distribution evolution of a system containing 3,456 monodisperse particles of diameter $d = 0.02\text{m}$, The particles initially are randomly packed into a box of size ($12d \times 48d \times 12d$) with periodic boundary conditions in x and z directions; subsequently they settle down to poured undisturbed bed with fill height $H/d = 20.7$. Then the containment vessel is subject to the intermittent harmonic oscillations of the floor as described in Section 4.3 and depicted in Figure 4.1. The vibration parameters are as follows: amplitude $b/d = 0.35$, frequency of oscillations

$\omega = 47.12\text{Hz}$. These parameters yield a dimensionless acceleration $\Gamma = 2.03$. The duration of one tap cycle is $t_b = 0.0667\,\text{sec}$. The relaxation time $t_p = 0.3\,\text{sec}$ is chosen to ensure that kinetic energy of the particles is nearly equal to zero. The vertical center distribution statistics are averaged over ten consecutive taps to minimize noise.

How does the crystal propagation occur for Discrete Element Method simulation? The vertical center distribution dependence shown in Figure 5.10 and Figure 5.11 is very similar to the analogous results from the Monte Carlo simulations with regard to the development of an 'ordered' structure. There is a similar arrangement of the ordered layers adjacent to the floor for the early stages of tapping. As the tapping continues, crystallization of the spheres advances from the floor as the initial random loose configuration is transformed to an 'ordered' packing. The maximum vertical coordinate of the spheres at the top $y_{\max}$ is lowered as the packing becomes more dense.

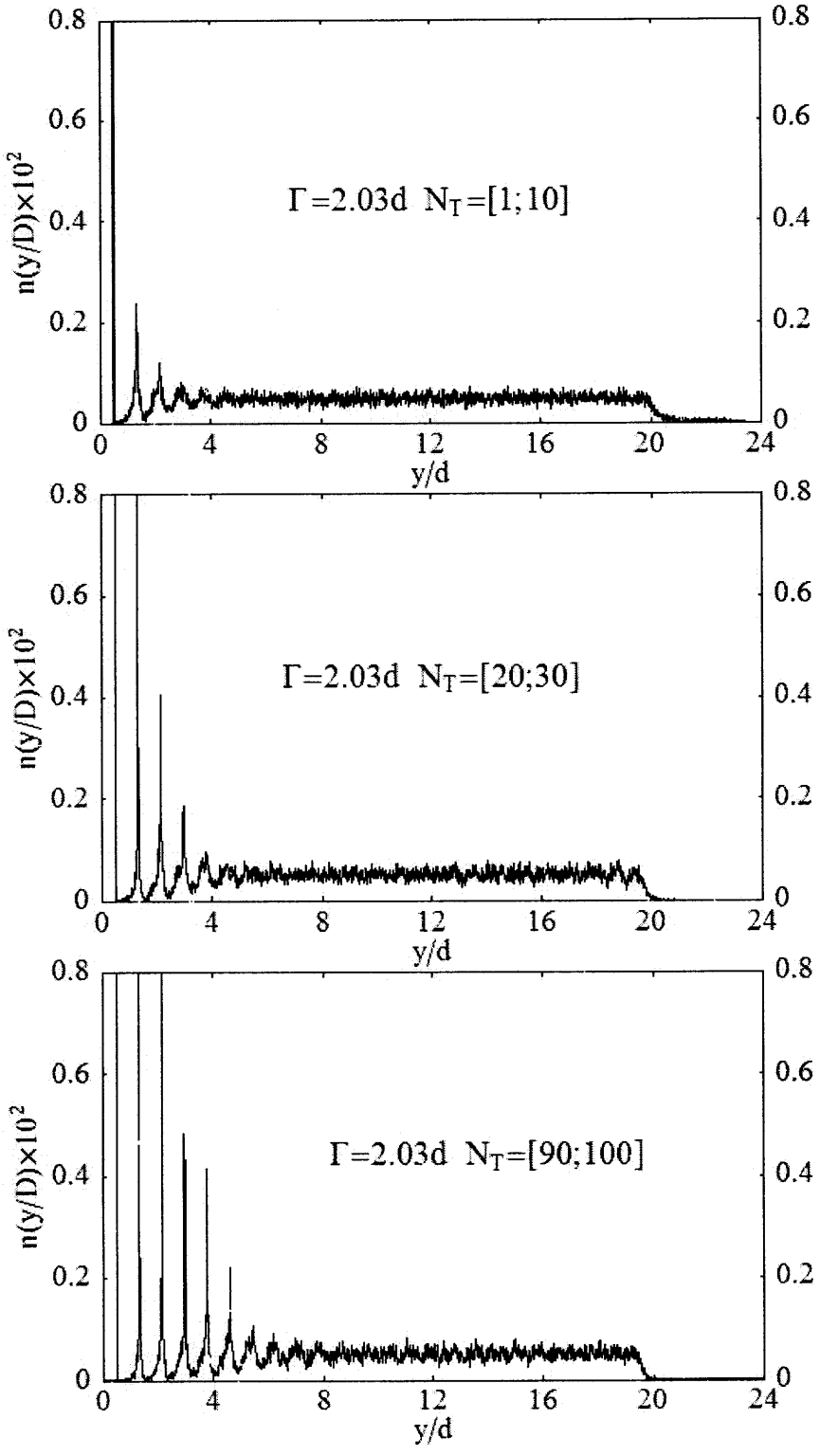

Figure 5.10 Crystallization at the early tapping levels for DEM simulation.

In spite of the qualitative similarities found for propagation mechanism in the Monte Carlo and Discrete Element simulations, a number of differences between them could be observed as well. First, the level of the peaks for the ordered layers is much higher for the DEM as compared with the MC simulation (see Figure 5.11). For instance, the maximum values of $n\left(y/d\right)$ for the second and third layers near to the floor $n\left(y_2/d\right)\Big|_{DEM} = 2.7\times10^{-3}$, $n\left(y_3/d\right)\Big|_{DEM} = 3.14\times10^{-3}$ are considerably higher for Discrete Element Method than for the relevant values for Monte Carlo simulation $n\left(y_2/d\right)\Big|_{MC} = 0.92\times10^{-3}$, $n\left(y_3/d\right)\Big|_{MC} = 6.34\times10^{-4}$. Secondly, the dynamics of propagation and structural reorganization are rather distinguishable. In contrast with Monte Carlo, the DEM vertical center distribution is exceptionally inhomogeneous with perceptibly separated regions of random loose structure in the heap of the vessel and clearly developed hexagonal-close packings close to the floor, and the limiting boundary at $11d$ for the state at $N_T \in [990,1000]$. The third obvious distinction is the presence of particle centers in the intervals between peaks for layers adjacent to the floor $(d \le y \le 5d)$. This effect may be due to the effect of the inter-particle friction that creates the contact bridge networks of the touching particles.

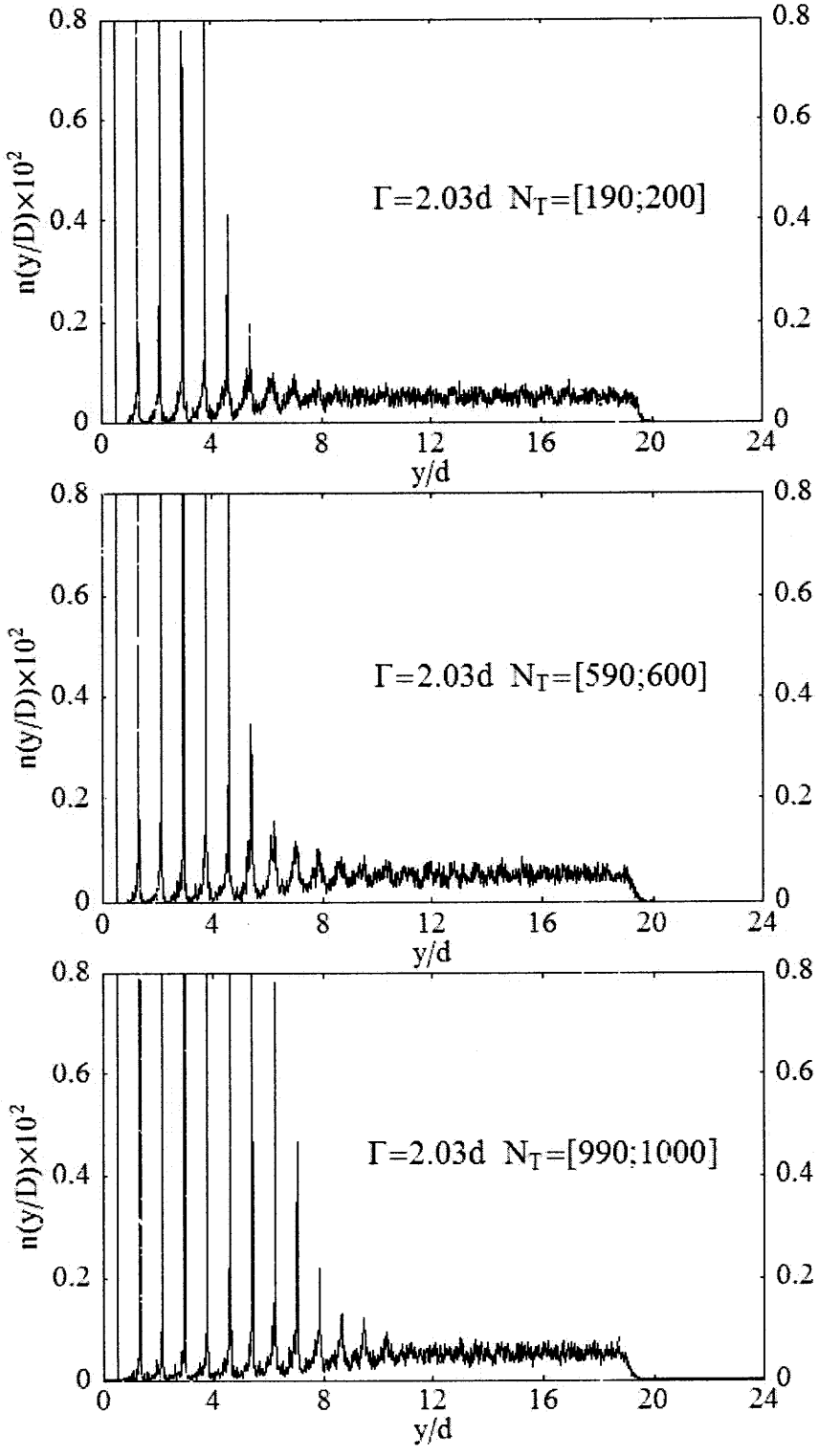

Figure 5.11 Crystallization at the middle and ultimate tapping levels for DEM simulation.

Figure 5.12 illustrates the average vertical center distributions of the tapping process at $N_T \in [990,1000]$ as compared with a hexagonal-close crystal structure (dashed blue lines). The locations of the vertical center distribution peaks strongly supports the hypothesis of the formation of the HCP-like geometry of the ordered layers located near the floor. It is worth noticing that the magnitude of the peaks steeply drops down for higher layers. This plunge in vertical center distribution may be due to the presence of voidage between hexagonally-close packed layers. It is remarked that the box geometry and the dimensions chosen for these simulations are not commensurate with that of a HCP crystal.

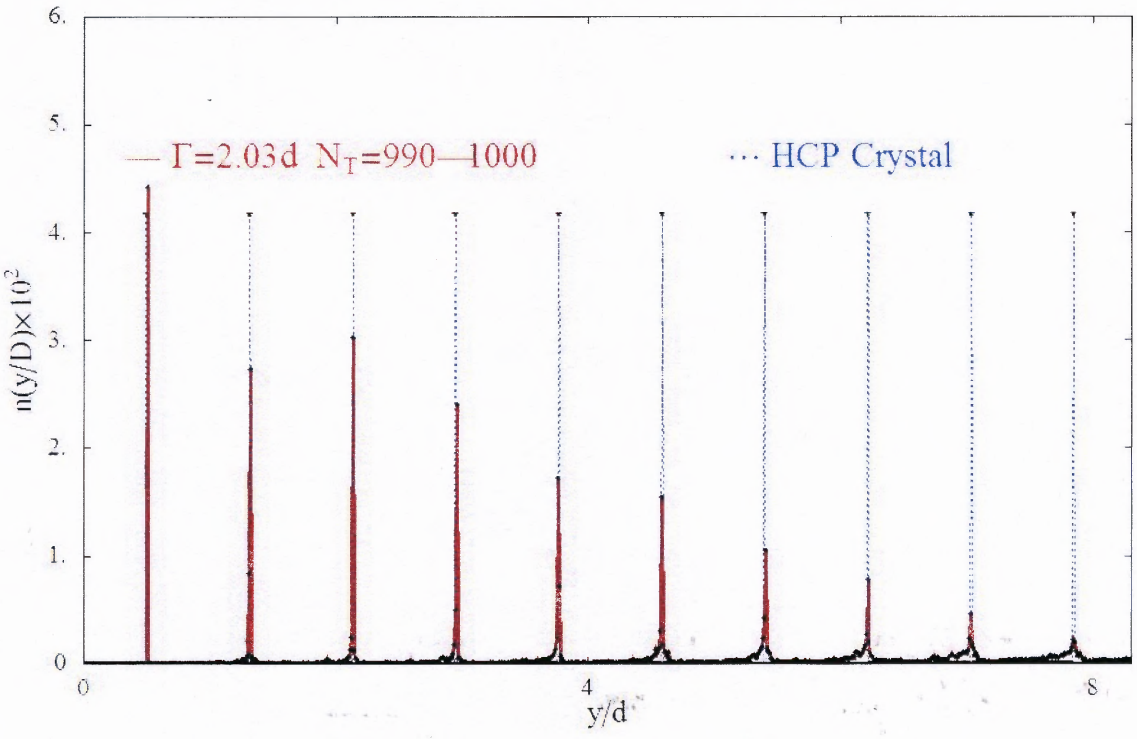

Figure 5.12 The comparison of the vertical center distribution for the system that corresponds to DEM configuration at $N_T = [990;1,000]$ (plotted by thick red lines) and the hexagonal-close crystal packing (marked out by dash-dotted blue lines). Both systems enclose 3,456 independent particles.

CHAPTER 6

CONCLUSIONS AND FURTHER WORK

6.1 Conclusions

Numerical simulation techniques (Monte Carlo and Discrete Element Method) were used to examine the density relaxation process arising from discrete taps applied to a granular material consisting of monodisperse hard spheres within a laterally periodic computational volume. In the MC simulations, which essentially use the Metropolis algorithm to generate stable configurations, the effect of a tap applied to the system is modeled using two different approaches: (1) application of the vertical position-dependent displacements to the particles (the so-called linear expansion) at intensity γ, and (2) uniformly lifting of the entire granular vessel on a small displacements above the supporting floor. For both methods the Metropolis algorithm was adapted so that motions which increase the system potential energy occur very rarely. Although not documented in this dissertation, the application of random lateral displacements in conjunction with the vertical expansion produced no effect on the final outcome. In order to accelerate the process and avoid trapping at local minima, the size of the neighborhood in which a particle is allowed to move was dynamically reduced as the system density increased. Also for both methodologies with tap intensity γ and lifting intensity Δ, the equilibrium value of the bulk solids fraction $\langle \nu(n) \rangle$ at tap n was computed as an ensemble average over a sufficient number of realizations to ensure a standard deviation of less than 0.001.

It was found that both methods resulted in an increase in the system density after many thousands of taps. Furthermore, we report that more dense systems were created at smaller tap and lifting intensities, but this was at the expense of an increasingly growing number of taps to reach equilibrium.

The following outcomes for the simulation using the linear expansion technique (1) were found. The evolution of the simulated data fit well to a hyperbolic tangent model of the form $\nu(n;\gamma)=\nu_0(\gamma)+[\nu_\infty(\gamma)-\nu_0(\gamma)]\tanh(A(\gamma)n)$ for tap intensities $1.2\le\gamma\le1.5$. For these energetic taps, poor correlation between the inverse log model $\nu(n)=\nu_\infty-\frac{\nu_\infty-\nu_o}{1+B\log(1+n/\tau)}$ and the simulation data was found because equilibrium was attained more rapidly than could be accommodated by this functional form. However, at smaller intensities that roughly corresponded to the magnitudes of the tap accelerations used in experiments [88], the inverse log model was consistent with the data. The fit of the data to this model and to the form $\nu=\nu_\infty-\frac{\nu_\infty-\nu_o}{1+Dn}$ indicated that the ratio $D\sim B/\tau$ is a relevant parameter for low tap intensities. A fit to the stretched exponential $\nu(n)=\nu_\infty-(\nu_\infty-\nu_o)\,e^{-(n/\tau)^\beta}$ showed reasonably good agreement with the data, albeit neither τ nor τ^β exhibited an expected decrease with intensity γ compatible with a time scale parameter.

Quantification of the microstructure via the radial distribution function $g(r/d)$ revealed local crystalline order consistent with a hexagonal-close packing crystal structure. In the densest tapped configuration $\nu_\infty=0.675$, a power-law singularity in $g(r/d)$ near $r/d=1$ was found, while at the lowest tapped solids fraction $\nu_\infty=0.583$,

the appearance of a double peak for $1.8 < r/d < 2.0$ resembled that seen in experiments and molecular dynamics simulations in the literature. The behavior of the mean coordination number, computed from the near-neighbor distributions, as a function of the equilibrium bulk solids fraction was found to be in good agreement with experimental measurement in the literature.

However, method (1) was exhibited a strong dependence of the final system density on the fill height, which has not been experimentally reported in the literature. On the other hand, this dependency was not seen when the expansion of type (2) was used. The MC evolution of the bulk solids fraction here was also found to be in qualitative agreement with an inverse log form that has been reported in the experimental literature. The simulated results illustrated that the bulk density is related to amount of the lift in method (2), with a critical value producing the most favorable results. Quite striking is the finding that as the taps evolve, the particles self-organize into quasi-crystalline layers, initiated by the planar floor.

Granular dynamics studies were performed using deterministic Discrete Element simulations, which employed force models of Walton and Braun [53] for uniform, inelastic, frictional soft spheres. The equations of motion were numerically integrated to obtain the coordinates and velocities of the particles. The container with confined granular material was tapped via a series of harmonic intermittent oscillations applied to the floor. After each tap, particles 'sediment' down under gravity and the system configuration finds its local potential energy minimum. The maximum vertical displacements of the particle layers showed a clearly nonlinear behavior (as a part of wave propagation through granular matter observed in the literature [157-159]) of the bed

expansion. Although (as expected), the response to the tapping for the MC simulations was not the same as for the discrete element simulations, the same type of self-organization into quasi-crystalline layers (first identified in the MC simulations) was found in the discrete element results. This supports the conjecture that this may be a universal mechanism of the density relaxation process.

6.2 Further Work

The product of this dissertation opens a fruitful area for complementary exploration of crystallization in granular systems. Some possible directions for further work are present below.

1. The author would like to encourage the examination by Monte Carlo Simulation of the nonlinear maximum vertical displacement that was the response to the harmonic oscillations (see Figure 4.4).
2. It would be particularly interesting to understand the ordered origin of the secondary peaks of the distribution of centers in y-direction seen for several cases for Monte Carlo simulation (for instance, Figure 5.5).
3. Using both simulation techniques, starting with a dense crystal structure, energetic taps should be applied to destroy the configuration in attempt to produce randomness.
4. The analysis of the correlation of the number of Monte Carlo steps per particle required to reaching equilibrium (given by Equation 2.7) and the average number of sphere collisions in the discrete element simulations appears to be very

promising. Moreover, it is suggested that analyses are made of the motions of a particles for both the Monte Carlo and Discrete Element simulations.

5. Perhaps a correlation could be made between the number of rejections by the overlap detection subroutine in the Monte Carlo and number of particle collisions with the relaxation time t_p in the discrete element simulations.
6. Further discrete element simulations could be done by using different tapping strategies (i.e., a uniform lift followed by gravity settling).
7. A detailed parameter study using discrete element simulations of the effects of taps of various intensities should be done (by varying amplitude, frequency and acceleration). As a first step, an analysis (i.e., Buckingham-Pi) should be done to identify governing dimensionless groups.

APPENDIX A

HEURISTIC DERIVATIONS OF THE INITIAL VALUE OF δ BASED ON FREE VOLUME APPROXIMATION

The choice of the initial value of the radius δ_0 of the hemisphere environment where a particle may be randomly displaced is justified by following heuristic derivations. First, the solids fraction $\bar{v}$ and voidage ε of the system of particles are defined as follows:

$$\bar{v} = \frac{V_{particles}}{V_{total}} \Rightarrow \varepsilon = 1 - \bar{v} = \frac{V_{free}}{V_{total}}$$

Then we define the volume of environment sphere (of diameter D) inside which the particle can move and the volume of a particle (of diameter d) as follows:

$$\begin{cases} V_{part.} = \dfrac{\pi d^3}{6} \\ V_{env.} = \dfrac{\pi D^3}{6} \end{cases}$$

This yields the free-volume between the particles as:

$$V_{free} = \frac{\pi}{6}\left(D^3 - d^3\right)$$

Now the relationship between D and solids fraction $\bar{v}$ becomes:

$$\frac{V_{free}}{\left(\frac{\pi D^3}{6}\right)} = 1 - \left(\frac{d}{D}\right)^3 = 1 - \bar{v} \Rightarrow \bar{v} \cong \left(\frac{d}{D}\right)^3 \Rightarrow D \cong \frac{d}{\sqrt[3]{\bar{v}}}$$

Since $\delta = \dfrac{D-d}{2} = \dfrac{1}{2}\left(\dfrac{d}{\sqrt[3]{\bar{v}}} - d\right) = r\left(\dfrac{1}{\sqrt[3]{\bar{v}}} - 1\right)$ the relationship between D and δ becomes:

$$\frac{\delta}{r} = \frac{1}{\sqrt[3]{\bar{v}}} - 1$$

Thus, for $\bar{v} = 0.58$ the initial δ is given as $\delta \approx 0.2r$, where r is the particle radius in comparison to the initial $2r$ used in current simulations. However, the higher value of δ chosen doesn't influence on the formation of the ordered structure in the system.

APPENDIX B

VERTICAL CENTRAL DISTRIBUTION FOR CRYSTALS

The distribution of the number of spherical centers for four crystal structures - hexagonal close packings (HCP), cubic (CCC), face-centered cubic (FCC) and body-centered cubic (BCC) - are considered. The first peak is located at $0.5d$, which exactly corresponds to the floor layer of spheres. The next peaks are equidistant from each other according to the periodic structure of each particular crystal.

1) Cubic crystal
Total number of particles: 1,728

$$\nu^{CCC} = 0.5236$$

$$\bar{N}_C = 6$$

$$F_{ij}^{CCC} = \begin{bmatrix} 1/3 & 0 & 0 \\ 0 & 1/3 & 0 \\ 0 & 0 & 1/3 \end{bmatrix}$$

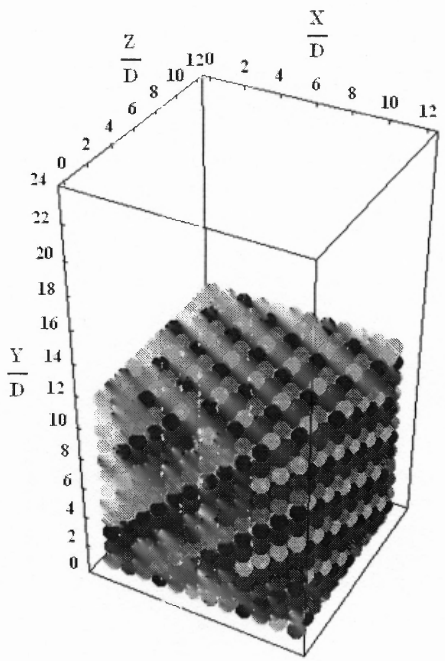

Figure B.1 Schematic representation of cubic crystal

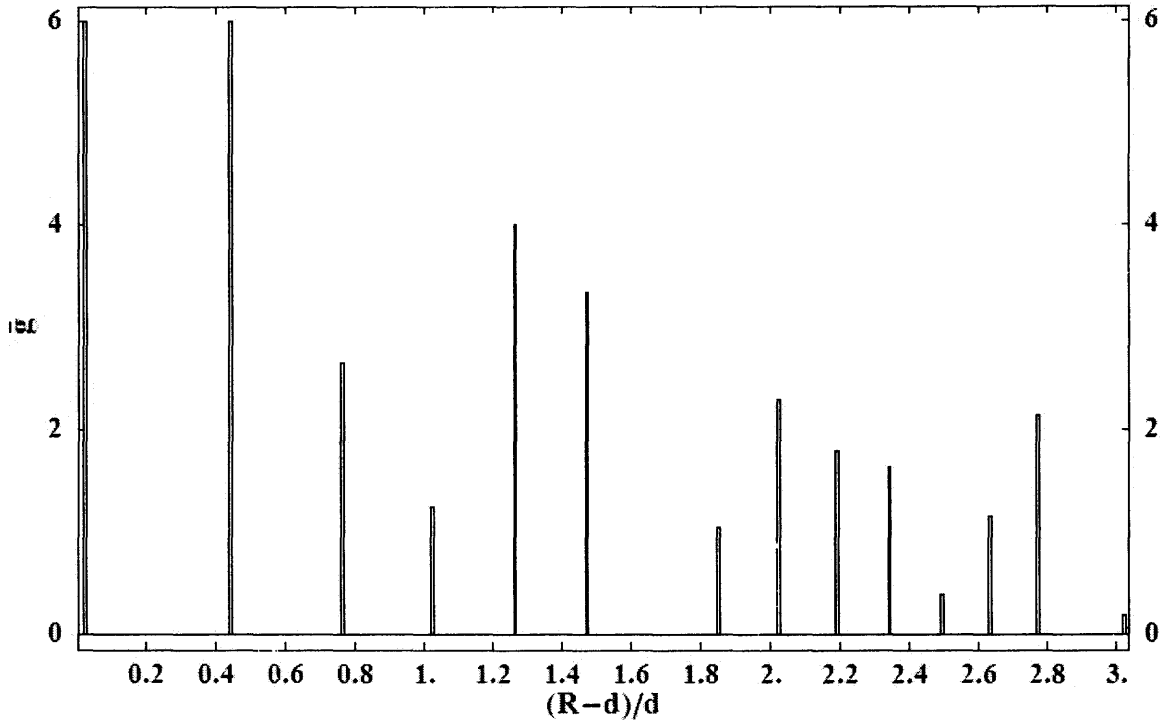

Figure B.2 The generalized radial distribution function for cubic crystal.

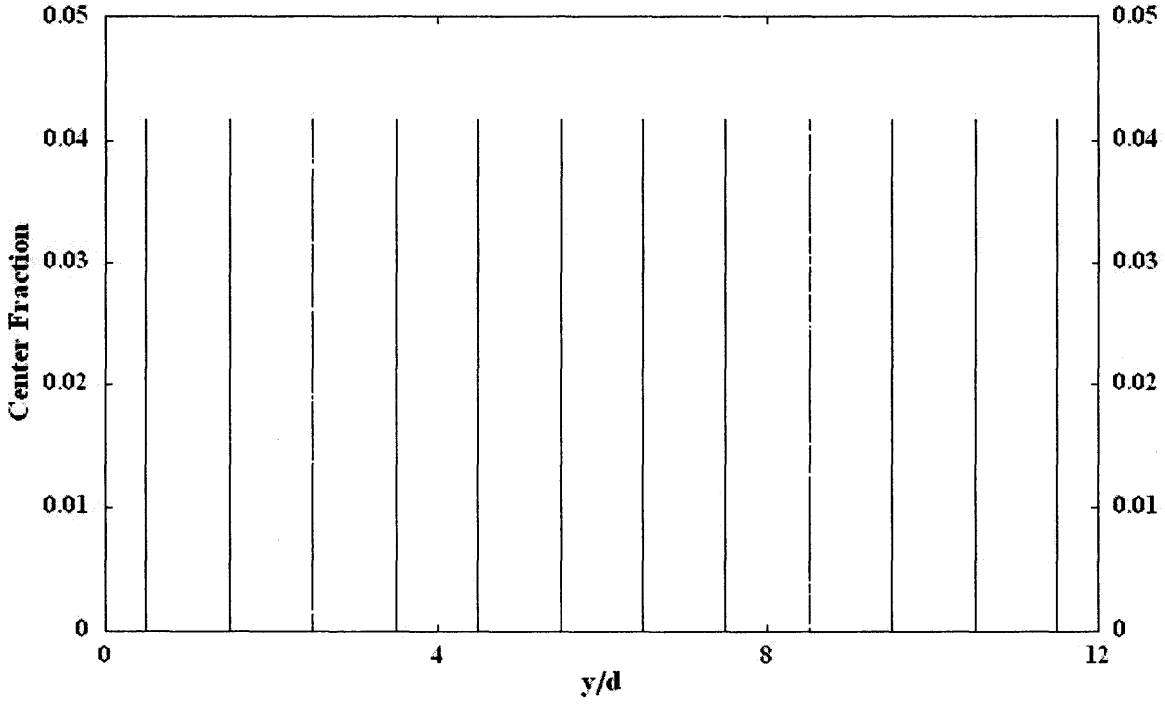

Figure B.3 The vertical center fraction distribution for cubic crystal (distance between each peaks equals to *d*)

2) Face-centered cubic crystal

Total number of particles: 6,336

$$v^{FCC} = 0.7405$$

$$\bar{N}_C = 12$$

$$F_{ij}^{FCC} = \begin{bmatrix} 1/3 & 0 & 0 \\ 0 & 1/3 & 0 \\ 0 & 0 & 1/3 \end{bmatrix}$$

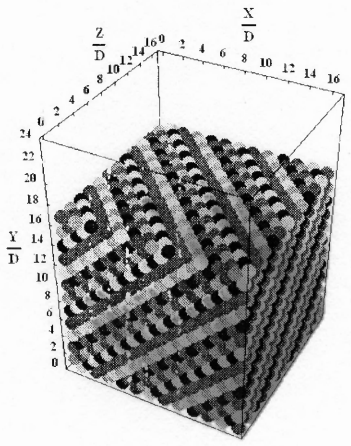

Figure B.4 Schematic representation of face-centered cubic crystal

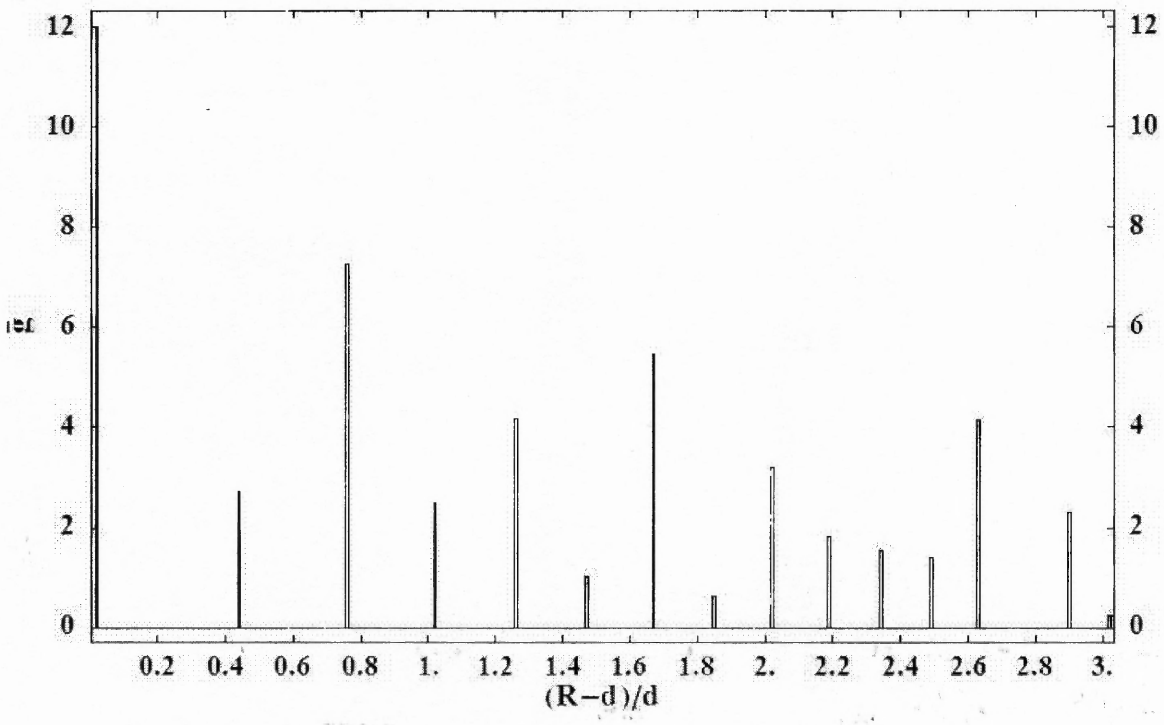

Figure B.5 The generalized radial distribution function for face-centered cubic crystal.

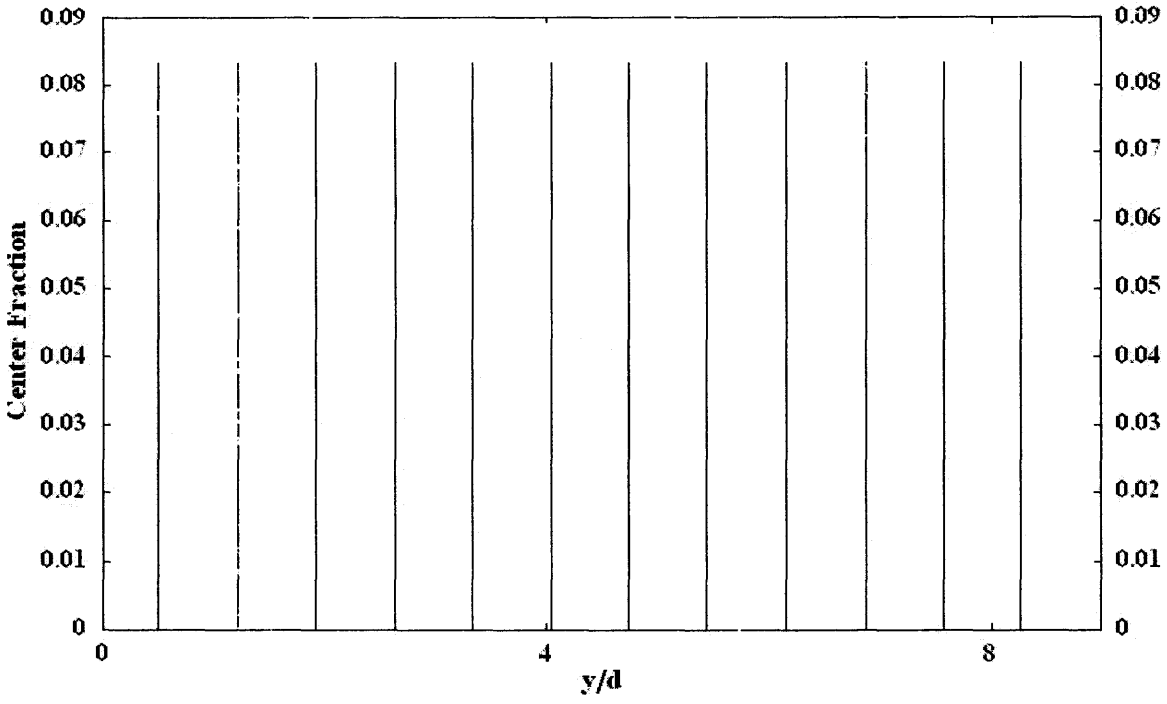

Figure B.6 The vertical center fraction distribution for face-central cubic crystal (distance between each peaks equals to ~0.71*d*)

3) Body-centered cubic crystal:

Total number of particles: 1,728

$$\nu^{BCC} = 0.68$$

$$\bar{N}_C = 8$$

$$F_{ij}^{BCC} = \begin{bmatrix} 1/3 & 0 & 0 \\ 0 & 1/3 & 0 \\ 0 & 0 & 1/3 \end{bmatrix}$$

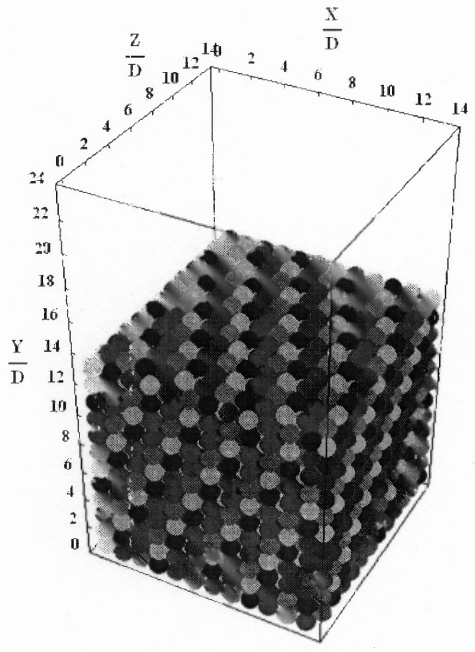

Figure B.7 Schematic representation of body-centered cubic crystal

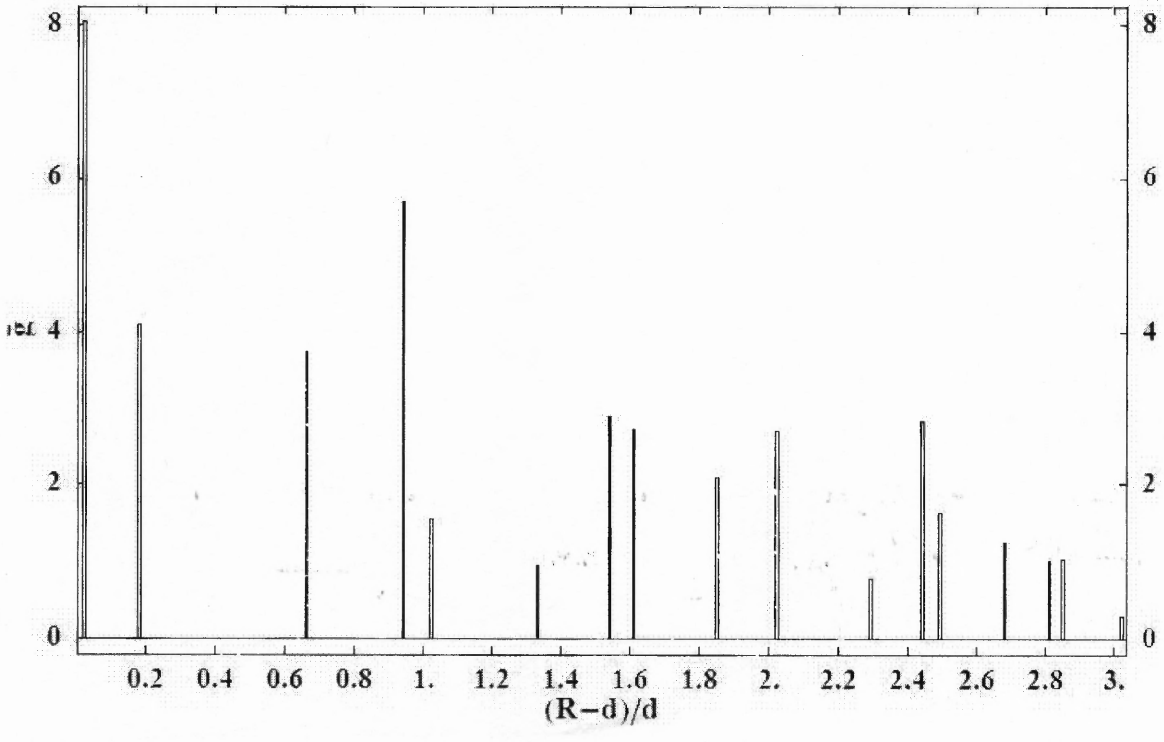

Figure B.8 The generalized radial distribution function for body-centered cubic crystal.

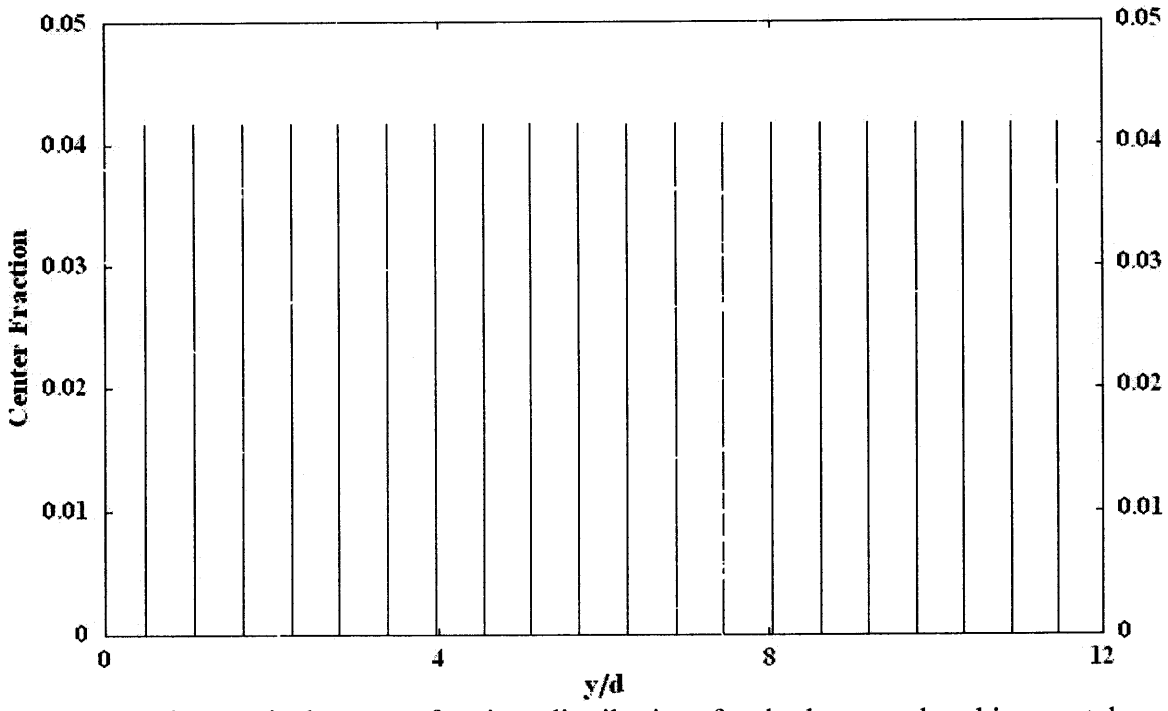

Figure B.9 The vertical center fraction distribution for body-central cubic crystal (distance between each peaks equals to ~0.58*d*)

4) Hexagonal close packing:

Total number of particles: 3,456

$$\nu^{BCC} = 0.7405$$

$$\overline{N}_C = 12$$

$$F_{ij}^{BCC} = \begin{bmatrix} 1/3 & 0 & 0 \\ 0 & 1/3 & 0 \\ 0 & 0 & 1/3 \end{bmatrix}$$

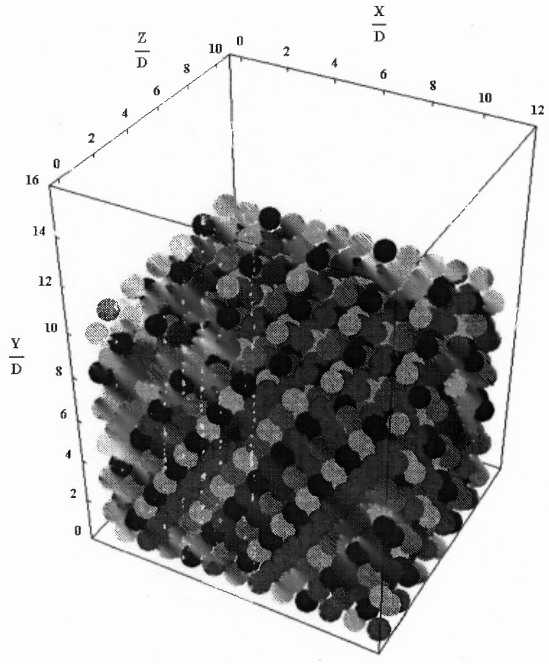

Figure B.10 Schematic representation of hexagonal-close packing

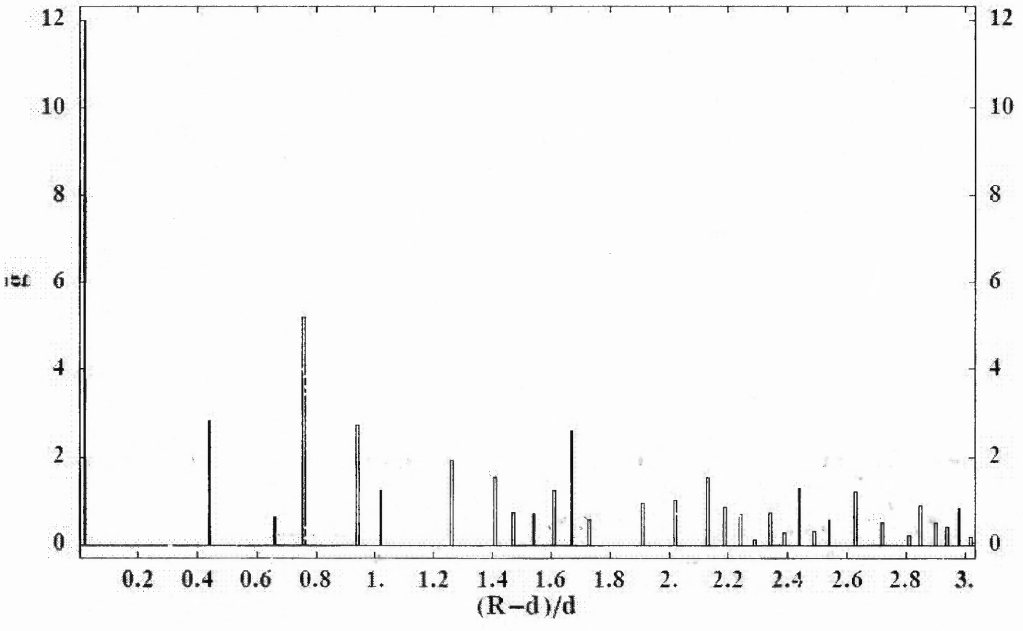

Figure B.11 The generalized radial distribution function for hexagonal-close packing

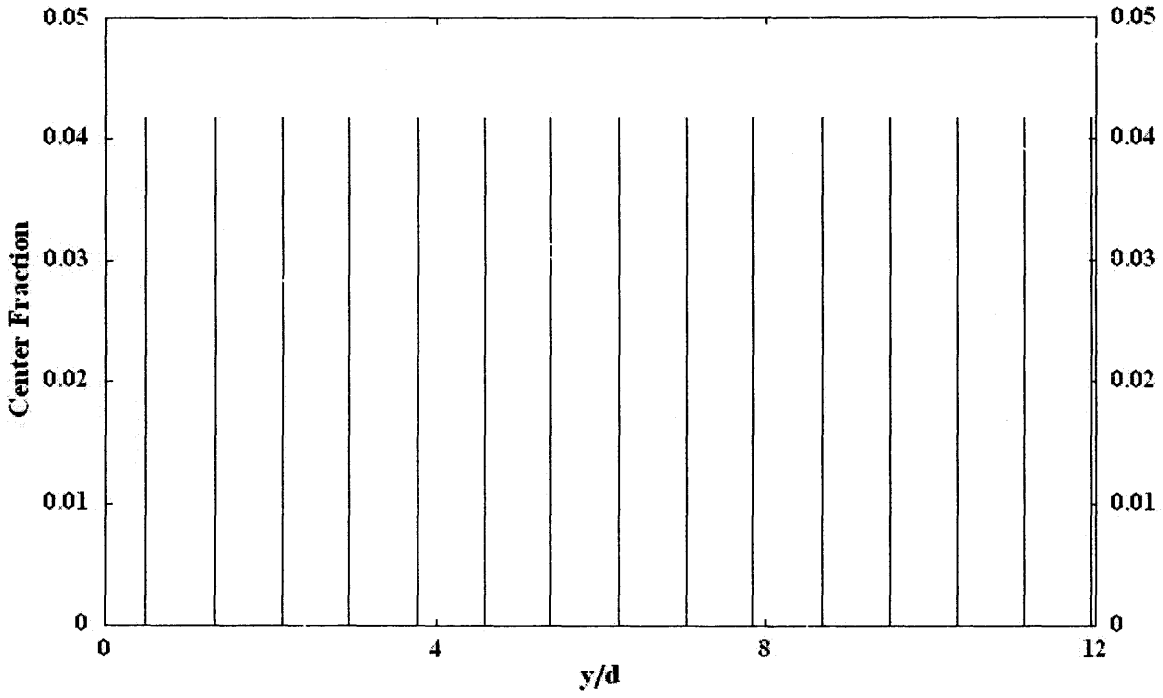

Figure B.12 The vertical center fraction distribution for hexagonal close packing crystal (distance between each peaks equals to ~0.82*d*)

APPENDIX C

DERIVATIONS OF THE GENERALIZED RADIAL DISTRIBUTION FUNCTION (RDF)

In this Appendix, a formula to compute the radial distribution function of spherical particles is given.

Number of particles $N(r)$ inside a spherical layer (r-Δr; r+Δr) is (See Fig. C):

$$N(r) := N(r-\Delta r; r+\Delta r)$$

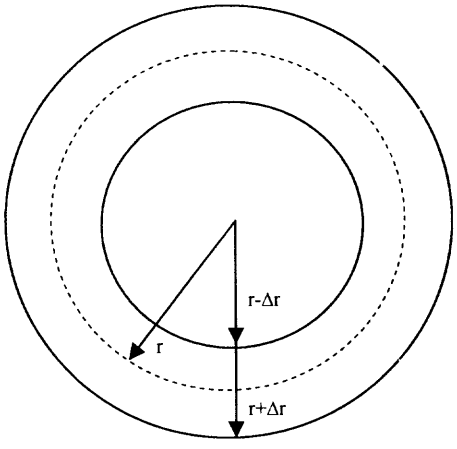

Figure C Spherical centers within a spherical layer of the thickness 2Δr that were counted to obtain radial distribution function.

Radial Distribution Function $g(r)$ is defined as:

$$g(r) := \frac{N(r)}{4\pi r^2 \Delta r}$$

Generalized radial distribution function $\overline{g}(r)$ could be expressed as follows:

$$\overline{g}(r) := \frac{g(r)}{\overline{\rho}} = \frac{N(r)}{4\overline{\rho}\pi r^2 \Delta r}$$

The physical term of bulk density is defined as number of particles inside some volume divided by the total volume:

$$\bar{\rho} := \frac{N(r)}{V_{tot}}$$

which is related with packing fraction $\bar{\nu}$:

$$\bar{\nu} = \frac{V_p}{V_{tot}} = \frac{N(r) \times \left(\frac{\pi}{6} d^3\right)}{V_{tot}}$$

as:

$$\bar{\rho} = \frac{6\bar{\nu}}{\pi d^3}$$

Therefore, the generalized radial distribution function $\bar{g}\left(\frac{r}{d}\right)$ could be written in the form of:

$$\bar{g}\left(\frac{r}{d}\right) = \frac{N(r)}{24\bar{\nu}\left(\frac{r}{d}\right)^2 \frac{\Delta r}{d}}$$

This form is later used to measure the radial distribution function of granular packings (word "generalized" is omitted for simplicity).

APPENDIX D

SAMPLE INPUT FILE FOR MONTE CARLO SIMULATION

This appendix gives the explanation of the sample of the input file (*input.dat*) that is used for Monte-Carlo Simulation and is described in Section 2.2.

```
xlength:      0.24d0  (length of the 3D box)
height:       0.48d0  (height of the 3D box)
width:        0.24d0  (width of the 3D box)
diameter:     0.02d0  (diameter of one monodisperse particle)
delta:        0.02d0  (initial value of δ as determined in Appendix A)
decr:         0.995d0 (multiplicator of dynamic reduction of δ)
dgap (diam):  0.2d0     (parameter that "distinguish" neighbors for the
coordination number computation)
packpr:       0.1d0   (if applicable, the step for layering analysis)
coef:         0.11d1  (linear expansion coefficient γ)
np:           1728    (number of monodisperse spheres in system)
mdiv:         8       (number of divisions of one side)
maxgen:       1000000 (max # of attempts in RINCFG.f)
MC steps:     1000000 (counter of every 1M MC steps for criterion 2.3)
navst:        5000000 (initial number of MC steps to meet criterion 2.3)
nrcg:         12001   (max # of taps-nrcgo to be simulated)
nrcgo:       10000     (original # of taps that is taken for the initial
config from coord.txt)
binwid:       0.01d0  (bin width used for radial distribution function)
dstinc:       2.0D-4  (parameter used for vertical center distribution)
Temperature: 2.73d2 (temperature T used for Metropolis algorithm)
density:      1.5d3   (density of a particle)
g:            9.81d0  (gravitational constant g)
floor:        yes     (flag of a rigid floor)
top:          yes     (flag of a rigid top)
x0wall:       no      (flag of a rigid wall at x=0)
x1wall:       no      (flag of a rigid wall at x=xlength)
z0wall:       no      (flag of a rigid wall at z=0)
z1wall:       no      (flag of a rigid wall at z=width)
method (pl/lr): pl    (way of solids fraction calculation: pl - planar
by , lr - method of volume confined in the layers)
iexist(1-no,2-yes): 1 (flag of existing coord.txt file)
```

APPENDIX E

CPU TIME USAGE BY MONTE-CARLO SIMULATION

Optimization of CPU time spent to provide simulation results was, is, and will be an essential task for any numerical simulation. In this appendix we report the computational time which is being used by Monte Carlo Simulation and Discrete Element Method codes on NJIT UNIX-platforms.

As seen from Figure E.1, the average number of particles in a cell is a crucial parameter for Monte-Carlo Simulation. By reducing the number of particles in a cell, we reduce the number of possible overlap detection attempts, however from the other side an increase of the number of cells means the check over the loop with more number of cells.

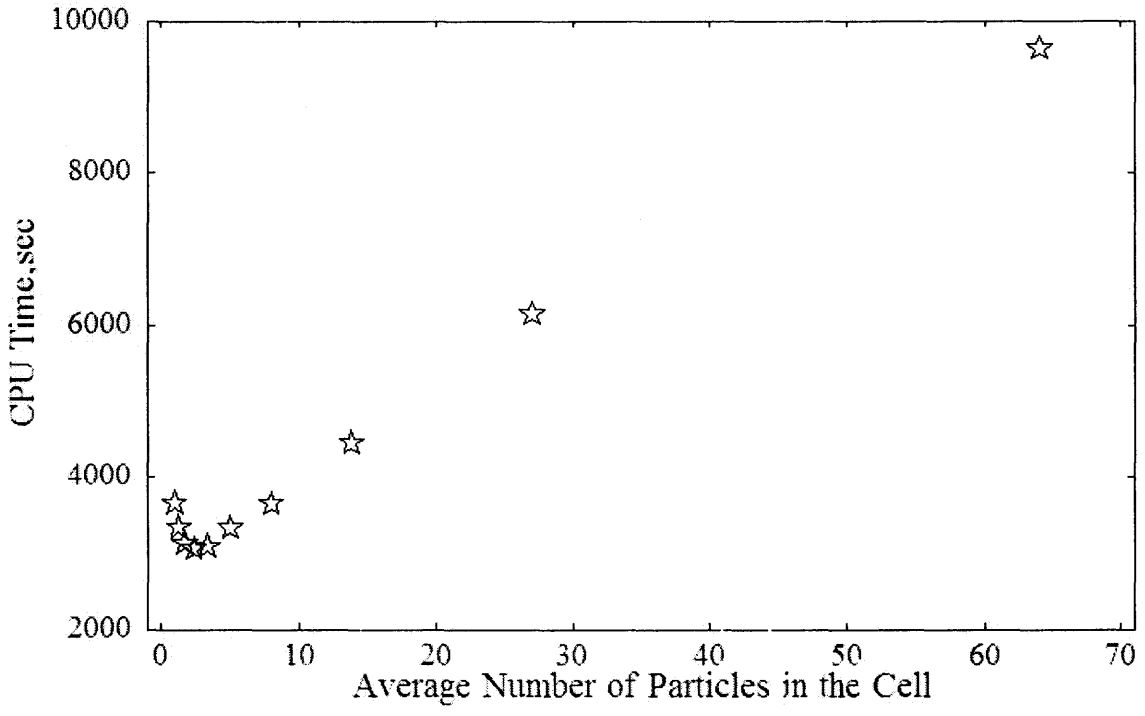

Figure E.1 CPU time usage dependence for one tap on the average number of particles in one cell.

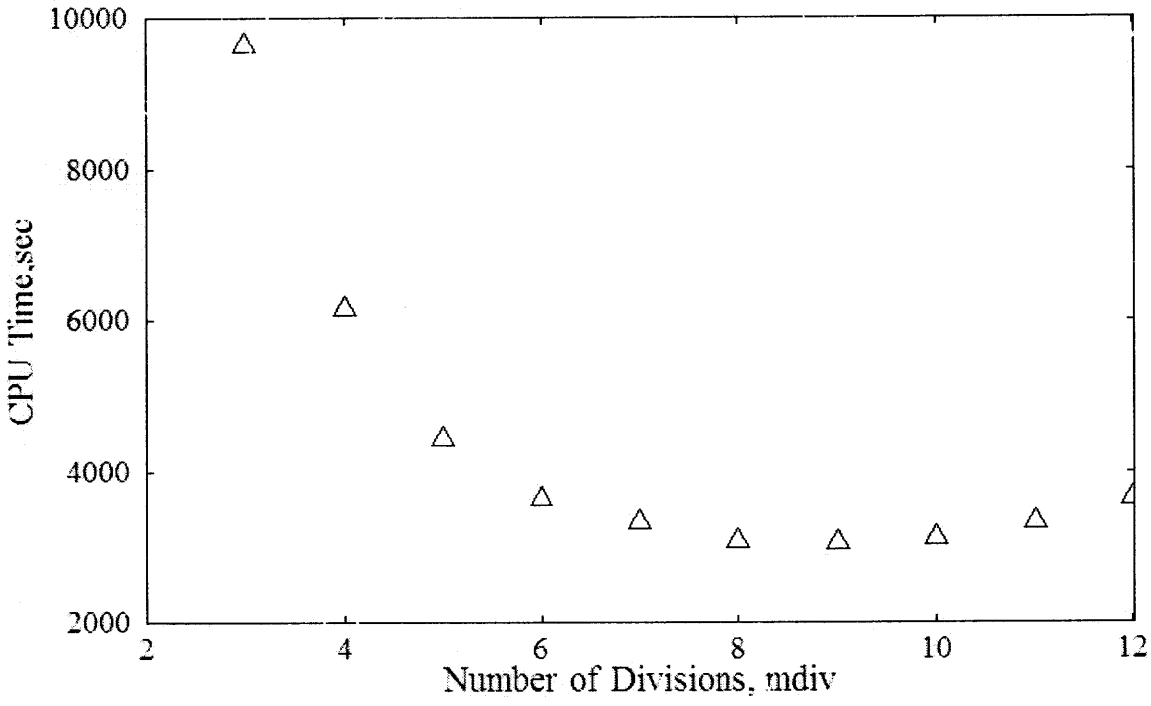

Figure E.2 CPU time usage dependence for one tap on the number of divisions of one side (i.e. length). The system considered is a box ($12d \times 24d \times 12d$) and 1,728 particles.

Figure E.2 above represents the influence of the number of one side divisions of the box on the computational time. Box sides (length, width and height) are divided into the cells of same dimensions and the number of divisions is very likely correlated with the average number of particles in the cell. The optimal numbers of divisions for different system sizes are tabulated in the Table E.1 below.

Table E.6.1 The optimal number of divisions for different system size.

Total number of particles, np	Number of side divisions, mdiv	Average number of particles in the cell, mp
729	6	3.37
1,000	7	2.91
1,728	8	3.37
3,375	10	3.37
8,000	14	2.91

APPENDIX F

CPU TIME USAGE BY DISCRETE ELEMENT METHOD SUBROUTINES

In this appendix we report the computational time which is being used by Monte Carlo Simulation and Discrete Element Method codes on NJIT UNIX-platforms. Spheres diameters chosen were equal to 0.02m and 0.002m and consequently different time-step intervals used by different DEM subroutines. Maximum time of run for both cases was 2.25×10^{-1} seconds. As seen from the Table F the most time-consuming subroutine is a subroutine *forces.f* where force model described in Chapter 4. Also it is very crucial to use a relatively moderate spherical diameter 2×10^{-2} m which results in moderate time-step 10^{-6} sec. The reduction of the time-step leads to several orders of the magnitude increase of CPU time use.

Table F The CPU time usage in seconds by various DEM subroutines for two different time-steps.

Subroutines	d=0.02m, $\Delta t\sim2.11\times10^{-6}$	d=0.002m, $\Delta t\sim6.69\times10^{-8}$
datain	0.0001	0.002
dumpread	0.	0.
init	0.0001	0.
avezon	2.77	2.87
findrad	0.	0.
datasav2	0.002	0.
update	1.57	12.57
initstep	8.12	264.11
forces	911.20	160720
integ1	16.07	515.99
diagnos2	22.44	705.43
integ2	21.33	680.13
bound	0.	0.001
deletem	0.	0.769
initcum1	0.002	0.
initcum2	0.001	0.
packfr	0.0397	0.0175
Total	983.54 sec	162 901 sec

APPENDIX G

APPLICATION OF PERIODIC BOUNDARY CONDITIONS IN DEM CODE

Given that in the previous versions of DEM code the lateral x and z boundaries were solid walls, the construction and implementation of the periodic boundary conditions for lateral x and z coordinates was naturally required. Let's consider a pair of neighboring spheres that are placed inside the box and suppose each of them touch opposite periodic boundary "walls". To take into account the periodic boundary conditions, one needs to create the "virtual image" particle from the opposite side with a shift of the proper coordinate for $\pm xcell$, where *xcell* stands for the box dimensions in x-direction:
Now the square of the central distance between two particles is calculated as the sum of the squared differences of the appropriate coordinates of centers (rx, ry, rz):

$$rijsq = rx^2 + ry^2 + rz^2$$

where $rx = x(j) - x(i)$, $rz = z(j) - z(i)$.

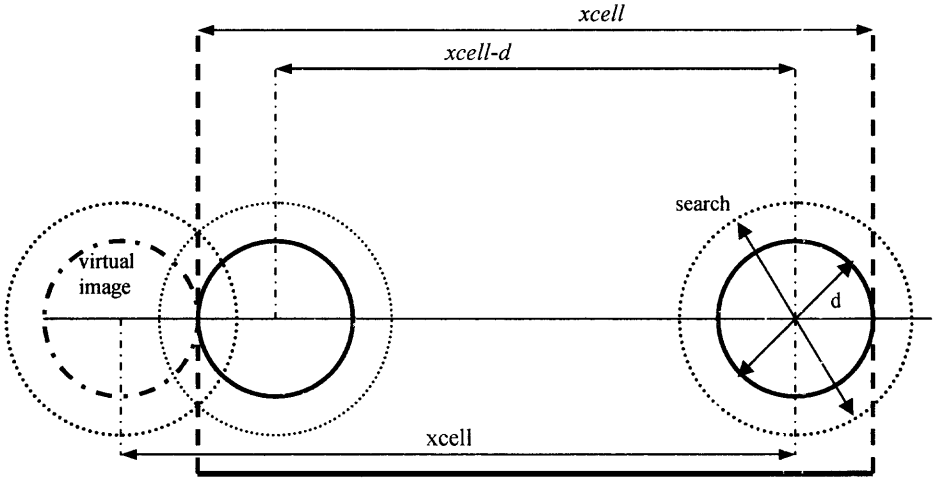

Figure G.1 The interpenetration of the search "envelopes" of two neighboring particles due to periodic boundary conditions.
This was done by modification of the inverse value of *xcelli* to:

$$xcelli = \frac{1}{xcell - (d + 2 \cdot search)}$$

REFERENCES

1. Aste, T., *Variations around disordered close packing.* J. Phys.: Condens. Matter, 2005. **17**: p. S2361-S2390.

2. Adams, D.J. and A.J. Matheson, *Computation of dense random packings of hard spheres* J. Chem. Phys., 1972. **56**: p. 1989-1994.

3. Arthur, J.R.F. and T. Dunstan, *Radiography measurements of particle packing.* Nature, 1969. **223**(2): p. 464-468.

4. Bennett, C.H., *Serially deposited amorphous aggregates of hard spheres.* J. Appl. Phys., 1972. **6**: p. 2727-2733.

5. Bernal, J.D. and J. Mason, *Co-ordination of randomly packed spheres.* Nature, 1960. **188**: p. 910-911.

6. Cumberland, D.J. and R.J. Crawford, *The Packing of Particles.* Handbook of Powder Technology, ed. J.C. Williams and T. Allen. Vol. 6. 1987: Elsevier.

7. Gotoh, K., W.S. Jodrey, and E.M. Tory, *A random packing structure of equal spheres - statistical geometrical analysis of tetrahedral configurations.* Powder Technology, 1978. **20**: p. 233-242.

8. Heesch, H. and F. Laves, *Uber dunne Kugelpackungen.* Z. Krist., 1933. **85**: p. 443-453.

9. Hilbert, D. and S. Cohn-Vossen, *Anschauliche Geometrie.* 1932, Berlin: Springer Verlag.

10. Onoda, G.Y. and E.G. Liniger, *Random loose packing of uniform spheres and the dilantancy onset.* Physical Review Letters, 1990. **64**: p. 2727-2731.

11. Scott, G.D. and D.M. Kilgour, *The density of random close packing of spheres.* British Journal of Applied Physics, 1969. **2**: p. 863-864.

12. Silbert, L.E., D. Ertas, G.S. Grest, T.C. Halsey, and D. Levine, *Geometry of frictionless and frictional sphere packings.* Phys. Rev. E 2002. **65**(3): p. 031304.

13. Smith, W.O., P.D. Foote, and P.F. Bussang, *Packing of homogeneous spheres.* Physical Review E, 1929. **34**(2): p. 1271-1274.

14. Torquato, S. and F.H. Stillinger, *New Conjectural Lower Bounds on the Optimal Density of Sphere Packings.* Experimental Mathematics, 2006. **15**(3): p. 307-332.

15. Tory, E.M., B.H. Church, M.K. Tan, and M. Ratner, *Simulated random packing of equal spheres.* Can. J. Chem. Eng., 1973. **51**: p. 484-493.

16. Berg, T.G.O., R.L. McDonald, and R.J.T. Jr., *The Packing of Spheres.* Powder Technology, 1969/70. **3**: p. 183-188.

17. Kelly, E.M., *Porosity of a layer of spheres deposited randomly on a close-packed layer.* Powder Technology, 1970. **4**(1): p. 56-57.

18. Cundall, P.A. and O.D.L. Strack, *A discrete numerical model for granular assemblies.* Geotechnique, 1979. **29**(1): p. 47-65.

19. Stewart, D.A., *High Quality Concrete.* 1951, London: Spon Publishers.

20. Evans, P.E. and R.S. Millman, *The Vibratory Packing of Powders.* Powder Met., 1964. **7**: p. 50-52.

21. Ayer, J.E. and F.E. Soppet, *Vibratory Compaction: I, Compaction of Spherical Shapes.* J. Am. Ceram. Soc., 1965. **48**(4): p. 180-181.

22. D'Appolonia, D. and E. D'Appolonia. *Determination of the maximum density of cohesionless soils.* in *3rd Asian Regional Conference on Soil Mechanics and Foundation Engineering.* 1967: Jerusalem Academic Press.

23. Dobry, R. and R.V. Whitman, *Compaction of Sand on a Vertically Vibrated Table.* 1973, American Society of Testing Materials: Philadelphia. p. 156-170.

24. Zhang, N. and A.D. Rosato, *Experiments and Simulations on Vibration Induced Densification of Bulk Solids.* KONA, 2006. **24**: p. 93-103.

25. Macrae, J.C., W.A. Gray, and P.C. Finlason, *Vibration packing of dry granular solids.* Nature, 1957. **179**: p. 1365-1367.

26. Takahashi, M. and S. Suzuki, *Numerical analysis of tapping behavior of ceramic powders.* Ceramic Bulletin, 1986. **65**: p. 1587-1590.

27. Kawakita, K. and K.-H. Ludde, *Some considerations on powder compression equations.* Powder Technology, 1971. **4**(2): p. 61-68.

28. Knight, J.B., C.G. Fandrich, C.N. Lau, H.M. Jaeger, and S.R. Nagel, *Density relaxation in a vibrated granular material.* Phys. Rev. E, 1995. **51**: p. 3957-3963.

29. Jaeger, H.M. and S.R. Nagel, *Granular solids, liquids, and gases.* Rev. Mod. Phys., 1996. **68**: p. 1259-1273.

30. Jaeger, H.M., S.R. Nagel, and R.P. Behringer, *The physics of granular materials.* Physics Today, 1996. **49**(4): p. 32-38.

31. Nowak, E.R., J.B. Knight, E.B. Naim, H.M. Jaeger, and S.R. Nagel, *Density fluctuation in vibrated granular materials.* Physical Review E., 1998. **57**: p. 1971-1982.

32. Nowak, E.R., J.B. Knight, M.L. Povinelli, H.M. Jaeger, and S.R. Nagel, *Reversibility and irreversibility in the packing of vibrated granular material.* Powder Technology, 1997. **94**(1): p. 79-83.

33. Nicolas, M., P. Duru, and O. Pouliquen, *Compaction of granular material under cyclic shear.* Europhysics Letters, 2002. **60**: p. 677-683.

34. Lumay, G., F. Ludewig, and N. Vandewalle, *Compaction of granular materials: experiments and contact dynamics simulations.* Journal of Physics: Conference Series, 2006. **40**: p. 133-143.

35. Rosato, A.D., K.J. Strandburg, F. Prinz, and R.H. Swendsen, *Why the Brazil nuts are on top: Size segregation of particulate matter by shaking.* Phys. Rev. Lett., 1987. **58**: p. 1038-1042.

36. Tobochnik, J. and P.M. Chapin, *Monte Carlo simulation of hard spheres near random closest packing using spherical boundary conditions.* Journal of Chemical Physics, 1988. **88**(9): p. 5824-5830.

37. Metropolis, N., A.W. Rosenbluth, M.N. Rosenbluth, A.H. Teller, and E. Teller, *Equation of state calculations by fast computing machines.* J. Chem. Phys., 1953. **21**(6): p. 1087-1092.

38. Rosenbluth, M.N. and A.W. Rosenbluth, *Further Results on Monte Carlo Equations of State.* Journal of Chemical Physics, 1954. **22**(5): p. 881-884.

39. Mehta, A. and G.C. Barker, *Vibrated powders: a microscopic approach.* Physical Review Letters, 1991. **67**(3): p. 394-397.

40. Barker, G.C. and A. Mehta, *Vibrated powders: structure, correlations and dynamics.* Phys. Rev. A, 1992. **45**(6): p. 3435-3446.

41. Barker, G.C. and A. Mehta, *Transient phenomena, self-diffusion, and orientational effects in vibrated powders.* Physical Review E, 1993. **47**(1): p. 184-188.

42. Coniglio, A., *Clusters and frustration in glass forming systems and granular materials.* Progress of Theoretical Physics Supplement, 1997(126): p. 281-287.

43. Coniglio, A., A. Fierro, M. Nicodemi, M.P. Ciamarra, and M. Tarzia, *Statistical mechanics of dense granular media.* Journal of Physics Condensed Matter, 2005. **17**(24): p. S2557-S2572.

44. Coniglio, A. and H.J. Herrmann, *Phase transitions in granular packings.* Physica A, 1996. **225**: p. 1-6.

45. Coniglio, A. and M. Nicodemi, *Jamming transition of granular media.* Journal of Physics Condensed Matter, 2000. **12**(29): p. 6601-6610.

46. Coniglio, A. and M. Nicodemi, *A statistical mechanics approach to the inherent states of granular media.* Physica A: Statistical Mechanics and its Applications, 2001. **296**(3-4): p. 451-459.

47. Nicodemi, M. and A. Coniglio, *Aging in out-of-equilibrium dynamics of models for granular media.* Phys. Rev. Letters, 1999. **82**: p. 916-919.

48. Nicodemi, M., A. Coniglio, and H.J. Hermann, *Density fluctuations in a model for vibrated granular media.* Phys. Rev. E, 1999. **Vol.59, N6**: p. 6830-6837.

49. Nicodemi, M., A. Coniglio, and H.J. Herrmann, *Frustration and slow dynamics of granular packing.* Physical Review E - Statistical Physics, Plasmas, Fluids, and Related Interdisciplinary Topics, 1997. **55**(4): p. 3962-3969.

50. Nicodemi, M., A. Coniglio, and H.J. Herrmann, *Compaction and force propagation in granular packings.* Physica A: Statistical Mechanics and its Applications, 1997. **240**(3-4): p. 405-418.

51. Nicodemi, M., A. Coniglio, and H.J. Herrmann, *The compaction in granular media and frustrated ising models.* Journal of Physics A: Mathematical and General, 1997. **30**(11): p. L379-L385.

52. Williams, J.R., G. Hocking, and G.G.W. Mustoe, *The theoretical basis of the discrete element method*, in *NUMETA Numerical Methods in Engineering, Theory and Applications*. 1985, A. A. Balkema: Rotterdam.

53. Walton, O.R., *Numerical simulation of inelastic, frictional particle-particle interactions*, in *Particulate Two-Phase Flow*, M.C. Roco, Editor. 1992, Butterworth: Boston. p. 884-911.

54. Schafer, J., S. Dippel, and D.E. Wolf, *Force schemes in simulations of granular materials.* J. Phys. I France, 1996. **6**: p. 5-20.

55. Luding, S., *Models and simulations of granular materials*, in *Theoretische Polymerphysik*. 1994, Albert-Ludwigs-Universitat: Freiburg. p. 125-138.

56. Liu, L.F., Z.P. Zhang, and A.B. Yu, *Dynamic Simulation of the Centripetal Packing of Mono-Sized Spheres.* Physica A, 1999. **268**: p. 433-453.

57. Cheng, Y.F., S.J. Guo, and H.Y. Lai, *Dynamic simulation of random packing of spherical particles.* Powder Tech, 2000. **107**: p. 123-130.

58. Liu, G. and K.E. Thompson, *Influence of computational domain boundaries on internal structure in low-porosity sphere packings.* Powder Tech, 2000. **113**: p. 185-196.

59. Rosato, A.D., D.L. Blackmore, N. Zhang, and Y. Lan, *A perspective of vibration-induced size segregation of granular materials.* Chemical Engineering Science, 2002. **57**: p. 265-275.

60. An, X.Z., R.Y. Yang, K.J. Dong, R.P. Zou, and A.B. Yu, *Micromechanical simulation and analysis of one-dimensional vibratory sphere packing.* Physical Review Letters, 2005. **95**: p. 205502.

61. Yang, R.Y., R.P. Zou, K.J. Donga, X.Z. An, and A. Yu, *Simulation of the packing of cohesive particles.* Computer Physics Communications, 2007. **177**(1-2): p. 206-209.

62. Remond, S. and J.L. Galias, *Simulation of Periodic Mono-Sized Hard Sphere Systems under Different Vibration Conditions and Resulting Compaction.* Physica A, 2006. **369**: p. 545-561.

63. Arsenovic, D., S.B. Vrhovac, Z.M. Jaksic, L. Budinski-Petkovic, and A. Belic, *Simulation Study of Granular Compaction Dynamics under Vertical Tapping.* Physical Review E, 2006. **74**: p. 061302-1-14.

64. Boutreux, T. and P.G. DeGennes, *Compaction of granular mixtures: a free volume model.* Physica A, 1997. **244**: p. 59-67.

65. Gavrilov, K.L., *Cluster model for compaction of vibrated granular materials.* Physical Review E, 1998. **58**(2): p. 2107-2114.

66. Linz, S.J., *Phenomenological Modeling of the Compaction Dynamics of Granular Systems.* Phys. Rev. E, 1996. **54**: p. 292501-292504.

67. Brey, J.J., F. Moreno, and J.W. Dufty, *Model kinetic equation for low-density granular flow.* Physical Review E - Statistical Physics, Plasmas, Fluids, and Related Interdisciplinary Topics, 1996. **54**(1): p. 445-456.

68. Head, D.A., *Phenomenological glass model for vibratory granular compaction.* Phys. Rev. E, 2000. **62**(2): p. 2439-2449.

69. Head, D.A. and G.J. Rodgers, *A coarse grained model for granular compaction and relaxation.* J. Phys. A, 1998. **31**: p. 107-122.

70. Adam, G. and J.H. Gibbs, *On the Temperature Dependence of Cooperative Relaxation Properties in Glass-Forming Liquids.* J Chem Phys, 1965. **43**(1): p. 139-146.

71. Peng, G. and T. Ohta, *Logarithmic density relaxation in compaction of granular materials.* Phys. Rev. E, 1998. **57**: p. 829-833.

72. Brey, J.J. and A. Prados, *Linear response of vibrated granular systems to sudden changes in the vibration intensity.* Physical Review E, 2001. **63**: p. 061301-1.

73. Brey, J.J., A. Prados, and B. Sanchez-Rey, *Thermodynamic description in a simple model for granular compaction.* Physica A: Statistical Mechanics and its Applications, 2000. **275**(3): p. 310-324.

74. Round, G.F. and R. Newton, *Random Packing of Equal Spheres on a Plane Surface.* Nature, 1963. **198**(4882): p. 747-750.

75. Josserand, C., A.V. Tkahenko, D.M. Mueth, and H.M. Jaeger, *Memory effects in granular materials.* Physical Review Letters, 2000. **85**(17): p. 3632-3635.

76. Rosato, A.D., D.L. Blackmore, N. Zhang, and Y. Lan, *A perspective on vibration-induced size segregation of granular materials.* Chemical Engineering Science, 2002. **57**(2): p. 265-275.

77. Powell, M.J., *Distribution of Near Neighbors in Randomly Packed Hard Spheres.* Powder Technology, 1980. **26**: p. 221-223.

78. Pouliquen, O., M. Belzons, and M. Nicolas, *Fluctuating Particle Motion during Shear Induced Granular Compaction.* Phys Review Letters, 2003. **91**(1): p. 1-4.

79. Williams, S.R. and A.P. Philipse, *Random Packings of Spheres and Spherocylinders Simulated by Mechanical Contraction.* Physical Review E, 2003. **67**(051301): p. 1-9.

80. Abreu, C.R.A., F.W. Tavares, and M. Castier, *Influence of particle shape on the packing and on the segregation of spherocylinders via Monte Carlo simulations.* Powder Tech, 2003. **134**: p. 167-180.

81. Coniglio, A., A. De Candia, A. Fierro, M. Nicodemi, and M. Tarzia, *Statistical mechanics approach to the jamming transition in granular materials.* Physica A: Statistical Mechanics and its Applications, 2004. **344**(3-4 SPEC. ISS.): p. 431-439.

82. Silbert, L.E., D. Ertas, G.S. Grest, T.C. Halsey, and D. Levine, *Analogies between granular jamming and the liquid-glass transition.* Physical Review E - Statistical, Nonlinear, and Soft Matter Physics, 2004. **65**(5): p. 1-6.

83. Brujic, J., P. Wang, C. Song, D.L. Johnson, O. Sindt, and H.A. Makse, *Granular dynamics in compaction and stress relaxation.* Physical Review Letters, 2005. **95**(12): p. 1-4.

84. Luding, S., E. Clement, A. Blumen, J. Rajchenbach, and J. Duran, *Studies of columns of beads under external vibrations.* Physical Review E, 1994. **49**(2): p. 1634-1641.

85. Ribiere, P., P. Philippe, P. Richard, R. Delannay, and D. Bideau, *Slow compaction of granular systems.* J. Phys.: Condens. Matter, 2005. **17**: p. S2743-S2754.

86. Ribiere, P., P. Richard, R. Delannay, and D. Bideau, *Importance of convection in the compaction mechanisms of anisotropic granular media.* Physical Review E, 2005. **71**: p. 011304.

87. Ribiere, P., P. Richard, R. Delannay, D. Bideau, M. Toiya, and W. Losert, *Effect of rare events on out-of-equilibrium relaxation.* Physical Review Letters, 2005. **95**(26): p. 1-4.

88. Knight, J.B., C.G. Frandrich, C.N. Lau, H.M. Jaeger, and S.R. Nagel, *Density relaxation in a vibrated granular material.* Physical Review E, 1995. **51**: p. 3957-3963.

89. Kim, K., J.K. Moon, J.J. Park, H.K. Kim, and H.K. Pak, *Jamming Transition in a Highly Dense Granular System under Vertical Vibration.* Physical Review E, 2005. **72**: p. 011302-1-4.

90. Budinski-Petković, L.J., M. Petković, Z.M. Jakšić, and S.B. Vrhovac, *Symmetry effects in reversible random sequential adsorption on a triangular lattice.* Physical Review E, 2005. **72**: p. 046118.

91. Jaeger, H.M., S.R. Nagel, and R.P. Behringer, *Granular Solids, Liquids and Gases.* Reviews of Modern Physics, 1996. **68**: p. 1259 - 1273.

92. Theuerkauf, J., P. Witt, and D. Schwesig, *Analysis of particle porosity distribution in fixed beds using the discrete element method.* Powder Technology, 2006. **165**: p. 92-99.

93. Linz, S. and A. Dohle, *Minimal relaxation law for compaction of tapped granular matter.* Phys. Rev. E, 1999. **60**(5): p. 5737-5741.

94. Wouterse, A. and A.P. Philipse, *Geometrical Cluster Ensemble Analysis of Random Sphere Packings.* The Journal of Chemical Physics, 2006. **125**: p. 194709-1-10.

95. Nicodemi, M., A. Coniglio, and H.J. Herrmann, *Density fluctuations in a model for vibrated granular media.* Physical Review E: Statistical Physics, Plasmas, Fluids, and Related Interdisciplinary Topics, 1999. **59**(6): p. 6830-6837.

96. Lumay, G., F. Ludewig, and N. Vandewalle, *Compaction of granular materials: Experiments and contact dynamics simulations.* Journal of Physics: Conference Series, 2006. **40**(1): p. 133-143.

97. McNamara, S. and S. Luding, *Energy flows in vibrating granular media.* Phys. Rev. E 1998. **58**: p. 813-822.

98. Ciamarra, M.P., A. Coniglio, and M. Nicodemi, *Thermodynamics and statistical mechanics of dense granular media.* Physical Review Letters, 2006. **97**(15).

99. Ciamarra, M.P., M. Nicodemi, and A. Coniglio, *Granular Packs under Vertical Tapping: Structure Evolution, Grain Motion and Dynamic Heterogeneities.* Physical Review E, 2007. **75**: p. 021303-1-10.

100. Pillai, K.K., *Voidage variation at the wall of a packed bed of spheres.* Chemical Engineering Science, 1977. **32**: p. 59-61.

101. Bernal, J.D. *The Geometry of the Structure of Liquids.* in *Liquids: Structure, Properties, Solid Interactions.* 1963. Warren, Michigan: Elsevier Publishing Company.

102. Scott, G.D., *Packing of spheres.* Nature, 1960. **188**: p. 908-909.

103. Berryman, J.G., *Random Close Packing of Hard Spheres and Disks.* Physical Review A, 1983. **27**(2): p. 1053-1061.

104. Haughey, D.P. and G.S.G. Beveridge, *Local voidage variation in a randomly packed bed of equal-sized spheres.* Chemical Engineering Science, 1966: p. 905-916.

105. Goodling, J.S. and M.S. Khader, *Coordination Number Distribution of Spherical Particles in a Packed Cylindrical Bed.* Powder Technology, 1985. **44**: p. 53-55.

106. Mason, G., *Radial Distribution Functions from Small Packings of Spheres.* Nature, 1968. **217**: p. 733-735.

107. Tory, E.M., N.A. Cochrane, and S.R. Waddell, *Anisotropy in simulated packing of equal spheres.* Nature, 1968. **220**: p. 1023-1024.

108. Nolan, G.T. and P.E. Kavanagh, *Computer Simulation of Random Packing of Hard Spheres.* Powder Technology, 1992. **72**: p. 149-155.

109. Nolan, G.T. and P.E. Kavanagh, *Octahedral Configurations in Random Close Packing.* Powder Technology, 1995. **83**: p. 253-258.

110. Finney, J.L., *Random packing and the structure of liquids. 1. The geometry of random close packing.* Proc. Roy. Soc. Lond. A, 1970. **319**: p. 479-493.

111. Bratberg, I., K.J. Maloy, and A. Hansen, *Validity of the Janssen law in narrow granular columns.* European Physical Journal E, 2005. **18**: p. 245-252.

112. Cargill, G.S., *Dense Random Packing of Hard Spheres as a Structural Model for Noncrystalline Metallic Solids.* J of Appl Physics, 1970. **41**(5): p. 2248-2250.

113. Sederman, A.J., P. Alexander, and L.F. Gladden, *Structure of Packed Beds Probed by Magnetic Resonance Imaging.* Powder Technology, 2001. **117**: p. 255-269.

114. Beresford, R.H., *Statistical Geometry of Random Heaps of Equal Hard Spheres.* Nature, 1969. **224**: p. 550-553.

115. Torquato, S., T.M. Truskett, and P.G. Debenedetti, *Is Random Close Packing of Spheres Well Defined?* Phys. Rev. Lett., 2000. **84**: p. 2064-2067.

116. He, D., N.N. Ekere, and L. Cai, *New Statistic Techniques for Structure Evaluation of Particle Packing.* Materials Science and Engineering, 2001. **A298**: p. 209-215.

117. Liao, Y.C., D.J. Lee, and P. He, *Microstructural Description of Packed Bed Using Voronoi Polyhedra.* Powder Technology, 2002. **123**: p. 1-8.

118. Gotoh, K., *Liquid Structure and the Coordination of Equal Spheres in Random Assemblage.* Nature, 1971. **231**: p. 108-110.

119. Gotoh, K. and J.L. Finney, *Statistical geometrical approach to random packing density of equal spheres.* Nature, 1974. **252**: p. 202-205.

120. Wu, Y., Z. Fan, and Y. Lu, *Bulk and Interior Packing Densities of Random Close Packing of Hard Spheres.* Journal of Materials Science, 2003. **38**: p. 2019-2025.

121. Iwata, H. and T. Homma, *Distribution of Coordination Numbers in Random Packing of Homogeneous Spheres.* Powder Technology, 1974. **10**: p. 79-83.

122. Aste, T., M. Saadatfar, and T.J. Senden, *Geometrical structure of disordered sphere packings.* Phys. Rev. E, 2005. **71**: p. 061302.

123. Matheson, A.J., *Computation of a Random Packing of Hard Spheres.* J. Phys. C: Solid State Phys., 1974. **7**: p. 2569-2576.

124. Mueller, G.E., *Numerically Packing Spheres in Cylinders.* Powder Technology, 2005. **159**: p. 105-110.

125. Dodds, J.A., *Simplest Statistical Geometric Model of the Simplest Version of the Multicomponent Random Packing Problem.* Nature, 1975. **256**: p. 187-189.

126. Kumar, V.S. and V. Kumaran, *Voronoi neighbor statistics of hard-disks and hard-spheres.* Journal of Chemical Physics, 2005. **123**: p. 074502.

127. Kumar, V.S. and V. Kumaran, *Voronoi cell volume distribution and configurational entropy of hard-spheres.* J. Chem. Phys., 2005. **123**(11): p. 114501-114503.

128. Levine, M.M. and J. Chernick, *A Numerical Model of Random Packing of Spheres.* Nature, 1965. **208**: p. 68-69.

129. Suzuki, M., K. Makino, M. Yamada, and K. Linoya, *A Study on the Co-ordination Number in a System of Randomly Packed, Uniform-Sized Spherical Particles.* International Chemical Engineering, 1981. **21**: p. 482-485.

130. Rumpf, J., *Grundlagen und Methoden des Granulierens.* Chemie-Ingenieur-Technik, 1958. **3**: p. 144–158.

131. Meissner, H.P., A.S. Michaels, and R. Kaiser, *Spontaneous Pelletization in Fine Powders.* Industrial and Engineering Chemistry Process Design and Development, 1964. **3**(3): p. 197-201.

132. Ridgway, K. and K.J. Tarbuck, *The Random Packing of Spheres.* British Chemical Engineering, 1967. **12**: p. 384-385.

133. Nakagaki, M. and H. Sunada, *Theoretical studies on structures of the sedimentation bed of spherical particles.* Yakugaku Zasshi, 1968. **88**: p. 651:5.

134. Ouchiyama, N. and T. Tanaka, *Estimation of the average number of contacts between randomly mixed solid particles.* Industrial and Engineering Chemical Fundamentals, 1980. **19**: p. 338-340.

135. Hill, T., *Statistical Mechanics.* 1956, New York: McGraw-Hill.

136. Powell, M.J., *Computer-simulated random packing of spheres.* Powder Technology, 1980. **25**: p. 45-52.

137. Rosato, A.D. and D. Yacoub, *Microstructure evolution in compacted granular beds.* Powder Technology, 2000. **109**: p. 255-261.

138. Qin, Y. and K. Fichthorn, *Molecular-Dynamics Simulation of Forces between Nanoparticles in a Lennard-Jones Liquid.* J Chem Phys, 2003. **119**(18): p. 9745-9754.

139. Gibson, W.G. and S.G. Byrnes, *Quantum-mechanical Radial Distribution Function for a Hard-sphere Gas at Low Density and High Temperature* Phys. Rev. A, 1975. **11**: p. 270 - 275.

140. Ascarelli, P., *Atomic Radial Distributions and Ion-ion Potential in Liquid Gallium.* Physics Review, 1966. **143**(1): p. 36-47.

141. Kirkwood, J.G., *Statistical Mechanics of Fluid Mixtures.* J Chem Phys, 1935. **3**: p. 300-313.

142. Morell, W.E. and J.H. Hilderbrand, *The Distribution of Molecules in a Model Liquid.* J Chem Physics, 1936. **4**: p. 224-227.

143. Bortz, A.B., M.H. Kalos, and J.L. Lebowitz, *A New Algorithm for Monte Carlo Simulation of Ising Spin Systems.* Journal of Computational Physics, 1975. **17**: p. 10-18.

144. Jansen, A.P.J., *Monte Carlo Simulations of Chemical Reactions on a Surface with Time-Dependent Reaction-Rate Constants.* Computer Physics Communications, 1995. **86**: p. 1-12.

145. Lukkien, J.J., J.P.L. Segers, P.A.J. Hilbers, R.J. Gelten, and A.P.J. Jansen, *Efficient Monte Carlo Methods for the Simulation of Catalytic Surface Reactions.* Physical Review E, 1998. **58**(2): p. 2598-2610.

146. Fichthorn, K.A. and W.H. Weinberg, *Theoretical Foundations of Dynamical Monte Carlo Simulations.* J. Chem. Phys., 1991. **95**(2): p. 1090-1096.

147. Carlson, P., M. Danielsson, M. Dejardin, K. Jon-And, and J. Sjolin, *Simulated Annealing and Neural Networks as Alternative Methods for Nonlinear Constrained Optimization.* Nuclear Instruments and Methods in Physics Research A, 1996. **381**: p. 152-156.

148. Sweetman, M., *Addition of a chain-cell search method and a van der Waals force model to a particle dynamics code*, in *Mechanical Engineering*. 2003, New Jersey Institute of Technology: Newark, NJ.

149. Allen, M.P. and D.J. Tildesley, *Computer Simulation of Liquids*. 1989: Oxford University Press. 385-387.

150. Talbot, J., G. Tarjus, and P. Viot, *Optimum Monte Carlo simulations: some exact results.* J. Phys. A: Math. Gen., 2003. **36**: p. 9009-9023.

151. Bouzida, D., S. Kumar, and R.H. Swendsen, *Efficient Monte Carlo methods for computer simulation of biological molecules.* Phys. Rev. A, 1992. **45**: p. 8894-8901.

152. Kohlrausch, R., *Theorie des elektrischen riicksandes in der leidener flasche.* Pogg. Ann. Phys. Chem, 1854. **91**: p. 179-214.

153. Williams, G. and D.C. Watts, *Non-Debye relation in condensed matter.* Trans. Faraday Soc., 1970. **66**: p. 80-81.

154. Haile, J.M., *Molecular Dynamics Simulation: Elementary Methods*. 1992: J. Wiley and Sons. 489-492.

155. Walton, O.R. and R.L. Braun, *Stress calculations for assemblies of inelastic spheres in uniform shear.* Acta Mechanica, 1986. **63**: p. 73-86.

156. Mindlin, R.D. and H. Deresiewicz, *Elastic spheres in contact under varying oblique forces.* J. Appl. Mech., 1953. **20**: p. 327-328.

157. Hostler, S.R. and C.E. Brennen, *Pressure wave propagation in a granular bed.* Physical Review E, 2005. **72**: p. 031303-1-031304-6.

158. Liu, C.H. and S.R. Nagel, *Sound in Sand.* Phys Review Letters, 1992. **68**(15): p. 2301-2304.

159. Makse, H.A., N. Gland, D.L. Johnson, and L. Schwartz, *Granular packings: Nonlinear elasticity, sound propagation, and collective relaxation dynamics.* Physical Review E - Statistical, Nonlinear, and Soft Matter Physics, 2004. **70**(6 1): p. 061302-1-061302-19.

160. Alcocer, F.J., V. Kumar, and P. Singh, *Permeability of Periodic Porous Media.* Physical Review E, 1999. **59**(1): p. 711-714.

161. Singh, P. and D.D. Joseph, *Dynamics of fluidized suspensions of spheres of finite size.* Int. J. Multiphase Flows, 1995. **21**: p. 1-26.